Non-invasive Monitoring of Oxygen Concentrations and Metabolic Function in Pancreatic Substitutes

A Dissertation
Presented to
The Academic Faculty

by

Jeffrey D. Gross

In Partial Fulfillment
of the Requirements for the Degree
Doctor of Philosophy in the
School of Biomedical Engineering

Georgia Institute of Technology
May 2007

Non-invasive Monitoring of Oxygen Concentrations and Metabolic Function in Pancreatic Substitutes

Approved by:

Dr. Athanassios Sambanis, Advisor
Department of Chemical & Biomolecular Engineering, Department of Biomedical Engineering
Georgia Institute of Technology

Dr. Dale Edmondson
Department of Biomedical Engineering
Emory University

Dr. Elliot Chaikof
Department of Biomedical Engineering
Georgia Institute of Technology

Dr. Robert Long, Jr.
Department of Radiology
Emory University

Dr. Ioannis Constantinidis
Division of Endocrinology
University of Florida

Date Approved: 3/26/2007

To my sister Angela Martino, an insulin dependent diabetic

ACKNOWLEDGEMENTS

I would first like to express my sincerest gratitude to my advisor, Dr. Athanassios Sambanis. The patience and dedication that he displayed on a daily basis in mentoring me has been unparalleled in my educational career. Most notably, the lessons in communication – specifically, in writing and presenting – that Dr. Sambanis has instilled in me will forever impact my professional career. I would like to thank Dr. Ioannis Constantinidis for his many contributions to my project, especially for his help while I visited the University of Florida every few months. In addition, I would like to thank Dr. Robert Long for his instrumental help in performing the *in vivo* experiments. Furthermore, I would like to express my gratitude to Drs Elliot Chaikof and Dale Edmondson whose input helped shape this project.

I would like to thank everyone at the University of Florida who helped with this project in so many ways. First and foremost, I would like to thank my friend Jim Rocca, an NMR specialist at the McKnight Brain Institute, who was there to help with my NMR needs no matter the time of day or night. I would also like to thank the members of the Constantinidis Laboratory (Jose Oca, Carol Sweeney, Chiab Simpson and Dr. Nicholas Simpson) for their assistance with experiments and many helpful discussions.

I am very thankful to have worked with some tremendous individuals over the years. Shing-Yi Cheng and Tony Tang were kind enough to mentor me when I first entered the lab and showed by example how to be a great scientist. Current lab members of the Sambanis Laboratory – Neil Mukherjee, Heather Bara, and Angela Gulino – have

contributed through many helpful discussions and through creating an especially enjoyable lab environment.

Special thanks go to the friends I made here in Atlanta and in particular, my classmates, Craig Duvall, Chris Gemmiti, and Charlie Gersbach. These guys made my Ph.D. career a lot more enjoyable by helping to balance research with a life outside the laboratory.

I would like to acknowledge my family. Mom and Dad, you're constant love, support, words of wisdom and encouragement created an environment in which I could pursue and attain any goal I desired and for this I'm eternally grateful. You both have always been the perfect role models. To my in-laws, Paul and Landy Labonte, thank you so much for your love, support and encouragement over the last 5 years. Finally, I would like to acknowledge my incredible wife, Taryn. The unconditional love that you give me on a daily basis gives me the strength to do so many things. I cannot thank you enough or express in words how much I appreciate everything you do for me. You are my best friend and I love you so very much.

This work was supported by grants from the ERC Program of the National Science Foundation under Award Number EEC-9731643, and the NIH (DK47858). Additionally, I wish to acknowledge the financial support received from NSF IGERT-0221600.

TABLE OF CONTENTS

LIST OF TABLES

Page

LIST OF FIGURES

SUMMARY

Design and characterization of tissue engineered substitutes rely on robust monitoring techniques that provide information regarding viability and function when exposed to various environmental conditions. *In vitro* studies permit the direct monitoring of cellular and construct changes because these substitutes remain accessible. However, upon *in vivo* implantation, changes in cell viability and function are often detected using indirect or invasive methods that make assessing temporal changes challenging. Thus, the development of non-invasive monitoring modalities may facilitate improved tissue substitute design and, ultimately, clinical outcome.

Nuclear magnetic resonance (NMR) spectroscopy and imaging are valuable tools to non-invasively monitor tissue substitutes *in vitro* and *in vivo*. However, due to sensitivity issues, monitoring the physiologic status of cells in substitutes after implantation by NMR is challenging. This limitation was overcome in this thesis by developing a method that non-invasively monitors the dissolved oxygen (DO) concentrations within tissue engineered constructs, since DO levels are known to effect cell viability and function. In these studies, a pancreatic substitute that consisted of a mouse insulinoma cell line sequestered in an alginate bead was used to develop the methodology. Specifically, the oxygenation within pancreatic substitutes was assessed via the incorporation of perfluorocarbon (PFC) emulsions into the construct; ^{19}F NMR was then used to measure T_1 relaxation rates, which inversely correlate to DO concentrations. This technique was developed by designing and building an NMR-compatible perfusion system capable of maintaining user-defined DO concentrations.

The completed system enabled the investigation of a pancreatic substitute composed of βTC-tet cells (a mouse insulinoma cell line) encapsulated into alginate beads .

One of the first challenges addressed in this thesis was the acquisition of DO and cell density gradients within the alginate beads. Although these profiles could be attained by using ^{19}F NMR chemical shift imaging, the magnet used in this thesis did not have the necessary gradients to perform such imaging. In addition, the long acquisition times associated with chemical shift imaging would be problematic upon moving to *in vivo* studies. This caveat was addressed by the development of a mathematical model. The model simulated changes in DO and cell density profiles based on Fickian diffusion equations, spatial limitations of alginate beads, oxygen consumption, and the growth and death characteristics of βTC-tet cells. Based on the model, correlations between the experimentally measurable average intrabead DO (AIDO) concentration and the cell number, cell density profiles and DO concentration gradients were established.

With these correlations established, the volume-averaged DO concentrations could be acquired by ^{19}F NMR and used to monitor the pancreatic substitute. The AIDO/mathematical model system was validated by exposing encapsulated βTC-tet cells to a range of DO concentrations (0.20 to 0.04 mM) within the NMR-compatible perfusion system. During this validation, the metabolic and bioenergetic states of the cells were assessed by DO sensors bracketing the bioreactor and ^{31}P NMR, respectively. In addition, AIDO measurements were acquired using ^{19}F NMR and an established calibration curve. Comparing the simulated and experimental data revealed that the AIDO/mathematical model system indeed could track the status of encapsulated cells, as long as the DO concentration immediately external to the beads is known. Measuring the

surrounding DO concentration is trivial in an *in vitro* setting, as DO sensors can be used, but this is not easily performed *in vivo*. Therefore, a dual-PFC system was developed that enabled simultaneous DO concentration acquisition from two bead populations. This capability was demonstrated using two populations of cell-free beads that were implanted into the peritoneal cavity of mice. The first set of beads contained the PFC perfluorotributylamine (PFTBA), along with a coating of poly-l-lysine (PLL), an inflammatory response initiator. The second set of beads had perfluoro-15-crown-5-ether (PFCE) sequestered in alginate-only beads. The close proximity of the chemical shifts of these two PFCs allowed simultaneous T_1 relaxation rate measurements, and thus simultaneous DO concentration measurements. Due to the induced fibrotic response by the PLL in the PFTBA beads, a lower DO concentration was indeed measured by the PFTBA compared to that measured by PFCE. These results provided validation that the dual-PFC system could be utilized *in vivo*.

The ability to monitor a pancreatic substitute by the AIDO/mathematical model system was then investigated under two simulated *in vivo* conditions. The first study was designed to mimic the changes in DO concentrations that often occur *in vivo* – either due to natural fluctuations at the site of implantation or an induced inflammatory response. During this study, AIDO measurements and the mathematical model were used in combination to estimate the cell density within alginate beads, while the external DO levels were changed. In the second study, the ability to measure cell death during a mimicked cytokine attack was assessed. Specifically, AIDO-estimated cell densities were acquired upon the addition of puromycin (an antibiotic that disrupts mRNA translation, thereby killing the cell). During both of the above studies, AIDO-estimated

cell densities were compared to estimates based on overall oxygen consumption rate measurements. It was concluded that the AIDO measurement was indeed capable of tracking a pancreatic substitute and could possibly aide in distinguishing between various modes of implant failure.

In the final portion of this thesis, the effect of PFC emulsions on encapsulated cells was investigated both experimentally and through mathematical modeling. In this experiment, βTC-tet cells were encapsulated in alginate beads that contained 0%, 5%, or 10% v/v PFTBA emulsion, and cell viability and stimulated insulin secretion were measured over a 16 day period. It was found that the presence of PFTBA had no effect on either cell viability or insulin secretion. Indeed, simulations by the mathematical model did not show any effect on cell viability during the first 8 days and only a slight increase in viability thereafter when PFC emulsions were incorporated. Lastly, the mathematical model was used to simulate the effect of PFCs on cell viability under additional environments. Specifically, the ability of PFCs to buffer the DO concentration within alginate beads upon transient reductions in the DO levels external to the beads was studied. It was found that PFCs are able to maintain higher AIDO concentrations within beads during short hypoxic episodes; however, these differences had only a small effect on the number of viable cells that could be sustained in the beads.

In conclusion, this thesis has established the ability to track pancreatic substitutes using DO concentration measurements acquired from sequestered PFC emulsions and a mathematical model. Future studies could expand this methodology to *in vivo* monitoring of pancreatic substitutes, as well as to additional tissue engineered constructs.

CHAPTER 1

INTRODUCTION

Insulin dependent diabetes comprises approximately 10% of the currently 18 million cases of diabetes in the United States and current health care costs are estimated to be over $130 billion. Despite being a treated disease, diabetics typically live 15 years less than the national average [1], primarily due to the long-term complications associated with the disease (e.g. retinopathy, neuropathy, nephropathy). Fortunately, research has shown that the long-term complications can be mitigated when blood glucose levels are kept under tighter (more physiologic) regulation [2]. Minimizing blood glucose concentration excursions currently requires the use of multiple insulin injections or the use of insulin pumps, and do not entirely eliminate the complications. Promising new therapies, such as islet transplantation, provide better physiologic control of blood sugar and avoid the need for painful traditional bolus insulin injections or insulin pumps. This procedure, which was discovered in 1973, has recently attracted more attention with the introduction of an improved implantation and immunesuppression regimen developed in 2000 [3]. However, the implantation of islets is greatly limited by the scarce supply and the immunosuppressant regimen needed to prevent rejection. Therefore, an alternative treatment that provides tight physiologic control and alleviates cell source issues would greatly benefit insulin-dependent diabetics.

The engineering of living tissues, or tissue engineering, to secrete insulin is a promising alternative. Research in this field primarily focuses on creating biologically-based tissue substitutes that repair, augment, or replace the function of diseased or malfunctioning tissue in the body [4]. One type of tissue substitute is created by

sequestering genetically modified cell lines – a continuous source of cells – that have the desired functional properties into a three-dimensional construct. The construct matrix provides mechanical support, allowing cells to remain viable and functioning. The encapsulation of insulin-secreting cells into a biocompatible material may become a viable treatment option for diabetics. Despite significant progress, the especially complex nature of cell-based therapies and the considerable characterization needed prior to use have precluded the development of such a pancreatic substitute.

Characterization, design and functional improvements of tissue substitutes are routinely accomplished through *in vitro* and *in vivo* testing. In such testing, parameters that can affect viability and function of sequestered cells are meticulously evaluated and monitored to determine consequences. Numerous tools are available to researchers for this i*n vitro* characterization and assessment of constructs, as the substitute is readily available and duplicates for destructive assays can be made. Nevertheless, upon transitioning to *in vivo* characterization, tools available for assessing the tissue substitute are limited. Typically, researchers must rely on monitoring constructs indirectly – in the example of a pancreatic substitute, blood glucose levels could be monitored – or at the end of an animal study when the implant is extracted. Such measurements are important in determining the functional quality of a substitute; however, discerning the mechanism for failure is difficult using such methods. The dissolved oxygen (DO) concentration cannot currently be measured by direct or indirect methods, yet is known to have a direct impact on both cell viability and function [5-9]. This impact has been demonstrated in numerous cell lines [5, 8, 10-18], especially in pancreatic substitutes, as insulin secretion is compromised in low oxygen environments. In addition, the effect of DO

concentrations on viability and function is not always proportional, as cellular function is often diminished at higher DO concentrations than those which would cause cellular apoptosis and death [8]. Thus, monitoring the DO concentration is equally as critical in evaluating a construct as determining the number of viable cells.

The overall objective of this thesis was to establish a method to monitor and track cells and the cellular environment within a tissue engineered substitute *in vitro* and *in vivo*. This was accomplished via ^{31}P NMR spectroscopy and through the incorporation of perfluorocarbon (PFC) emulsions for the monitoring of DO concentration by ^{19}F NMR spectroscopy. The first aim of this thesis was to develop a method that tracked the state of cells and of the cellular environment within alginate constructs during perfusion studies in which the perfusing medium DO concentrations were changed over time or cells were exposed to a cytotoxic antibiotic. Due to challenges in acquiring DO concentration gradient information within beads, a second aim was to develop a mathematical model that would calculate gradients from experimentally acquired volume averaged DO concentrations; thus, significantly enhancing the robustness of tracking the alginate beads. Lastly, since the PFC emulsions used in the study may affect cell viability and function, a third aim was to characterize, experimentally and via modeling, the effect of several PFC emulsion concentrations on the encapsulated βTC-tet cells. The thesis chapters are organized by the order in which they were published (CHAPTERS 3 and 4) and by the order in which they were performed (CHAPTERS 5 and 6).

Previous studies have shown that the DO concentration can be monitored using ^{19}F NMR when PFC emulsions are employed. Specifically, the inverse of the T_1 relaxation time of specific perfluorinated chemical groups directly correlate with the DO

concentration surrounding the emulsion [19, 20]. Given that ^{19}F is the second most sensitive nucleus after ^{1}H and that there is no significant amount of ^{19}F normally present in tissues, ^{19}F NMR spectroscopy is particularly suitable for monitoring constructs in NMR-compatible bioreactors and *in vivo*. Additional background material is provided in CHAPTER 2 of this thesis.

An encapsulated cell system was utilized to establish the methodology described in this thesis. The pancreatic substitute consisted of βTC-tet cells (a mouse insulinoma cell line) encapsulated into alginate beads. Despite extensive characterization by our group, this substitute presented many challenges within this thesis, as the use of continuous cell lines causes substantial remodeling within the construct [21, 22]. This redistribution of cells creates a continuously changing DO concentration profile and would therefore require one, two, or three dimensional chemical shift imaging of the construct, to reconstruct such profiles. However, if intra-construct oxygen profiles are to be acquired using ^{19}F chemical shift imaging, long acquisition times would be required, which are a caveat to *in vivo* applications due to the lengthy anesthesia times required of experimental animals. In contrast, collecting signal from the entire tissue construct is a more rapid process; thus, a quantitative mathematical model was created that describes the cellular remodeling and changes in DO concentration profiles when proliferative cells are encapsulated in hydrogel beads (CHAPTER 3). The model uses parameters based on a permissive material, which does not directly influence cell growth and in which remodeling of the cell distribution occurs only from interplay between DO concentrations and spatial constraints. Simulated changes of the oxygen and cellular profiles with time are first presented and the latter is compared with previously obtained experimental

results, offering a preliminary validation. The model was then used in a reverse fashion to decipher cell and oxygen distributions from measurements of the average intrabead DO concentration – the same measurement that would be acquired by ^{19}F NMR averaged over a pancreatic substitute.

The use of a mathematical model and ^{19}F NMR to monitor alginate encapsulated cells first required the development of several technologies. The system required: (1) the design and construction of an *in vitro* perfusion circuit and bioreactor, (2) the selection of a suitable PFC that could be made into an emulsion, and (3) the generation of a calibration curve relating the inverse T_1 relaxations of the PFC emulsion to the DO concentration.

In brief, the computer controlled NMR-compatible perfusion bioreactor and circuit was designed and built (fully described in section 4.3.2 of the thesis and illustrated in Figure 4.1) according to the following criteria: (1) the system had to fit on a cart so that it could be brought in and out of an NMR room, i.e. maximum portability; (2) constant temperature (37°C) had to be sustained for the media entering the bioreactor; (3) media oxygenation had to remain constant going into the bioreactor and be capable of being changed at will by the operator to desired concentrations; (4) the system had to be capable of sustaining nutrient concentrations; (5) the system had to be capable of delivering alternative test media to the bioreactor when desired, and (6) the system had to remain aseptic.

Several PFC emulsions have been reported in the literature for use as an oxygen sensor [19, 20, 23-29]. In this thesis, the PFC perfluorotributylamine (PFTBA), was chosen since it is reportedly non-toxic [30, 31] and the T_1 relaxation is highly sensitive to

changes in surrounding DO concentrations [20]. Using the NMR-compatible perfusion system, a calibration curve was created for alginate encapsulated PFTBA emulsion (CHAPTER 4), allowing the assessment of DO concentrations within pancreatic substitutes. APPENDIX I of the thesis provides additional characterization studies of the PFTBA emulsion – e.g., distribution within alginate beads, leak from the beads, effect on βTC-tet cells at low concentrations, and the rate at which T_1 relaxations change in response to changes in DO concentrations.

With the capacity to assess intrabead DO concentrations, we next investigated the ability to track a pancreatic substitute by combining experimental measurements with mathematical modeling of the construct. Encapsulated βTC-tet cells were propagated in the above described NMR-compatible perfusion bioreactor and subjected to DO concentration step changes over the course of 50 hours. The overall cellular metabolic activity was monitored by the oxygen consumption rate (OCR) of the culture and by the level of intracellular nucleotide triphosphates (NTP), measured by ^{31}P NMR spectroscopy. The cellular oxygenation state was monitored by measuring the average intrabead DO concentration (AIDO) as a function of time by ^{19}F NMR. To test the validity of the model, the mathematical model was then used to predict the viable cell number and cellular oxygenation state when subjected to the same external DO concentrations measured experimentally. In the mathematical calculations, the model inputs were the intrinsic parameters for βTC-tet cells in alginate beads (CHAPTER 3) and the measured external DO concentration during the experiment. The model output was the time-dependent cell and DO distributions, from which the total viable cell number and a volume-average intrabead DO were calculated and compared against

experimental results. It was found that the mechanistic model of the encapsulated system was in general agreement with the experimentally acquired data, thus providing model validation.

Upon the implantation of tissue substitutes, such as the artificial pancreas described above, two types of immune reactions may compromise the function and viability of the implant due to biocompatibility issues. A non-specific host response can cause a dense fibrotic layer to form around the construct, severely limiting the transport of oxygen to the cells and, as mentioned previously, causing malfunction or death of the implant. In the second type of response, cytokines are released at the site of implantation, causing cell death within the substitute. To determine the utility of the mathematical model/^{19}F NMR system in distinguishing between these *in vivo* scenarios, these two conditions were mimicked *in vitro* (CHAPTER 5). First, the ability of the mathematical model and ^{19}F NMR to track cell growth in alginate beads that were cultured for one week prior to being placed in the NMR-compatible perfusion system and then subjected to DO concentration step changes is evaluated. This initial study is designed to reproduce monitoring that may occur during *in vivo* experiments, where parameters influencing cell function and viability are not continuously monitored and the DO concentration can vary widely from day to day. The second study monitors cell death as would occur via a cytotoxic immune response. Specifically, the AIDO and medium DO concentration are used to assess the cell density within alginate beads after the addition of puromycin, a toxic antibiotic.

Since the goal of the system developed in this thesis is to monitor constructs *in vivo*, the ability to measure the DO concentrations in an animal model was demonstrated

in CHAPTER 4. It should be noted that several investigators have demonstrated the ability to measure DO concentrations from PFC-loaded alginate beads *in vivo* [24, 32]. However, the mathematical model developed in this thesis requires a measurement of both the AIDO and the external DO concentrations; therefore, in CHAPTER 4, a novel dual PFC system is used to simultaneously monitor the DO concentrations in two distinct bead populations implanted in the peritoneal cavity of mice. Specifically, the method involved placing PFTBA and a second PFC emulsion, perfluoro-15-crown-5-ether (PFCE), whose chemical shifts are only separated by 9 ppm, into two types of beads, allowing for simultaneous T_1 relaxation measurements. The beads containing the PFTBA emulsion were coated with PLL, while no additional coating was placed on beads containing PFCE. The beads coated with PLL elicited a strong inflammatory response, thus causing a statistically lower DO concentration measurement within these beads.

Lastly, the use of PFC emulsions in tissue engineered constructs and the culturing of cells has gained considerable interest among researchers recently [33-42]. As mentioned above, the DO concentrations within tissue engineered constructs, combined with the inherently low solubility of oxygen in water, often limit the number of cells that can be supported within a substitute. Hence, any method that can enhance the solubility of oxygen or increase its effective diffusivity into a construct is desirable. PFC emulsions accomplish both of these objectives, as the solubility of oxygen is 15-20 fold higher in PFC emulsions than water [35] and the effective diffusivity is also increased by their presence [38]. However, since these emulsions are in constant equilibrium with the surrounding aqueous phase, which is determined by the partition coefficient, it would seem that the benefit is only transient and that, at steady-state, the only benefit would be

due to the increased diffusivity of oxygen. To explore this issue in greater detail, the mathematical model developed in CHAPTER 3 was augmented to account for the presence of PFC emulsion (CHAPTER 6). The model was first used to simulate the proliferation of βTC-tet cells encapsulated in alginate under incubator-type conditions with and without PFC emulsion. To provide validation, these simulations were compared to experimentally acquired data of the same system. Finally, the model was used to simulate the effect of having the PFC emulsion under changing DO concentrations, as is often observed upon implantation of constructs and due to naturally occurring fluctuations [24, 43].

Utilization of the combined mathematical model and ^{19}F NMR system to monitor the DO concentration within a pancreatic substitute and to assess cell viability and function are discussed further in CHAPTER 7. Direction for future research based on this method is also given.

Finally, I had the opportunity to participate in the two year NSF-sponsored IGERT Technological Innovation Generating Economic Results (TI:GER) program that spanned across Georgia Institute of Technology and Emory University. The program brought together Ph.D. candidates and M.B.A. students from Georgia Tech with two J.D. students from Emory University to learn about commercializing research. During the two years, my team developed a commercialization and business plan around a technology aimed at assessing the quality of islets destined for implantation. In APPENDIX II, the executive summary from the business plan is given, as well as a description of the technology that I helped develop.

CHAPTER 2

BACKGROUND

2.1 Diabetes

Diabetes is now one of the fastest growing diseases and leading cause of both morbidity and mortality worldwide. In the United States alone, 18 million people are afflicted with either Type 1 or Type 2 diabetes. The disease is characterized by the inability to maintain normal blood glucose levels, which causes major secondary health complications. Type 1 diabetes, which accounts for approximately two million of those affected, is an autoimmune disease that has been growing at a rate of 7.2% each year (i.e. 130,000 new cases per year). In this disease, the immune system attacks and kills all the insulin-producing β cells within the pancreas and without the ability to produce insulin, blood glucose levels cannot be sustained in the physiological range. Such an inability to regulate blood glucose levels causes major complications, and even death [44]. Currently, there is no cure for diabetes, only various treatment options.

2.2 Current and Future Therapies

The most common treatments for Type 1 diabetes are multiple daily injections of insulin and insulin pumps. Monitoring blood glucose levels combined with daily insulin injections provides patients with a near normal life. Still, bolus insulin injections fail to provide the minute-to-minute maintenance of normoglycemia that a pancreas or pancreatic substitute provides and long-term complications therefore arise. Some of these complications of include: nephropathy, retinopathy, problems with circulation, and

neuropathy. A study performed in the early 1990s showed that most of these complications are mitigated with tighter glucose control [2]. Thus, researchers have focused efforts on developing cell-based pancreatic substitutes capable of providing more physiologic control. One such procedure, the implantation of naked islets – cell clusters in the pancreas that produce insulin and control blood sugar – has shown promising results as a pancreatic substitute. However, several major limitations of implanting naked islets or whole pancreases currently exist, such as the need for chronic immunosuppressive drug therapy and islet donor availability (islets must be harvested from cadavers [45]). Therefore, such therapies are usually reserved for patients that are incapable of controlling blood glucose with exogenous insulin and have end-stage renal disease. Issues of donor availability could be minimized by the use of xenogeneic islets, but the ability to keep the animals disease free is a daunting task with many complications.

2.3 Tissue Engineered Pancreatic Substitutes

An alternative to islet or whole pancreas transplantation is the use of a tissue engineered pancreatic substitute. The field of tissue engineering is devoted to designing and creating biological substitutes that replace or repair a function in the body. In the realm of diabetes, this translates to the engineering of a pancreatic substitute, which typically consists of insulin secreting cells encapsulated in a biomaterial. The use of biocompatible materials for cell encapsulation circumvents the need for heavy immunosuppressive drugs by acting as a barrier, giving the sequestered cells partial immunoprotection. Since vital cell nutrients like glucose and oxygen, as well as insulin

are much smaller molecules than most immune response elements, the biomaterial does not impose a permeability barrier to these molecules, thus allowing the encapsulated cells to sense the surrounding glucose levels and respond with insulin secretion accordingly [46-48].

Lim and Sun developed one of the most widely used encapsulation techniques in 1980 [48], involving the encapsulation of cells in a three-layered biomaterial. By dispensing droplets of the alginate-cell suspension into calcium chloride, the previously uncross-linked alginate solution gels. This cross-linking of the alginate solution sequesters the cells in a spherical alginate bead. To give the construct greater mechanical strength, and to establish a semi-permeable coating, a layer of poly-l-lysine is used to cover the alginate bead [49, 50]. A final layer of alginate is then formed around the bead to maintain biocompatibility.

Alginate is a polymer found abundantly in nature and is composed of mannuronic acid and guluronic acid (Figure 2.1). Through manipulation of the ratio of mannuronic acid to guluronic acid, the sequential order of the residues, and the molecular weight, the overall physical characteristics and properties of alginate gels can be changed. For example, alginates containing larger amounts of mannuronic acid are softer, have faster degradation times, and are less porous when compared to alginate beads containing larger amounts of guluronic acid residues [46, 47, 51]. The effects of alginate composition have also been linked to growth characteristics of encapsulated cells, as well as the overall metabolic and secretory attributes of the cells. These studies demonstrated that high guluronic acid content transiently hinders metabolic and secretory activity of βTC3 cells, a mouse insulinoma cell line, due to growth inhibition. Conversely, a larger amount of

mannuronic acid allows an increase in the overall metabolic and secretory activity because of rapid cellular growth within the construct [51]. Given the ability of cells to grow uninhibited within the high-mannuronic acid alginates, these alginates are often referred to as permissive matrices.

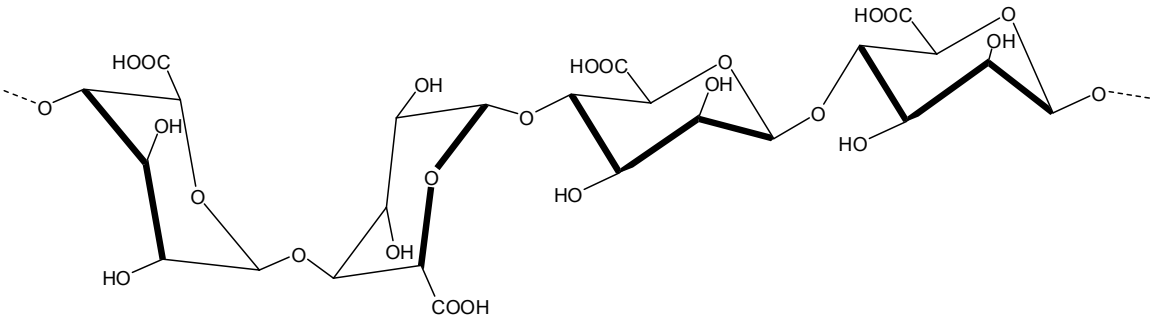

Figure 2.1 Molecular structure of an alginate fragment – (--L-GulA-α-1,4-L-GulA-α-1,4-D-ManA-β-1,4-D-ManA-β-1,4--)

2.4 Insulin-secreting Cells

There have been several cell sources studied for their use as pancreatic substitutes. In general, sources included harvested islet cells of Langerhans, differentiated stem/progenitor cells, transformed β cells, and genetically engineered non-β cells, each of which has their own advantages and disadvantages. Despite a much more physiologic insulin release profile from harvested islet cells, islets have several caveats that impede their use as pancreatic substitutes. For example, islets cannot be expanded in tissue culture and when one considers that allogeneic islets only account for 1-2% of a pancreas and that two or more cadavers are needed for one transplant, the scale-up to widespread clinical use of islets as pancreatic substitutes seems impracticable. Attractive renewable sources of insulin secreting cells are differentiated embryonic or adult stem

cells. The differentiation of both human and mouse embryonic and adult stem cells into β-like cells has been demonstrated [52-54]. However, several significant challenges currently impede the use of stem cells, including: low insulin content of differentiated adult cells, the chance of growing a teratoma upon *in vivo* implantation, as well as ethical issues involved with embryonic stem cells, to name a few. Transformed β cells alleviate the issue of cell source availability since such cells can be expanded in cell culture. However, the disadvantage of transformed β cells is that many have sub-optimal insulin secretion characteristics, i.e. the cells are hypersensitive to glucose and continuously secrete insulin when glucose is in the normal physiologic range [55]. This increased sensitivity of the transformed β cells to surrounding glucose may lead to hypoglycemia, a serious condition that can lead to coma or death. Genetically engineered cells that have transcriptionally controlled insulin release are often significantly slower at releasing insulin than islets [56-58]. Thus, a thorough characterization of any β cell line is needed before the cell line is used clinically.

The development of continuous β cell lines has been led by the laboratory of Dr. Shimon Efrat [55, 59-61]. A library of these β cells was created by expressing the simian virus 40 tumor antigen gene under the control of the insulin promoter in transgenic mice [60]. One of the early β tumor cell (βTC) lines, βTC3, has been well characterized in terms of bioenergetics and the metabolic and secretory properties both in monolayer and in calcium alginate-polylysine-alginate (APA) beads by our group [16, 62-66]. The reduced oxygen requirements needed to maintain βTC cell function is an additional benefit. However, due to the hypersensitivity of these cells to glucose, βTC3s would not be suitable for an implanted pancreatic substitute, as hypoglycemic events would occur.

A more recent cell line that has emerged from Dr. Efrat's laboratory is βTC-tet cells [67]. βTC-tet cells are closely related to βTC3 cells, but exhibit a growth control mechanism. Specifically, the growth of these cells is controlled by a well-known tetracycline operon system. In this system, βTC-tet cell proliferation is halted by exposure to tetracycline; when the tetracycline is removed, the cells regain their ability to divide. The insulin secretion characteristics of βTC-tet cells have been reported to be closer to those of islets, making them an appealing cell source [61, 68]. Additionally, βTC-tet cells encapsulated in alginate were shown to restore normoglycemia in non-obese diabetic mice for up to 8 weeks without inducing an inflammatory response [69]. Given the scale-up capability of continuous cell lines, these cells have become an attractive alternative to islet transplantation. However, as mentioned above, there are some key attributes of these cell systems that must be fully understood if they are to be of therapeutic use.

2.5 Perfluorocarbons (PFCs)

Due to their ability to dissolve large amounts of gases and their general chemical and biologic inertness, perfluorinated carbons have been used in a variety of medical applications, as well as tissue engineering. These hydrophobic organic compounds gained the interest of the medical community in 1966 when Clark and Gollan demonstrated that a mouse submerged in such a PFC liquid could sustain life [70]. Since then, PFCs have been combined with emulsifying agents and investigated for use as blood substitutes, oxygen reservoirs, and as a tool for monitoring oxygen concentrations non-invasively by ^{19}F nuclear magnetic resonance (NMR) [36, 37, 41, 71, 72]. However,

prior to use in any medical application, careful consideration must be given to the type of PFC, the emulsifying agent, stability, droplet size, and aseptic preparation.

A number of types of PFC molecules have been characterized as blood substitutes and as NMR imaging agents, since the early 1980s [23, 28, 29, 71, 73-81]. Fluosol-DA (combination of perfluorodecalin and perfluorotripropylamine), perfluorooctylbromide (PFOB), perfluoro-15-crown-5-ether (PFCE), perfluorotributylamine (PFTBA), and perfluorohexane (PFH) are just a few that have been reported in the literature. Of these, PFTBA and PFCE were chosen for use in this thesis. PFTBA has been used as an oxygen carrier with no reports of adverse effects in cells [31]. Additionally, the relatively high sensitivity of PFTBA to oxygen (discussed in section 2.5.2) [20] made it a clear choice. In this thesis, PFCE is used as a second PFC in the development of a dual-PFC system, enabling monitoring of oxygen concentrations within two constructs simultaneously. PFCE was chosen primarily because its chemical shift is close to that of PFTBA (enabling simultaneous T_1 relaxation measurements) and secondly, because it has a high signal-to-noise ratio (the 20 fluorine atoms of PFCE all resonate at a single frequency [74]).

As mentioned previously, PFCs must be emulsified due to the hydrophobic nature of the molecules. During emulsification, an amphiphilic molecule is used at the interface between the PFC phase and the surrounding aqueous phase, which is diagramed in Figure 2.2. An emulsion droplet size of approximately 0.2 μm is typically created by either sonication or high pressure homogenization. In medical applications, the choice of an emulsifying agent (surfactant) is based on biocompatibility and stability. Surfactants that have been commonly used in blood substitutes include Pluronic-68, egg yolk lecithin

(phosphotidylcholine), and triglycerides [75, 82]. In this thesis, egg yolk lecithin was chosen because it has been shown to create micelles that are very stable (little change in emulsion diameter over 80 days at 37°C) [83], and it does not cause immune complement activation [30, 31].

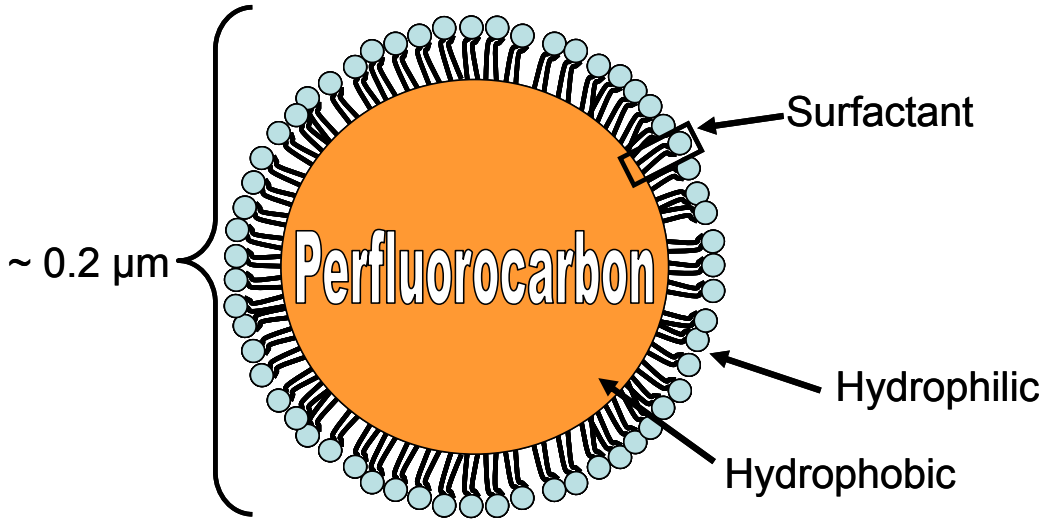

Figure 2.2 Diagram of a perfluorocarbon micelle.

2.5.1 PFCs as Oxygen Reservoirs

PFC emulsions are known to have an oxygen solubility that is 15-20 fold higher than that of water [35]. An example of this capacity is shown in Table 2.1, where the solubilities of oxygen and carbon dioxide are given for PFTBA and PFOB, along with that of water. Also, the amount of oxygen dissolved in the PFC is linearly related to the partial pressure of oxygen in the surrounding medium. This inherent high solubility of oxygen in PFC emulsions has led several research groups to study the effect of incorporating these emulsions into medium – static and perfused – and sequestering the emulsion directly into tissue engineered substitutes [33, 38, 42, 84]. In 1988, the use of

PFC in organ preservation (specifically, pancreas preservation) was demonstrated as a component of the two-layer method by Kuroda et al. [85]. During this study, the pancreas was suspended between a layer of PFC and Euro-Collins' solution, which was later replaced by University of Washington (UW) solution. The PFC-UW two-layer method (TLM) increased the preservation of canine pancreata from up to 24 hours to up to 96 hours [86]. Additionally, the use of PFCs has been shown to improve survival of pancreata after transplantation and to increase the yield of purified islets [37, 40]. Further characterization of the effect of PFCs on cultured islets indicated that despite having significant benefit in transportation, islet stimulated insulin secretion was compromised by the TLM [87]. However, Brandhorst et al. [88] determined that preserving islets by a one-layer method (PFC-only) had no detrimental effect on stimulated insulin secretion. Thus, it is essential that a full characterization of the effect of PFCs on the function of cells be performed prior to implementation in any tissue engineered device.

Table 2.1 Solubility of oxygen and carbon dioxide in water and two PFCs at 1 atm and 37°C. In parentheses, the fold increase in solubility above water is given.

Liquid	Oxygen	Carbon Dioxide
Water	0.21 mM	5.44 mM
Perfluorotributylamine (PFTBA)	3.36 mM (16x)	11.7 mM (2.2x)
Perfluorooctylbromide (PFOB)	4.2 mM (20x)	17.7 mM (3.2x)

In the context of tissue engineered substitutes, PFCs have been used to increase DO concentrations within constructs and in perfused bioreactors. Specifically, Radisic et al. [38] demonstrated through experimentation and a mathematical model that adding the commercially available PFC emulsion, Oxygent, to medium perfusing a parallel plate cardiac bioreactor, increases the DO concentration throughout the bioreactor and consequently supports a greater density of cardiomyocytes. In these studies, the oxygen partial pressure of the medium entering the bioreactor was kept constant at 160 Torr; hence, after releasing the oxygen within the bioreactor, PFCs were reloaded in the gas exchanger. In a study by Khattak et al. [33], the presence of sequestered PFC emulsions in alginate capsules caused an enhanced proliferation of HepG2 cells compared to beads without PFC over two weeks. Additionally, improved metabolic activity of the HepG2 cells was demonstrated at the physiologically relevant DO concentration of 5% oxygen (0.04 mM). Although these results are promising, the mechanism for such increased viability and metabolic activity remains unclear, as PFC sequestered within an encapsulated cell system are unable to be reoxygenated after equilibration with the surrounding aqueous phase. However, if the surrounding DO concentration were cycled to higher levels (which did not occur in the studies by Khattak et al), the PFC emulsions would indeed be capable of being reoxygenated and therefore maintain a higher DO concentration within the encapsulated cell system.

2.5.2 PFCs as Oxygen Monitors

PFC emulsions are ideal for non-invasively monitoring DO concentrations *in vivo* by ^{19}F NMR since (1) the inverse T_1 relaxation rates of the fluorines are linearly correlated to the surrounding DO concentration; (2) Fluorine is not found in natural

abundance in the body; and, (3) the ^{19}F nucleus is the second most sensitive nucleus with a sensitivity 0.83 times that of ^{1}H.

The T_1, or spin-lattice, relaxation rate is an NMR parameter that is defined by the time it takes nuclear spin to be restored to 63% of the original magnitude (M_0) after being placed into disequilibrium by a radio-frequency pulse, see Figure 2.3. This rate is directly influenced by the environment around the nuclei. Thus, oxygen, a paramagnetic molecule, in the surrounding environment shortens the relaxation rate of ^{19}F. Figure 2.4 shows one of the early calibration curves for a PFC emulsion (Fluosol-DA) which was developed by Reid et al. [19].

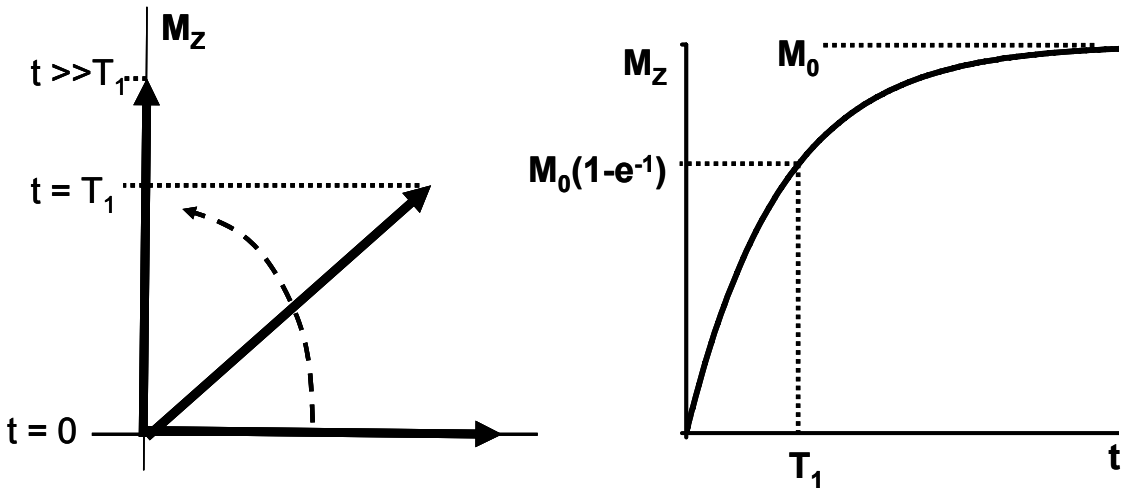

Figure 2.3 An illustrative representation of a T_1 relaxation, where M_Z is the direction of the applied magnetic field along the z-axis and M_0 is the net macroscopic magnetization of nuclear spins.

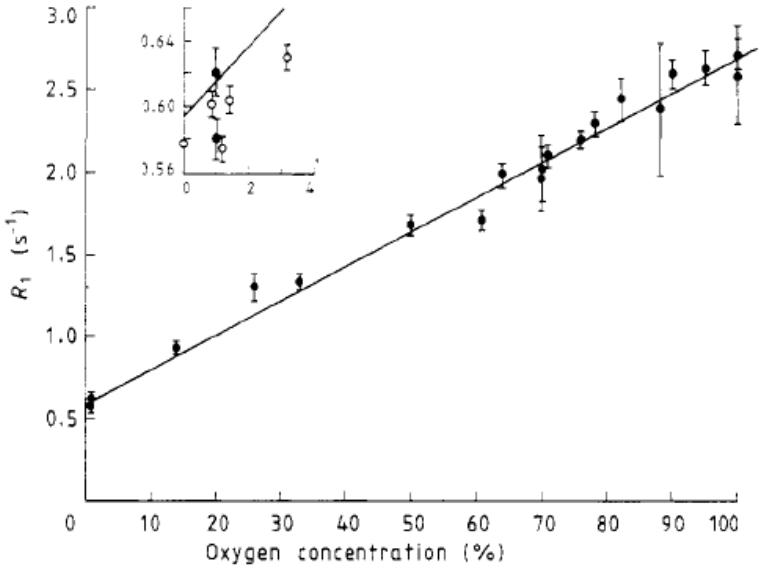

Figure 2.4 Calibration curve relating the R_1 ($1/T_1$) of Fluosol-DA to the surrounding oxygen concentration (adapted from Reid et al. [19])

^{19}F NMR has been used extensively in the evaluation of tumor oxygenation [25, 89-93], since knowing the oxygen tension within tumors is an important parameter during radiotherapy treatments [94, 95]. In these experiments, investigators inject a PFC emulsion intravascularly, which subsequently circulates into perfused regions of tumors. ^{19}F NMR imaging of the tumor is then performed, thus quantifying the mean oxygen tensions at various locations within the tumor. More recently, the use of PFCs as molecular imaging agents has been explored [96-100]. Specifically, the surfactant is functionalized for molecular imaging by the addition of homing ligands, such as those used in a study by Lanza et al. [99]. Since then, paramagnetic chelates, such as gadolinium, have also been attached to the PFC emulsions, creating enhanced NMR imaging contrast [96].

The immobilization of PFCs into alginate beads to measure oxygen tensions at various locations within the human body has also been demonstrated [24, 32]. In the study by Noth et al. [24], perfluorobutyl-ethylene (F-44E) was encapsulated into cell-free barium alginate capsules at a concentration of 50% v/v. The capsules were then implanted into the peritoneal cavity, the *musculus quadriceps femoris*, and beneath the kidney capsule of rats. The DO concentrations at these sites were capable of being quantified by ^{19}F NMR for over three months. It should be noted that the peritoneal cavity and the kidney capsule were found to have the lowest oxygen concentrations. In addition, the greatest variability and range were observed in the peritoneal cavity (14±9% air saturation). This study by Noth et al. was significant as it demonstrated the range of DO concentrations that an implanted tissue substitute may experience; however, knowledge of intra-construct sharp oxygen gradients that are created by cellular oxygen

consumption are also expected to have a significant impact in dictating the functionality of the encapsulated cells, in addition to the DO concentration surrounding such implants.

Pilatus et al. [101] and McGovern et al. [102] demonstrated the utility of ^{19}F NMR in measuring oxygen consumption rates of encapsulated cells. Specifically, McGovern et al. [102] encapsulated a PFC emulsion into alginate gels that contained EMT6/Ro murine tumor cells and used DO concentration measurements to determine oxygen consumption rates of cells. However, the technique was limited to a system in which cell distribution was homogeneous and thus was unable to account for the well documented cellular remodeling that typically occurs in such systems [103]. Conversely, Pilatus et al. [101] placed cell-free alginate beads containing a PFC emulsion at both the inlet and outlet of a bioreactor to acquire oxygen consumption rates of both breast and prostate cancer cells by ^{19}F NMR. However, such a technique is limited to quantifying oxygen consumption rates only in an *in vitro* system, where other methods exist to quantify such rates more accurately (e.g. fiber-optic DO sensors). Thus, neither the technique by McGovern et al. or Pilatus et al. is capable of assessing the DO concentration experienced by implanted cells at various locales within constructs *in vivo*, which is of significance in the overall function of encapsulated cell systems.

2.6 Alternative Methods for Monitoring Oxygen

As mentioned previously, the importance of oxygen availability to cellular growth and function has been demonstrated for many cell systems, including the sequestered cells in APA beads. There are several techniques that can be used to monitor oxygen levels available to cells, some of which are given below.

2.6.1 Polarographic Probes

Polarographic probes have been used to monitor oxygen concentrations within cell culture systems *in vitro* and within tissues *in vivo* [8, 9, 16, 94, 95, 104, 105]. These sensors rely upon DO reacting with the silver cathode, resulting in an ion flux to the silver or lead anode and this ion flux (current) measured by the probe is proportional to the surrounding oxygen tension. The reaction of DO with the silver cathode consumes small quantities of oxygen during the process; thus, DO gradients may develop at the tip of polarographic probes, which subsequently results in erroneous measurements. The invasiveness of polarographic sensors and their need for frequent calibration are additional obstacles to their use *in vivo*.

2.6.2 Fiber Optic Probes

Similar to polarographic probes, these probes represent an invasive method of measuring dissolved oxygen. The long-term stability of the probe calibration is an improvement over the polarographic probes. Additionally, these probes do not consume oxygen, rather, they rely upon fluorescence quenching of a sequestered material at the tip of the probe. A spectrometer at the base of the probe correlates the amount of quenching with the oxygen tension surrounding the probe using the Stern-Volmer equation [106], shown here:

$$\frac{I_O}{I} = 1 + k \cdot [pO_2]$$

Where, I_o is the fluorescence intensity when no oxygen is present, I is the fluorescence intensity at a given oxygen tension, k is a constant inherent to the fluorescent material, and $[pO_2]$ is the surrounding oxygen tension.

2.6.3 Near-Infrared Spectroscopy (NIRS)

This non-invasive technique is currently used clinically to monitor dissolved oxygen. The method relies on a molecule, such as hemoglobin or myoglobin, to absorb the light emitted into the tissue. Despite being a non-invasive technique, the penetration depth of this method is at maximum 2-6 cm [107]; thus, for this method to be used in monitoring implanted pancreatic substitutes a probe placed inside the peritoneal cavity would be needed, making the technique invasive.

2.6.4 ^{17}O NMR

^{17}O NMR has recently been used to study oxygen concentrations within a human brain [108]. Despite the ability to measure oxygen non-invasively, this method suffers from a lack of sensitivity. In addition, inhalation of gaseous ^{17}O is required for the technique to work, as ^{17}O is not found naturally in the body.

2.6.5 Electron Paramagnetic Resonance

Electron paramagnetic resonance (EPR) is a relatively non-invasive method of measuring DO concentrations within tissues. For example, oxygenation within the brain and tumors has been demonstrated by this technique [109, 110]. However, it has two significant caveats: (1) it requires the injection of a paramagnetic oxygen-sensitive material, prior to being monitored; and, (2) significant heating of the material is a problem and therefore is restricted to small tissue sizes.

2.7 Nuclear Magnetic Resonance

In the realm of non-invasive monitoring, NMR is a potent tool that can track and image tissue engineered constructs *in vivo* and *in vitro*. This is accomplished by aligning

nuclei that have a spin greater than zero with a powerful external magnetic field. The alignment is then perturbed using an electromagnetic field pulse. The resulting response of the nuclei to the external perturbation is the phenomenon that is exploited in NMR spectroscopy and imaging. Specifically, after nuclei are perturbed – i.e. forced to a higher energy state – the nuclei will spin back to equilibrium, which creates radio frequency signals that can be detected by a receiver coil. This spin back to equilibrium, known as relaxation, comes in two forms: T_1 and T_2. Using this method, a wealth of information can be obtained about living systems. Specifically, through monitoring of various nuclei, the intracellular metabolite fluxes (^{13}C), the bioenergetics (^{31}P), and viable cell number and distribution (^{1}H) (to name a few) can all be ascertained.

Due to the strong sensitivity of the ^{1}H nuclei, ^{1}H NMR has been used broadly in both imaging and spectroscopy. Images are acquired by placing gradients within the bore of an NMR magnet. ^{1}H NMR imaging has been used to study the structural integrity of tissue engineered constructs and more specifically, it has recently been used to acquire detailed information on alginate and agarose encapsulation systems [111, 112]. The NMR techniques used by Simpson et al. [111] demonstrated the ability to quantify the guluronic acid content, as well as several other characteristics of alginate beads. Additional studies using ^{1}H NMR spectroscopy, have demonstrated the ability to accurately assess the viable cell number within agarose disk-shaped constructs, *in vitro* and *in vivo* [112, 113]. To accomplish this, localized, water-suppressed ^{1}H spectroscopy of the total-choline peak – a peak comprised of choline-related metabolites – was directly correlated to the number of viable cells within a disk-shaped pancreatic substitute.

^{31}P NMR spectroscopy has proven to be a robust tool in determining total concentrations of intracellular metabolites, specifically, nucleotide triphosphates, inorganic phosphates, and phosphoesters, to name a few. These intracellular metabolites become increasingly important in the studies of insulin secreting cell lines since ATP and ADP are directly involved in the glucose-stimulated insulin secretion of these cells [114]. Research from our laboratory has used ^{31}P NMR spectroscopy to study the effects of nutrients, such as oxygen and glucose levels on alginate encapsulated βTC3 cells [9, 15, 16]. In these studies, alginate beads were placed into an NMR-compatible perfusion system and monitored constantly for 38 days [9, 16]. The DO concentration entering the bioreactor was reduced to hypoxic levels at various points throughout the experiment for 3-4 days. It was found that decreasing the DO concentration in the surrounding medium drove encapsulated cells to a more anaerobic glycolytic metabolism, increased glucose consumption rates, and reduced the rates of oxygen consumption and insulin secretion. Upon re-oxygenation, all parameters returned to their prehypoxic levels. Shorter term hypoxic studies (24 hr) revealed that a decrease in ATP and an increase in glucose consumption rate correlated positively to hypoxic environments, regardless of the amount of cellular remodeling that took place within the alginate beads [15]. However, glucose-induced insulin secretion was suppressed by short-term hypoxia only after beads were perfused for 10 days. This was attributed to changes in cell number and distribution within the pancreatic substitutes, which resulted in lower average oxygenation of cells relative to the fresh capsules.

CHAPTER 3

MODELING OF ENCAPSULATED CELL SYSTEMS[1]

3.1 Abstract

Tissue engineered substitutes consisting of cells in biocompatible materials undergo remodeling with time as a result of cell growth and death processes. With inert matrices that do not directly influence cell growth, remodeling is driven mainly by the concentration of dissolved oxygen (DO). Insulin-secreting cell lines encapsulated in alginate-based beads and used as a pancreatic substitute represent such a case. Beads undergo remodeling with time so that an initially homogeneous distribution of cells is eventually replaced by a dense peripheral ring of primarily viable cells, whereas inner cells are mostly necrotic. This paper develops and analyzes a mathematical model of an encapsulated cell system of spherical geometry that tracks the viable and dead cell densities and the concentration of DO within the construct as functions of radial position and time. Model simulations are compared with experimental histology data on cell distribution. Correlations are then developed between the average intrabead DO concentration (AIDO) and the total viable cell number, as well as between AIDO and the radial cell and DO distributions in beads. As AIDO can be measured experimentally by incorporating a perfluorocarbon emulsion in the beads and acquiring ^{19}F nuclear magnetic resonance (NMR) spectroscopic data, these correlations can be used to track the

---

[1] Modification of a paper published in **Journal of Theoretical Biology**, 244(3): 500-510 (2006).

remodeling that occurs in the construct *in vitro* and potentially *in vivo*. The usefulness of mathematical models in describing the dynamic changes that occur in tissue constructs with time, and the value of these models at obtaining additional information on the system when used interactively with experimental measurements, are discussed.

3.2 Introduction

The engineering of living tissues, or tissue engineering, involves the use of living cells, manipulated through their extracellular environment or genetically, to develop biological substitutes for implantation into the body and/or to foster the remodeling of tissue in some other active manner [115]. Tissue substitutes often consist of cells in hydrogel materials, such as collagen, agarose, or calcium alginate, in appropriate three-dimensional configurations that enable cell and construct function and permit handling of the substitute for *in vitro* manipulations and *in vivo* implantation. Substitutes may undergo significant remodeling with time, especially when the cells can proliferate in the matrix environment. Remodeling occurs as a result of cell growth and death processes and does not necessarily involve cell migration within the matrix [21, 22, 116]. The matrix itself may directly affect the cellular growth kinetics and the type of remodeling that occur, as is the case with proliferative βTC mouse insulinomas encapsulated in calcium alginate/ poly-L-lysine/ alginate (APA) beads made using high guluronic alginate [21, 116]. Although plausible explanations for the observed effects have been proposed, the precise mechanism remains unclear. On the other hand, with permissive matrices which do not inhibit cell growth, there exists ample experimental evidence that cellular reorganization is driven by the concentration of available oxygen. For example,

βTC insulinomas encapsulated and homogeneously distributed in APA beads made with permissive high manuronic alginate, form, after a period of 14-16 days, a dense peripheral ring of mainly viable cells, whereas inner cells are mostly necrotic [116]. This type of remodeling occurs because, as cells at the bead periphery - where oxygen is more abundant - grow, oxygen gradients across the bead radius become steeper, hence inner cells are exposed to increasingly hypoxic conditions and eventually die.

To directly monitor the dynamic changes that occur in tissue constructs with time, *in vitro* and post-implantation *in vivo*, our group has been developing methods based on nuclear magnetic resonance (NMR) imaging and spectroscopy. While NMR imaging allows the assessment of structural features of the construct, localized NMR spectroscopy enables the evaluation of the number of viable cells and of the cellular metabolic state in a volume of interest (VOI) contained within the construct [113, 117-121]. For instance, the resonance of total cellular choline, measured by water-suppressed ^{1}H NMR spectroscopy, correlates positively and linearly with the viable cell number, hence it is a reliable estimate of the latter [113, 121, 122]. The resonances of intracellular metabolites measured by ^{31}P NMR, which include nucleotide triphosphates and phosphorylcholine, offer an assessment of the cellular bioenergetic status [119, 123].

Due to the sensitivity of the ^{1}H nucleus, ^{1}H NMR spectroscopy can be performed both *in vitro* and *in vivo*. On the other hand, ^{31}P NMR spectra have, thus far, been obtained from tissue engineered constructs only *in vitro* [113, 118-121, 123]. To indirectly assess the cellular metabolic state, one could alternatively use measurements of dissolved oxygen (DO) concentration within the construct. Indeed, DO is a critical parameter determining many aspects of cell function, including viability, metabolism and

protein secretion [5, 8, 9, 18, 124-126]. Given this importance of oxygen, our laboratory, as well as others [102, 127], are developing NMR–based methods to measure DO concentration in tissue constructs by incorporating a perfluorocarbon emulsion in the hydrogel. Using the linear correlation between DO concentration and the inverse of the T_1 relaxation of ^{19}F [102, 127] the average oxygen concentration in a VOI can be measured. It should be noted that ^{19}F is the second most sensitive nucleus after ^{1}H and there is no significant amount of ^{19}F normally present in tissues, hence ^{19}F NMR spectroscopy is particularly suitable for constructs in NMR-compatible bioreactors and *in vivo* situations.

As a construct remodels, the distributions of viable cells, cellular metabolic states, and DO change with time. To evaluate these distributions non-invasively, one could collect spectra from a series of VOIs within the construct using chemical shift imaging in one, two, or possibly three dimensions, as previously reported in one dimension *in vitro* with encapsulated cells [9, 16, 122, 123]. However, even if feasible, these are time-consuming techniques with limited applicability especially *in vivo* due to cost and the long anesthesia times required for experimental animals. Since collecting signal from the entire tissue construct is a more rapid process, a methodology that permits an evaluation of the cellular and oxygen distributions from concentration measurements averaged over the entire construct, or by measuring the overall metabolic activity of the construct, would thus be highly desirable.

In this paper, we present the development of a quantitative mathematical model describing the cellular remodeling and changes in DO profile when proliferative cells are encapsulated in hydrogel beads. The model considers only a permissive material, which

does not directly influence cell growth and in which remodeling of the cell distribution occurs only in response to the available oxygen. Model parameters were representative of mouse insulinoma βTC cells in permissive high manuronic calcium alginate beads. This encapsulated cell system constitutes a model pancreatic substitute appropriate for *in vitro* and small animal *in vivo* experiments [9, 16, 69, 116]. Model solutions on changes of the cellular and oxygen profiles with time are first presented and compared with experimental results. Importantly, the model was also used in a reverse fashion, specifically to decipher cell and oxygen distributions – both critical in determining the functional ability of a construct – from measurements of the average oxygen concentration in the tissue substitute or of the total oxygen consumption rate by the construct. The use of the model in synergy with experimental measurements to obtain spatial information on intra-construct gradients, and the significance of such information, are discussed.

3.3 Mathematical Model and Assumptions

A number of assumptions were incorporated in the development of the model and are listed below. These assumptions were based on experimental data collected with βTC3 mouse insulinoma cells encapsulated in calcium alginate and agarose matrices [113, 118-121, 123]. Hence, the assumptions are realistic for this and likely other similar systems of proliferative cells in inert permissive hydrogels.

1. DO is the only nutrient that limits cell proliferation. Thus, all other essential nutrients are assumed to be in excess throughout the construct.

2. Spatial constraints are the only other factor besides DO concentration that limits the rate and extent of cell proliferation within the construct.
3. Cells do not migrate within the matrix, hence the observed remodeling in cell distribution is due entirely to cellular growth and death at each locale. This is supported by the fact that cells do not attach to alginate hydrogels without modification of the alginate by grafting adhesion molecules [128, 129].
4. The values of the model parameters, including the effective diffusivity of DO through the encapsulated system, remain constant over the time period of the simulations.
5. There is no external boundary layer effect. This is a reasonable assumption for systems in which there is significant velocity of the medium relative to the surface of the beads, as is the case in perfusion bioreactors where beads are retained in place while medium flows through the bed.

The model equations for spherical geometry are as follows.

$$\frac{\partial C(r,t)}{\partial t} = D_{eff}\left(\frac{\partial^2 C(r,t)}{\partial r^2} + \frac{2}{r}\cdot\frac{\partial C(r,t)}{\partial r}\right) - S(r,t) \qquad (1)$$

$$\frac{dX(r,t)}{dt} = X(r,t)\left(\mu_g - \mu_d\right) \qquad (2)$$

In the above equations, t is time and r is radial position in the construct; $C(r,t)$ and $X(r,t)$ are the concentration of oxygen and the cell density, respectively, as functions of radial position and time; D_{eff} is the effective oxygen diffusivity; $S(r,t)$ is the rate of oxygen consumption per unit volume as a function of radial position and time; and μ_g and μ_d are

the specific cell growth and death rates, respectively. Equations (1) and (2) need two initial and two boundary conditions to be solved, which are given below.

$C\big|_{t=0} = C_o$ (3) (the initial concentration of oxygen is constant throughout the spherical construct and known)

$X\big|_{t=0} = X_o$ (4) (the cells are initially distributed homogeneously throughout the construct at a known density)

$\frac{\partial C}{\partial r}\big|_{r=0} = 0$ (5) (symmetry condition for oxygen concentration at the center of the sphere)

$C\big|_{r=R} = C_b$ (6) (the concentration of oxygen at the surface of the construct is equal to the concentration in the surrounding medium, which is known)

The expressions used for the kinetics of oxygen consumption by the cells, cell growth and cell death are as follows.

$$S(r,t) = X(r,t) \cdot \frac{\nu_{max} C(r,t)}{K_m + C(r,t)} \quad (7)$$

(Monod's model with kinetic parameters ν_{max} and K_m)

$$\mu_g = \frac{\mu_{g,max} C(r,t)}{K_g + C(r,t)} \left(1 - \frac{X(r,t)}{X_{max}}\right) \quad (8)$$

(Monod's model with kinetic parameters $\mu_{g,max}$ and K_g, accounting for spatial constraints)

$$\mu_d = \mu_{d,\max} - \left(\mu_{d,\max} - \mu_{d,\min}\right)\frac{C(r,t)}{K_d + C(r,t)} \quad (9)$$ (modified Monod's model maximizing the cell death rate at C=0 and minimizing it at $C>>K_d$)

In the above equations, $\mu_{g,max}$ and $\mu_{d,max}$ are the maximum specific growth and death rates, respectively; $\mu_{d,min}$ is the minimum death rate, which prevails under an abundance of oxygen; K_g and K_d are Monod model parameters; and X_{max} in the maximum cell density that can be accommodated in the construct. The ratio X/X_{max} is thus the fractional maximum occupancy at a particular locale in the construct.

The cumulative number of dead cells $D(r,t)$ as a function of time and position can be obtained by integrating over time the specific death rate multiplied by the cell density, as in the following equation.

$$D(r,t) = \int_0^t X(r,t)\mu_d dt \qquad (10)$$

3.3.1 Baseline Model Parameters

Baseline parameter values for the above mathematical model are representative of βTC3 mouse insulinoma cells encapsulated in calcium alginate beads and are listed in Table 3.1. The continuous βTC3 cell line, a member of the βTC family of insulinomas established by Efrat and co-workers [60, 130, 131], has been extensively studied by our group and others both as such and following alginate encapsulation as a model tissue engineered pancreatic substitute [8, 9, 16, 116, 126].

Table 3.1 Baseline parameter values used in simulating the spatio-temporal profiles of cells and oxygen in a system of βTC3 cells encapsulated in spherical calcium alginate/ poly-L-lysine/ alginate (APA) beads.

Parameter		Value	Reference
Effective Diffusivity	D_{eff}	1.4 cm^2/day	(Tziampazis and Sambanis 1995), (Mehmetoglu, Ates et al. 1996), (Stabler 2004)
Maximum O_2 Consumption	v_{max}	2.88 mmole/(day●10^9cells)	(Tziampazis and Sambanis 1995)
Monod Parameter – O_2	K_m	0.01 mM	(Tziampazis and Sambanis 1995)
Maximum Specific Growth Rate	$\mu_{g,max}$	0.35 day^{-1}	Monolayer growth rate, (Stabler, Wilks et al. 2001)
Maximum Specific Death Rate	$\mu_{d,max}$	1.4 day^{-1}	(Graeber, Osmanian et al. 1996)
Minimum Specific Death Rate	$\mu_{d,min}$	0.00273 day^{-1}	Tziampazis et al. (unpublished)
Monod Parameter – Growth	K_g	0.01 mM	Tziampazis et al. (unpublished)
Monod Parameter – Death	K_d	0.001 mM	Tziampazis et al. (unpublished)
Maximum Cell Density	X_{max}	$9x10^8$ cells/ml	Calculated based on a 10μm diameter cell

The maximum oxygen consumption rate, v_{max}, and parameter K_m were estimated from reported results for encapsulated βTC3 cells as 2 μmole/(min·10^9cells) and 0.01 mM, respectively [125, 132, 133]. The maximum specific death rate $\mu_{d,max}$ was estimated using published rates of hypoxia-induced apoptosis. Oncogenically transformed cells (with wild-type p53) exposed to low DO concentrations (<0.0001 mM) had an approximate 15% viability after 24 hours [6], which corresponds to a specific death rate of 1.9 day^{-1}. The p53 gene status of βTC3 cells is not known. Thus, for the mathematical model presented here, a conservative maximum specific death rate of 1.4 day^{-1} was assumed. The maximum specific growth rate was estimated from growth rates observed in T-flask experiments where death is negligible. In particular, T-175 flasks seeded with βTC3 cells at a surface density corresponding to 35 cm^2 became confluent (at 175 cm^2) in five days, which results in a specific growth rate of 0.32 day^{-1}. Thus, a value of 0.35 day^{-1} was used for a maximum growth rate. This estimate is also compatible with data from freshly encapsulated cells [116], in which the glucose consumption rate (GCR) doubled over a period of 50 hours. Although the per cell GCR depends on the DO concentration, encapsulated cells are all well oxygenated before remodeling occurs [116, 132], hence GCR is a measure of viable cell number under these conditions. In the sensitivity analysis section of this paper, the effect of $\mu_{g,max}$ and $\mu_{d,max}$ on the steady state cell and DO profiles is investigated.

To estimate the maximum cellular density, X_{max}, which can be accommodated in the calcium alginate matrix, βTC3 cells were assumed to be 10 μm in diameter. At this diameter, the maximum viable cell density with no void space is 1.9x10^9 cells/ml. To account for space occupied by the matrix, for dead cells, and for voids revealed by

histology even after extensive cell growth [16, 21, 116], the baseline value of X_{max} was set equal to 1/2 of the theoretical maximum, or $9x10^8$ cells/ml. A sensitivity analysis was also performed on the effect of changing X_{max} from its baseline value in regards to the resulting cell and oxygen profiles.

The effective diffusivity of oxygen D_{eff} in cell-loaded alginate beads was estimated as follows. Using the Wilke-Chang equation, the oxygen diffusivity in water at 37ºC is calculated to be $1.8x10^{-3}$ cm^2/min [132]. Oxygen diffusivity is lower in cell-free and, more so, cell-containing alginate beads [134]. In cell-free alginate beads, the oxygen diffusivity was found to be $1.53x10^{-3}$ cm^2/min [135]. In cell-containing beads, reported values of the effective oxygen diffusivity range from $0.764x10^{-3}$ cm^2/min to $1.39x10^{-3}$ cm^2/min [132, 135]. An intermediate value of $0.972x10^{-3}$ cm^2/min, or 1.4 cm^2/day, was chosen for the simulations in this study. It should be noted that, since D_{eff} depends on cell density, it likely changes with time at a particular radial position in the beads as remodeling occurs. In this initial study, however, a constant value of D_{eff} – independent of time and position – was assumed; a sensitivity analysis was performed by changing D_{eff} from its baseline value for all positions within the bead.

3.3.2 Numerical Methods

The steady state solution was calculated numerically using finite difference equations programmed in MatLab software. Accuracy was verified by ensuring that the solution did not change by decreasing Δr.

The transient model equations were also solved using finite difference equations programmed in MatLab. Convergence of the calculations was ensured by keeping the Δt

component much smaller than Δr [136]. Specifically, for all simulations presented here the following relationship was maintained:

$$\frac{\Delta t}{\Delta r^2} \leq 0.4 \qquad [\text{day/cm}^2]$$

The accuracy of the simulations was then verified by (i) ensuring that the transient solution after 150 days closely approximated the steady state solution, and (ii) confirming that the solution did not change by decreasing Δr.

3.4 Results

3.4.1 Steady State Solution

The steady state oxygen and cell density profiles were calculated by setting the time derivatives equal to zero. Hence, equation (1) was reduced to

$$D_{eff}\left(\frac{d^2C(r)}{dr^2}+\frac{2}{r}\cdot\frac{dC(r)}{dr}\right)-X(r)\frac{\nu_{\max}C(r)}{K_m+C(r)}=0 \tag{11}$$

and equation (2) to

$$X(r)[\mu_g-\mu_d]=0 \tag{12}$$

Substituting Equations (8) and (9) in Equation (12), the following is obtained:

$$\frac{\mu_{g,\max}C(r)}{K_g+C(r)}\left(1-\frac{X(r)}{X_{\max}}\right)-\left(\mu_{d,\max}-\left(\mu_{d,\max}-\mu_{d,\min}\right)\frac{C(r)}{K_d+C(r)}\right)=0 \tag{13}$$

By a simple algebraic manipulation, the cell density, *X(r)*, is found as a function of *C(r)* resulting in the following equation

$$X(r)=X_{\max}\left(1-\frac{\mu_{d,\max}\left(K_g+C(r)\right)}{\mu_{g,\max}C(r)}+\frac{\left(\mu_{d,\max}-\mu_{d,\min}\right)\left(K_g+C(r)\right)}{\mu_{g,\max}\left(K_d+C(r)\right)}\right) \tag{14}$$

Equation (14) was then substituted in Equation (11) and the resulting equation was solved numerically. Results are shown in Figure 3.1A and 3.1B for a 1.0 mm diameter bead and external DO concentrations of 0.20 mM and 0.06 mM, respectively. The DO concentration of 0.20 mM corresponds to normal incubator conditions, while 0.06 mM is representative of the peritoneal environment. The cellular profile in Figure 3.1A illustrates the viable cell ring at the periphery which has been observed experimentally by histological sectioning of the beads [16, 21, 116].

Reported results on the effect of oxygen on the βTC3 cell line indicated that cellular metabolism shifts to enhanced anaerobic glycolytic activity below 0.032 mM (25 mmHg), whereas insulin secretion becomes inhibited as DO is reduced to 0.01 mM (7 mmHg) or lower [8]. As seen in Figure 3.1, for beads exposed to 0.20 mM external DO, 0.032 mM DO occurs at a position approximately 136 μm from the bead's periphery, and the lower 0.01 mM DO occurs at 224 μm from the periphery. Hence, at steady state, 2% of the cells have their secretory capacity compromised under these conditions. On the other hand, with beads exposed to 0.06 mM external DO, the DO concentration reached 0.032 mM and 0.01 mM only 37 μm and 124 μm, respectively, from the bead's periphery. Thus, in this case, 6% of the cells have their secretory capacity compromised. The steady state oxygen profiles correspond to average intrabead DO concentrations (AIDO) of 0.073 mM and 0.020 mM for 0.20 mM and 0.06 mM external DO, respectively. The average viable cell densities in the beads are 6.52×10^8 and 3.88×10^8 cells/ml and the total cell numbers are 3.41×10^5 and 2.03×10^5 cells/bead for the high and low value of the external DO, respectively.

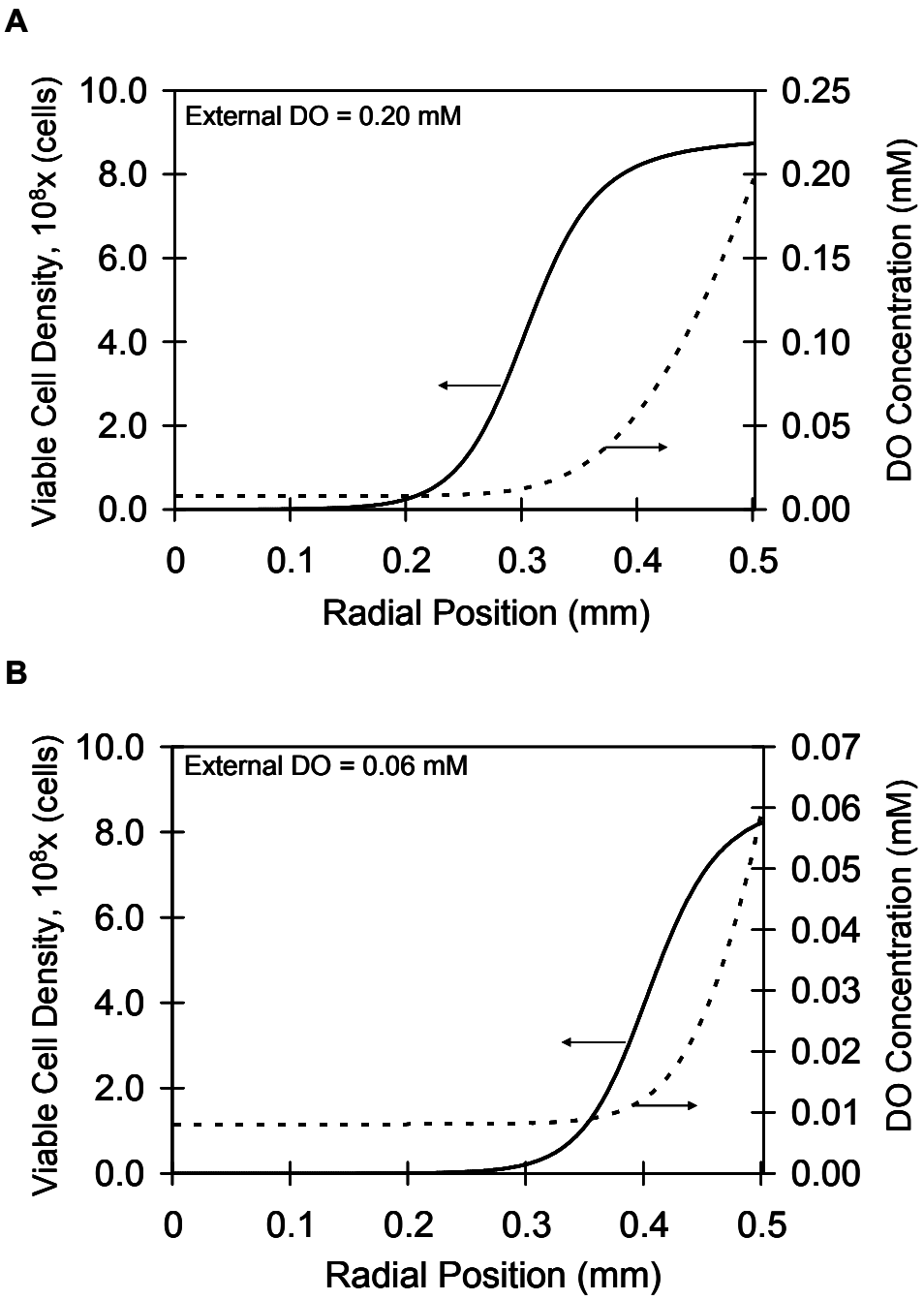

Figure 3.1 Steady state viable cell density and DO profiles in a 1.0 mm diameter bead at two external DO concentrations. (A) External DO equal to 0.20 mM. At the periphery (radial position equal to 0.5mm), the cell density reaches 8.74 x 10^8 cells/ml due to the high DO concentration (0.20 mM). The cell density declines towards the center of the bead attaining its lowest value of 1.8 x 10^5 cells/ml at the center where the DO concentration is 0.008 mM. (B) External DO equal to 0.06 mM. The maximum cell density at the periphery is 8.23 x 10^8 cells/ml. At the center where the oxygen concentration is 0.008 mM, the cell density declines to 5.0 x 10^3 cells/ml.

3.4.2 Sensitivity Analysis of the Steady State Solution

A sensitivity analysis was performed to evaluate the effect D_{eff} on the steady state viable cell density and DO concentration in beads. Figures 3.2A and 3.2B show the simulated steady state cell density and DO profiles, respectively, at an external DO concentration of 0.20 mM and with values of D_{eff} ranging from 1.0 to 2.0 cm^2/day. As the diffusivity was increased, the thickness of the dense peripheral band of cells also increased and oxygenated conditions extended to longer distances from the bead periphery. Decreasing K_d caused the cell density profile to become steeper (results not shown). Parameter K_g had little effect on the steady state solutions. In regards to the maximum specific growth and death rates, Equation (14) indicates that it is the ratio of these two parameters that determines the viable cell distribution in beads. Figure 3.3 (A and B) shows the sensitivity of the steady state cell and oxygen profiles for different values of $\mu_{g,max}/\mu_{d,max}$ around the baseline value of 0.25. The effect of the two oxygen consumption parameters, v_{max} and K_m, on the steady state solutions was comparable to previous reported findings [17, 137] and was as follows. Increasing v_{max} resulted in steeper cell density gradients and a decrease in the number of viable cells that could be supported towards the center, as oxygen concentrations quickly reached hypoxic levels away from the bead periphery. Similarly, increasing v_{max} resulted in sharper DO gradients. Changing K_m from the baseline value had little effect on the viable cell and DO profiles compared to v_{max} (results not shown).

To investigate the sensitivity of steady state solutions to X_{max}, model solutions were obtained with this parameter increased and decreased by 50% from the baseline value. Changes in X_{max} influence primarily the cell density close to the bead periphery, as

the cell density closer to the center is determined mainly by the DO concentration. Thus, increasing X_{max} resulted in steeper cell density profiles and, conversely, decreasing X_{max} made the steady state cell density distribution more homogeneous (results not shown).

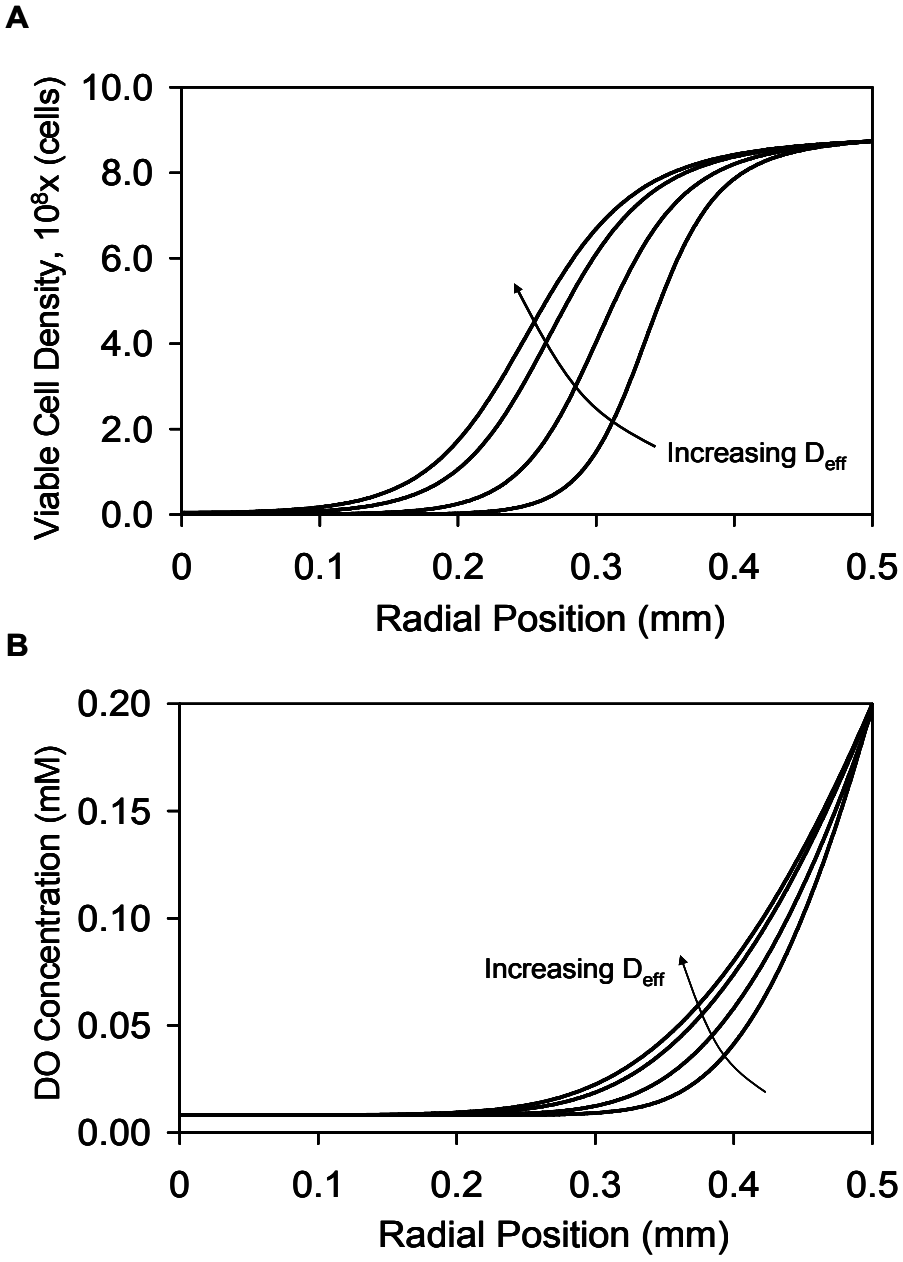

Figure 3.2 Sensitivity analysis of the steady-state cell (A) and DO (B) distributions in a 1.0 mm diameter bead at 0.20 mM external DO for effective diffusivity values of 1.0, 1.4, 1.8, and 2.0 cm^2/day.

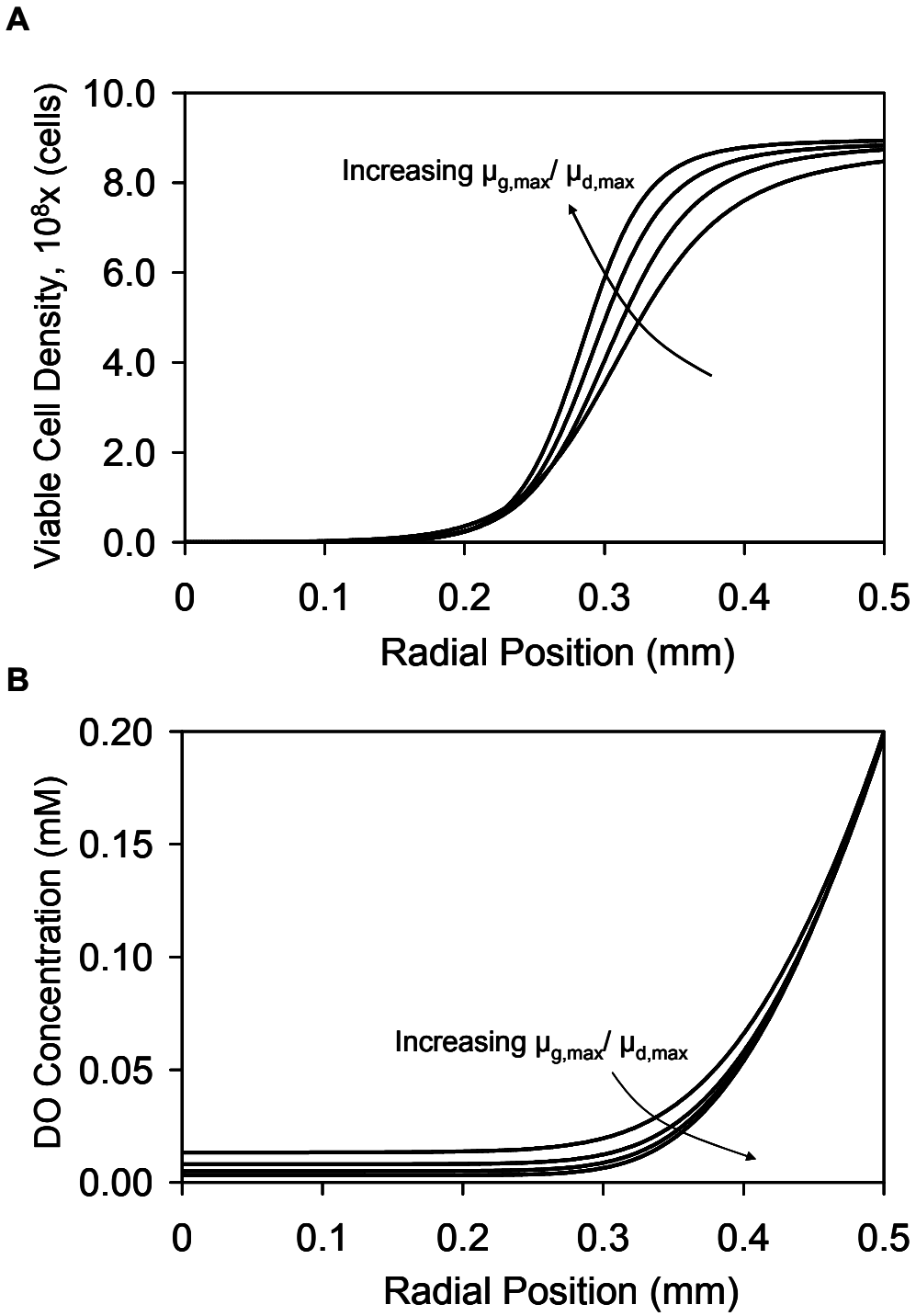

Figure 3.3 Sensitivity analysis of the steady-state cell (A) and DO (B) distributions in a 1.0 mm diameter bead at 0.20 mM external DO for $\mu_{g,max}/\mu_{d,max}$ values of 0.125, 0.25, 0.5, and 1.0.

3.4.3 Unsteady State Solutions

Using the parameters listed in Table 1, the changes in cellular and oxygen profiles in spherical geometry were tracked over 30 days. Figures 3.4A and 3.4B illustrate the radial changes in cell density and DO concentration starting from a uniform cell density of 5 x 10^7 cells/ml alginate and a uniform DO concentration of 0.20 mM. Initially, the dissolved oxygen concentration throughout the bead is sufficient to facilitate cell proliferation regardless of radial position (Figures 3.4A and 3.4B, days 1-5). However, as the cell density at the periphery increases, the DO concentration towards the center of the bead decreases, consequently the number of cells that can be supported at this locale also decreases. The proliferation of cells at the periphery continues until spatial constraints are reached, whereas at positions closer to the center the equilibrium cell density is determined by the equilibrium DO concentration (Figures 3.4A and 3.4B, days 5-30). Comparing the steady state and unsteady state solutions, the viable cell number in a bead reaches 95% of its steady state value within 16 days. This is consistent with the growth profiles observed experimentally, where the total metabolic activity of a culture reaches a plateau after approximately 15 days [116]. Figure 3.4C shows the spatiotemporal accumulation of dead cells in the beads. Interestingly, the highest accumulation of dead cells at later time points occurs not at the center of the beads, but at intermediate radial positions.

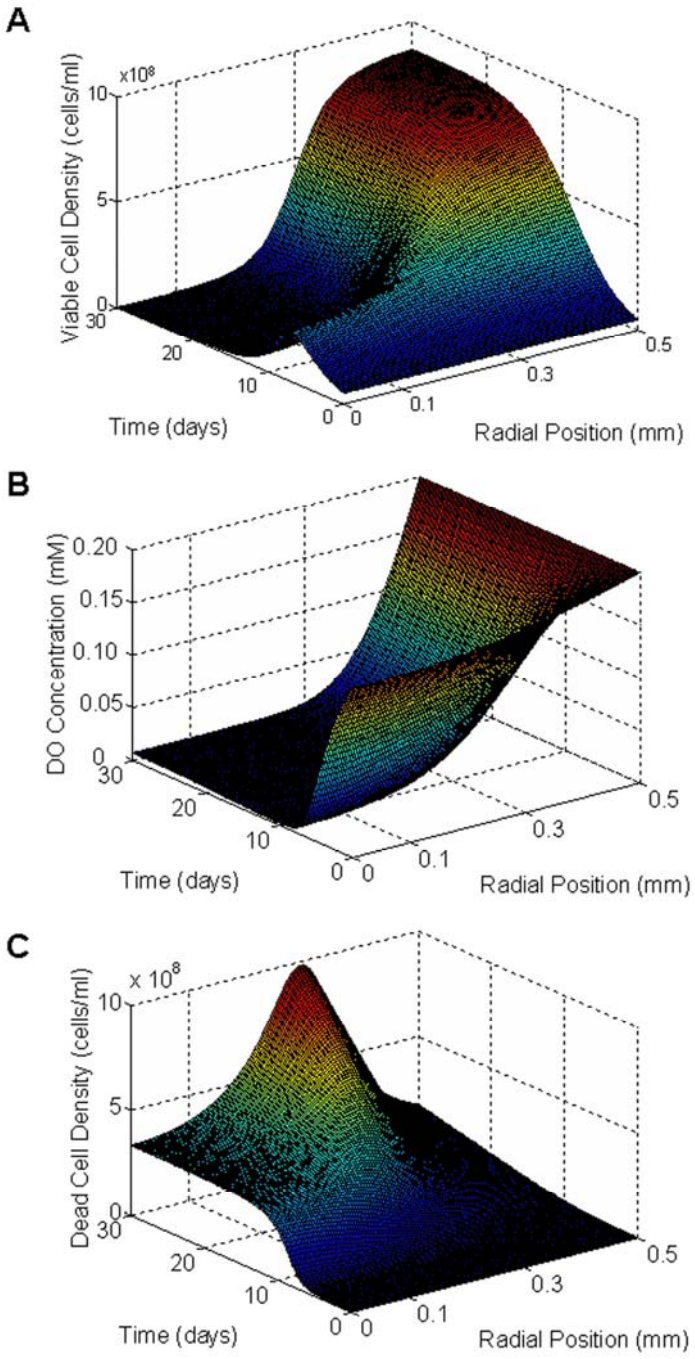
A
x10^8
10
5
0
Viable Cell Density (cells/ml)
30
20
10
0
Time (days)
0
0.1
0.3
0.5
Radial Position (mm)
B
0.20
0.15
0.10
0.05
0
DO Concentration (mM)
30
20
10
0
Time (days)
0
0.1
0.3
0.5
Radial Position (mm)
C
x 10^8
10
5
0
Dead Cell Density (cells/ml)
30
20
10
0
Time (days)
0
0.1
0.3
0.5
Radial Position (mm)

Implant antigens exiting the bead are thought to be recognized by the host and invoke an immune response via the indirect antigen presentation pathway [138]. Antigens are released in the capsule as a result of cellular death and lysis, possibly also protein secretion. For this reason, the accumulation of dead cells was tracked using Equation 10 for two different initial cell densities (1.0 and 10 x 10^7 cells/ml) and at external DO concentrations of 0.20 mM and 0.06 mM. The temporal accumulation of dead cells in beads is shown, along with the corresponding accumulation of viable cells, in Figures 3.5A and 3.5B. At both external DO concentrations, the rates of dead cell accumulation reached the same values irrespective of initial cell density (1.1 x 10^4 cells/day at 0.20 mM external DO, Figure 3.5A, and 1.3 x 10^4 cells/day at 0.06 mM external DO, Figure 3.5B), as shown by the equal slopes of the lines at later time points in the simulations. However, at the DO concentration of 0.20 mM, the beads with the higher initial cell density reached 95% of the steady state dead cell accumulation rate within 10 days, whereas the beads started with the lower initial cell density reached the 95% value on day 18. The times to reach 95% of the steady state rate were somewhat higher at the lower external DO, and they were equal to 13 and 23 days for the high and low initial cell densities, respectively.

As is seen in equations 7, 8, and 9 above, the final viable cell number within a construct is a function of both the available oxygen and spatial constraints. Because of this relationship, the total viable cell number and the viable cell distribution within a bead are the same at steady state for a given external DO, irrespective of the initial cell density. Figures 3.5A and 5B show the temporal profiles of the viable cell numbers in a bead at two different external oxygen concentrations—0.20 mM and 0.06 mM—and two initial

densities (1 and 10 x 10^7 cells/ml). At each external DO, the cell number plateaued at the same level, irrespective of initial conditions. Reducing the external DO by 70%, or from 0.20 mM to 0.06 mM, decreased the steady state viable cell number by 59%. This difference in percentages is due to the spatial constraints. When oxygen is more abundant (0.20 mM), the cells at the periphery are predominantly affected by the spatial constrains, while at lower oxygen levels the DO concentration is the major contributor to the steady state cell density throughout the bead, including the periphery.

Simulated changes in cellular distribution were compared against experimental data obtained with βTC3 mouse insulinomas encapsulated in high mannuronic alginate APA beads and reported by Stabler et al. [116]. Initially, the cells were homogeneously distributed in the beads, but with time in culture the cells proliferated at the periphery creating a ring of cells at the bead's edge. Histological data on the cell distribution on days 1, 7, 16 and 29 post-encapsulation [116] are in agreement with the model-predicted cell redistribution at these time points. Furthermore, the model-predicted thickness of the cell ring is in agreement with experimentally measured values by MR imaging [139].

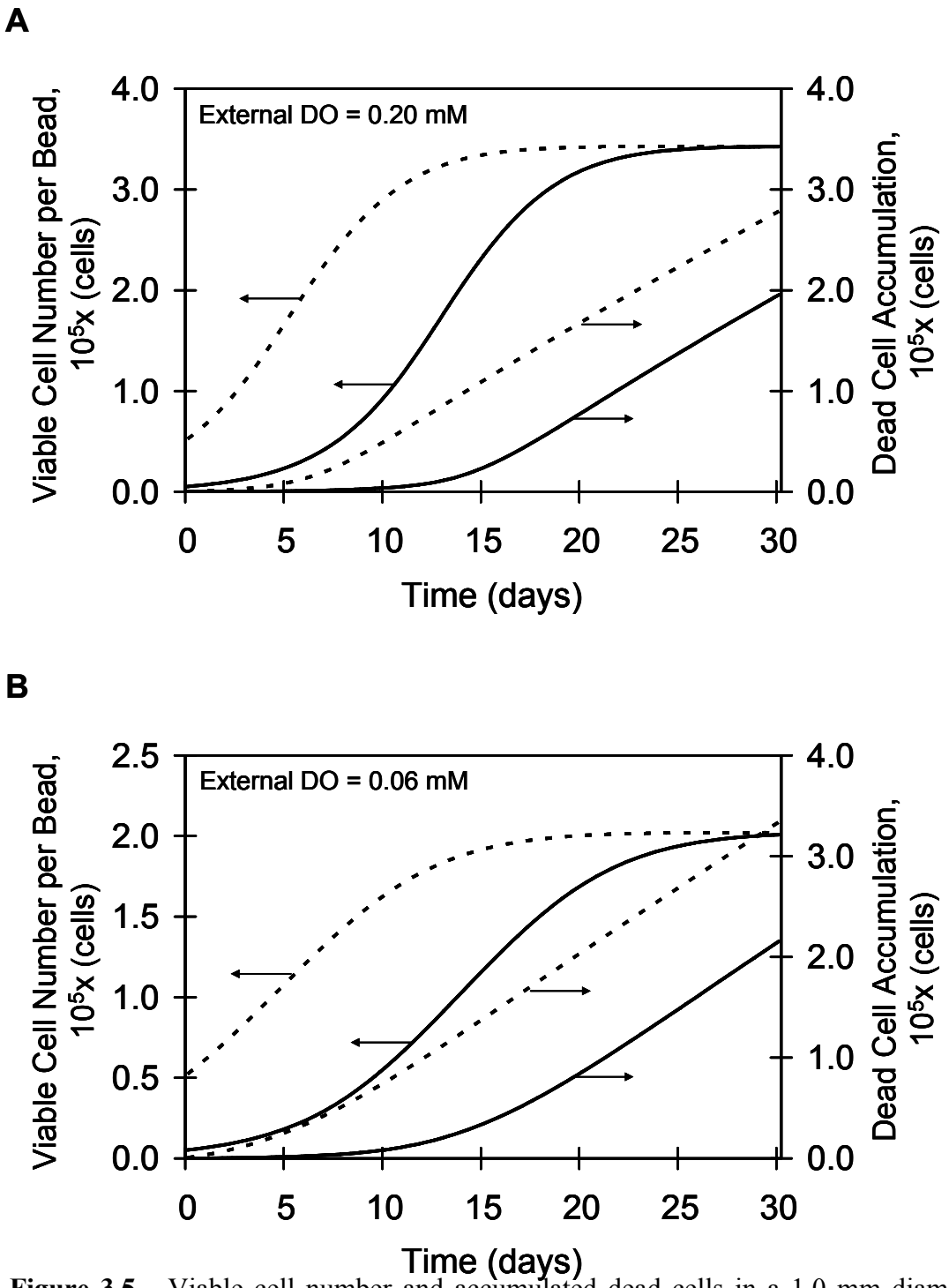

Figure 3.5 Viable cell number and accumulated dead cells in a 1.0 mm diameter bead as a function of time for 0.20 mM (A) and 0.06 mM (B) external DO concentrations. At each external DO concentration, simulations were performed with two initial cell densities – 1.0 and 10 x 10^7 cells/ml. All constructs eventually attain the same viable cell number per bead and rate of cell death (equal slopes of the accumulated dead cells vs. time curves); however, the total number of accumulated dead cells correlates positively with the initial loading density.

3.4.4 Experimentally Useful Correlations

To investigate whether measurements of the average intrabead DO concentration (AIDO), which are acquired through a single T_1 NMR relaxation from an entire bead, could offer information on the number and distribution of cells and on the DO gradients in a bead, pertinent correlations were developed and the following graphs were constructed. Figure 3.6 shows the total viable cell number in a bead vs. AIDO for different initial cell densities and for two DO concentrations in the surrounding medium. For a given external DO, all points fall on the same curve, irrespective of the initial cell density. Time is a parameter along each curve. Thus, these graphs demonstrate that with a given external DO, an AIDO value uniquely identifies the number of viable cells within a construct, irrespective of the initial cell density. It should be noted that similar correlations are obtained when the viable cell number is plotted vs. the total oxygen consumption rate (OCR) exhibited by a certain number of beads (results not shown). The latter can be measured *in vitro* when the beads are in a perfusion bioreactor with dissolved oxygen sensors positioned upstream and downstream of the bed [9, 16]. With beads implanted in experimental animals, however, OCR cannot be measured and AIDO is the useful measurement.

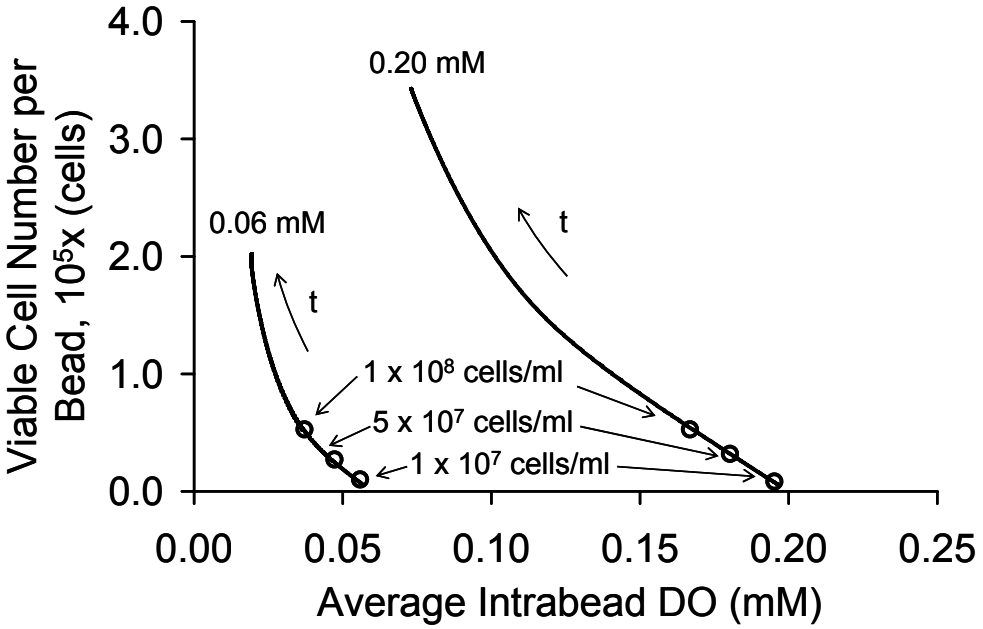

Figure 3.6 Correlation between the total viable cell number in a bead and the average intrabead dissolved oxygen concentration (AIDO) for two external DO levels. For a given external DO, the correlation is independent of the initial cell density. Time (t) is a parameter along the trajectories.

To evaluate whether AIDO could offer information on the cell distribution within a bead for a particular external DO, the distances from the bead periphery to the points at which the cell density dropped to 50% and 90% of the peripheral cell density – which is the maximum in the bead - were adopted as measures indicative of cell distribution. Figure 3.7 shows this distance as a function of AIDO for two external DO concentrations. Each curve was obtained by performing calculations with different initial cell densities and again all points fell on the same curve, irrespective of the initial density; time is a parameter along each curve. When the distance is 0.5 mm, i.e., it extends all the way to the bead center, this means that the cell density is relatively uniform and does not drop to

either 50% or 90% of the maximal even at the bead center. This occurs with fresh bead preparations, in which oxygen-driven remodeling has not yet occurred and for which AIDO is relatively high. However, as the density of cells close to the periphery increases, the position of 50% and 90% maximum cell density shifts closer to the bead's edge. Additionally, the AIDO decreases while this redistribution occurs. Hence, this correlation can be used to assess the cell distribution in the bead from experimentally measured AIDO. It should be noted that similar correlations are obtained when the measures of cell distribution are plotted vs. the OCR exhibited by a certain number of beads (results not shown).

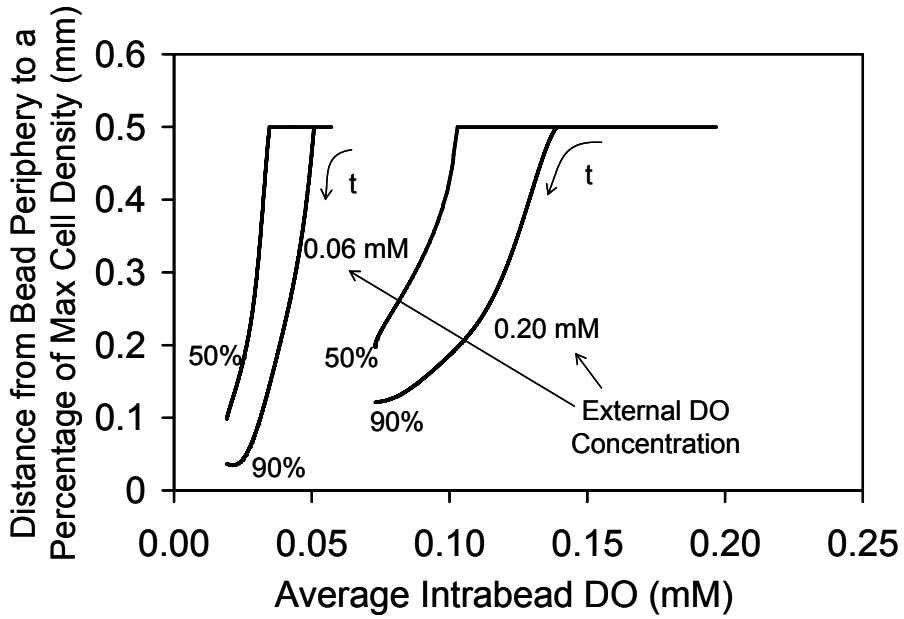

Figure 3.7 Correlation between a measure of the cellular distribution in beads (distance from the periphery to the points corresponding to 50% and 90% of maximum viable cell density) and AIDO for two external DO levels. For a given external DO, the correlation is independent of the initial cell density. Time (t) is a parameter along the trajectories.

To determine the correlation between the oxygen profile and the AIDO, the distances from the bead's edge to the radial positions at which the DO concentration is 20% and 50% of the external DO (indicative of intrabead DO distribution) were plotted against AIDO. As is seen in Figure 3.8, at a high AIDO, the DO concentration within the bead is everywhere higher than 20% and 50% of the external DO, hence the plotted distance extends to the center of the bead. However, as the AIDO decreases, so does the distance from the periphery to which 20% and 50% of external DO is reached. Thus, as with cell distribution, experimentally measured AIDOs can be used to assess the DO distribution in this encapsulated cell system. Again, similar correlations are obtained when the measures of DO distribution are plotted vs. the OCR of a certain number of beads (results not shown).

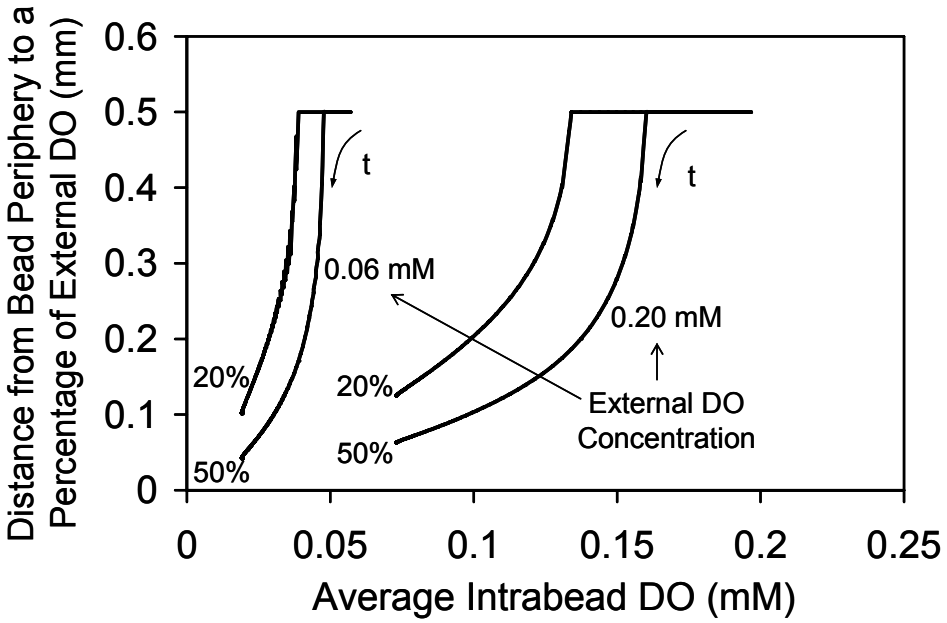

Figure 3.8 Correlation between a measure of the DO distribution in beads (distance from the periphery to the points corresponding to 20% and 50% of the external DO concentration) and AIDO for two external DO levels. For a given external DO, the correlation is independent of the initial cell density. Time (t) is a parameter along the trajectories.

3.5 Discussion

Understanding the oxygen-driven remodeling in tissue engineered substitutes in general and encapsulated cell systems in particular is essential in determining how tissue constructs will ultimately function. The mathematical model developed in this paper simulated the microenvironment within a spherical pancreatic substitute in regards to the cell and oxygen profiles. The surrounding dissolved oxygen concentration and spatial constraints were the two parameters that had the greatest influence over the final cell distribution. The influence of the DO concentration and spatial constraints parameters were seen in the sensitivity analysis. For the simulations presented here, external mass transport limitations were not accounted for, which is a reasonable approximation for perfusion and well mixed *in vitro* culture systems. On the other hand, boundary layer effects are likely to be present *in vivo*, with beads implanted extravascularly, such as intraperitoneally, in experimental animal models. The maximum oxygen consumption rate v_{max} dictated the distance to which dissolved oxygen could diffuse before being reduced to hypoxic levels. The maximum cell density, X_{max}, also influenced the cell profile, specifically the cell density within 200 μm of the construct's edge. After approximately 15 days, equilibrium was essentially reached, where the rate of cell growth equaled the rate of cell death at all radial positions. The simulated growth profile and cellular remodeling closely matched data from βTC insulinoma cells encapsulated in high mannuronic, growth permissive alginate beads. Simulating cellular remodeling within non-permissive materials would require additional constraints within the mathematical equations. As the precise nature of the cell-material interactions for non-permissive

matrices is currently unclear, a robust mechanistic model describing such a system cannot presently be developed.

Given the strong dependence of cell viability and insulin secretion on the DO concentration a cell experiences, the ability to non-invasively monitor DO concentration profiles would be beneficial in determining how a construct is functioning *in vivo*. For instance, in experiments with diabetic small animal models, an animal is made diabetic by an injection of streptozotocin, a chemical which specifically destroys the insulin-secreting β cells of the pancreas; a tissue engineered substitute is then implanted and its efficacy is evaluated by monitoring blood glucose levels during normal feeding or glucose injection episodes. However, the implant itself is evaluated only at the end of the experiment when the animal is euthanized and the construct is explanted. Non-invasive monitoring of cell viability and construct function on the same animal during the course of an experiment is thus especially useful in establishing an important link between implantation and end-point physiologic effects. Monitoring the DO concentration in a tissue substitute offers an indirect but clear indication of cell function within the construct.

Previous literature demonstrated the capacity of ^{19}F and ^{1}H NMR spectroscopy to quantify oxygen concentrations and the number of viable cells in a VOI, respectively. Nonetheless, determining the local DO concentrations and viable cell number using chemical shift imaging requires a significant amount of time that may limit *in vivo* applications. We have demonstrated in this paper the feasibility of using a mathematical model to evaluate cellular and oxygen profiles from a single ^{19}F NMR measurement (AIDO), which can be performed relatively quickly.

For a given external DO, the AIDO uniquely identified the viable cell number per bead irrespective of the initial cell density (i.e. a construct with 2 x 10^8 viable cells had the same AIDO regardless of whether it started with 1 x 10^7 or 5 x 10^7 cells/ml). At lower external DO concentrations, the correlation between AIDO and viable cell number becomes more difficult to discern, in the sense that a certain change in AIDO corresponds to a larger difference in viable cell number. However, if AIDO measurements are used in combination with ^{1}H NMR measurements performed on the same VOI, it is reasonably expected that a more accurate assessment of viable cell number can be made.

For a given external DO, cellular and DO profiles were also uniquely identified by the AIDO regardless of initial cell density. Indeed, at higher AIDO concentrations, the cell density is low and homogeneous enough to allow proliferation throughout the bead, and a drop to 90% of maximum density or below is not attained. Similarly, at a low cell density the oxygen consumption is not sufficient to reduce the DO concentration to less than 50% of the external DO. At lower external DO concentrations, the measures of cell and DO distribution become more difficult to decipher from an AIDO measurement, as small changes in AIDO correspond to large changes of the distributions.

Tissue engineered constructs are fabricated in many shapes and sizes, and the modeling framework presented here can be easily adapted to other construct geometries. Simulations for a disk-shaped construct of the type reported by Stabler et al. [113, 121] have also been performed (results not shown), and there was generally good agreement between simulated and experimentally measured viable cell numbers over a 14 day period. For the disk-shaped construct, too, AIDO could be used to assess viable cell

number and cell and DO distributions for a given external DO through correlations similar to those shown in Figures 3.6 - 3.8.

Current work in our laboratory involves further validating the model by measuring the intra-bead DO distribution *in vitro* using magnetic resonance techniques. The model will then be applied to *in vitro* and *in vivo* experimental systems in order to assess the viable cell number and cell and DO distributions from non-invasive measurements of AIDO by ^{19}F NMR.

CHAPTER 4

MONITORING OF DISSOLVED OXYGEN AND CELLULAR BIOENERGETICS WITHIN A PANCREATIC SUBSTITUTE[2]

4.1 Abstract

This work investigated the use of nuclear magnetic resonance (NMR) spectroscopy in combination with a mathematical model of an encapsulated cell system as a method for rapidly assessing the status of a pancreatic substitute. To validate this method, an *in vitro* experiment was performed in which the encapsulated cells were perfused in an NMR-compatible system and the dissolved oxygen (DO) concentration of the perfusing medium was lowered from 0.20 to 0.05 mM, then returned to 0.20 mM in a stepwise fashion. The cellular metabolic activity and bioenergetics were evaluated by measuring the oxygen consumption rate (via DO sensors) and nucleotide triphosphate levels (via ^{31}P NMR). By incorporating a perfluorocarbon emulsion into the alginate beads, the cellular oxygenation state was monitored by measuring the average intrabead DO (AIDO) concentration by ^{19}F NMR. The *in vitro* measurements were then compared with model predictions based on the measured external DO concentration and time. Model-predicted cell growth and AIDO closely matched the experimentally acquired data. As the DO concentrations both external to and within the pancreatic substitute are needed to apply this methodology *in vivo*, the feasibility of measuring the DO concentration from two distinct bead populations implanted in the peritoneal cavity of mice was established. It is concluded that PFC incorporation and ^{19}F NMR

---

[2] Modification of a paper published in **Biotechnology and Bioengineering**, in press (2007).

measurements, in combination with a mechanistic model of the encapsulated system, allow the tracking of the state of a pancreatic substitute *in vitro* and potentially *in vivo*.

4.2 Introduction

Tissue engineered substitutes, consisting of cells and biomaterials organized in specific three-dimensional architectures, have the potential to provide effective replacement of the function of natural tissues that have failed as a result of disease or injury [4]. Function of these substitutes is influenced by a variety of mechanical, chemical and possibly electrical cues. During *in vitro* culturing, conditions are monitored and controlled, so the development and function of tissue constructs are at least somewhat predictable. However, post-implantation *in vivo*, a multitude of poorly known factors affect the function of implanted cells and of a construct as a whole, hence also the achieved therapeutic effect. Thus, non-invasive methods to monitor construct integrity and function are invaluable. In particular, non-invasive *in vivo* monitoring allows investigators to establish important links between implant function and end-point physiologic effects during the entire life of an animal and not only at the end of an experiment when the animal is euthanized and the construct explanted for examination.

In previous studies, we established that nuclear magnetic resonance (NMR) spectroscopy and imaging are effective methods to non-invasively monitor tissue engineered pancreatic substitutes [9, 16, 112, 113, 140, 141]. ^{1}H NMR imaging was used to visualize construct integrity and localized, water-suppressed ^{1}H NMR spectroscopy to obtain information on the number of viable cells in a construct by monitoring the resonance of choline-related metabolites. Studies were performed with βTC3 mouse

insulinoma cells encapsulated in calcium alginate/ poly-L-lysine/ alginate (APA) beads and perfused in a packed bed reactor [141]; also, with βTC3 cells encapsulated in disk-shaped agarose constructs and cultured *in vitro* [113] or implanted in the peritoneal cavity of mice [112]. Additionally, use of ^{31}P and ^{13}C NMR provides information on the bioenergetic status and metabolic pathways of cells in pancreatic constructs [9, 140, 142]. However, due to the low sensitivity of ^{31}P and ^{13}C, use of these nuclei is currently limited to the *in vitro* setting for tissue engineered substitutes. A method that directly or indirectly monitors the physiologic status of cells *in vitro* and *in vivo* would thus be highly beneficial.

A key parameter affecting cellular function is the concentration of dissolved oxygen (DO). Several studies have shown that the DO concentration influences cell viability, apoptosis [6, 7] and various aspects of cellular function. Importantly, hypoxia may inhibit cellular function without affecting viability. For instance, reducing the DO concentration to below 60 mmHg inhibits insulin secretion from perfused pancreatic islets. This effect is rapidly reversed upon reoxygenation, which demonstrates that it is not associated with cell death [5, 18]. βTC3 mouse insulinomas have been found to be more resistant to hypoxia, having their insulin secretory capacity compromised only at DO concentrations below 7 mmHg [8].

Due to its low solubility in aqueous media, oxygen is the most challenging nutrient to deliver to cells in three-dimensional constructs. Furthermore, even when properly designed for all cells to be properly oxygenated shortly after fabrication, tissue substitutes undergo remodeling with time due to cell growth, death, and possibly cell migration processes. Such remodeling changes the DO concentrations to which cells in

the construct are exposed. Interactions of a substitute with the host post-implantation *in vivo* are also likely to alter the cellular oxygen environment. For instance, development of a fibrotic layer as a result of a non-specific host response towards a construct may severely limit the delivery of oxygen to the cells within and cause malfunction or death of the implant. In most cases, implant failure is only detected at the point of complete loss of function, and at this endpoint discerning the true mode of failure may be problematic. A method allowing for the continuous monitoring of cellular viability and function in an implanted construct could help decipher the mechanism of implant failure and thus lead to improved design and ultimately enhanced clinical outcome.

Previous studies have shown that the DO concentration can be monitored using ^{19}F NMR when perfluorocarbon (PFC) emulsions are employed. Specifically, the inverse of the T_1 relaxation time of specific perfluorinated chemical groups are known to vary linearly with the DO concentration surrounding the emulsion [19, 25, 26, 103, 143] and we, as well as others, have incorporated PFC emulsions into constructs to quantify the DO concentration available to encapsulated cells. It should be noted that ^{19}F is the second most sensitive nucleus after ^{1}H and that there is no significant amount of ^{19}F normally present in tissues, hence ^{19}F NMR spectroscopy is particularly suitable for constructs in NMR-compatible bioreactors and *in vivo* situations. Nonetheless, if intra-construct oxygen profiles are to be acquired using ^{19}F chemical shift imaging, long acquisition times are required, which are a caveat to *in vivo* applications due to the long anaesthesia times required of experimental animals. To overcome this limitation, one can acquire a single DO concentration from the entire construct, representing a volume-average measurement of the oxygen profile within the volume-of-interest (VOI); a

mathematical model can then be used to assess the cellular and oxygen spatial profiles within the construct, thus allowing for rapid measurements *in vivo* [144] (CHAPTER 3).

In this work, we investigated the ability to track a pancreatic substitute by combining experimental measurements with mathematical modelling of the construct. Encapsulated cells were propagated in an NMR-compatible perfusion bioreactor and subjected to a series of step-wise decreases followed by step-wise increases of DO in the perfusion medium. The overall cellular metabolic activity was monitored by the oxygen consumption rate (OCR) of the culture and by the level of intracellular nucleotide triphosphates (NTP), measured by ^{31}P NMR spectroscopy. The cellular oxygenation state was monitored by measuring the average intrabead DO concentration (AIDO) as a function of time by ^{19}F NMR. To test the validity of the model, the model-predicted viable cell number and cellular oxygenation state were compared with the experimental results. For construct monitoring *in vivo*, both the AIDO and the external DO need to be measured with time, hence the ability to simultaneously monitor the DO concentrations in two distinct bead populations was demonstrated in mice. The importance of characterizing the dynamic responses of tissue constructs to changing environmental conditions, and the implications of such results in understanding the construct function *in vitro* and *in vivo*, are discussed.

4.3 Materials and Methods

4.3.1 Cells and Cell Encapsulation

βTC-tet cells [67] were obtaind from the laboratory of Shimon Efrat, Albert Einstein College of Medicine, Bronx, NY. Cells were cultured as monolayers in T-flasks

with culture medium changed every 2-3 days. Culture medium consisted of Dulbecco's Modified Eagle's Medium (DMEM, Sigma Chemical Co., St. Louis MO) with 25 mM glucose, supplemented with 10% fetal bovine serum, 1% penicillin-streptomycin and L-glutamine to a final concentration of 6 mM. Cell monolayers that reached 80% to 90% confluence were trypsinized with 0.05% trypsin-EDTA (Sigma) and split at a 1:5 ratio; passage number increased by one at each splitting. Cells of passage number 36-40 were used in this study.

Cells were harvested by trypsin-EDTA and encapsulated at a density of $7x10^7$ cells/ml alginate in 2% w/v low viscosity high mannuronic content alginate (product LVM, NovaMatrix, Drammen, Norway) containing 4 µl/ml of perfluorotributylamine (PFTBA) emulsion (see below). Using an electrostatic droplet generator (Nisco Engineering Inc., Zurich, Switzerland), cells were encapsulated according to the procedure of Stabler et al. [51], except that a PLL and a final alginate layer were not added. The final bead size was 960±50 µm in diameter. Some beads prepared for the *in vivo* study (described below) were coated with PLL (MW = 19,200, Sigma), without a final alginate coat, to form alginate/PLL beads. The PLL coating was performed as described previously [51]. The final layer of alginate was not added to ensure that the beads would induce an inflammatory response *in vivo*.

The PFTBA and a second PFC used in the *in vivo* studies, perfluoro-15-crown-5-ether (PFCE) (Exfluor Research Corp, Round Rock, TX), were prepared following a protocol adapted from Joseph et al. [23]. An amount of 95mg of egg yolk lecithin (~99% purity, Sigma) was added to 600 µl of cold Tyrode's salt solution (pH 7.4). While being stirred in a 0°C ice bath, the mixture was sonicated twice for 15 seconds at 300 Watts

with a 1 minute interval between sonications. A volume of 400 µl of the desired PFC was then added and the mixture was sonicated for 15 seconds at 300 W seven times with a 1 minute interval between each sonication. The emulsion was filtered through a 0.4 µm membrane filter and mixed with alginate at a ratio of 4 µl emulsion per ml of alginate.

4.3.2 Perfusion System

Figure 4.1 is a schematic of the computer controlled bioreactor and the perfusion circuit, which consisted of a perfusion, a replenishing, and a switching medium circulation loops. The perfusion loop allows for continuous delivery of nutrients and dissolved oxygen to the cells located in the bioreactor. The replenishing loop is capable of maintaining desired nutrient (e.g., glucose) concentrations during long-term perfusion experiments; however, this was not needed for experiments described in this paper. The switching medium loop is utilized to deliver an alternative medium, e.g. medium with a higher or lower glucose concentration. The volume in the medium reservoir was held constant by a second tube that was placed at the desired level and continuously pumped additional medium out of the reservoir.

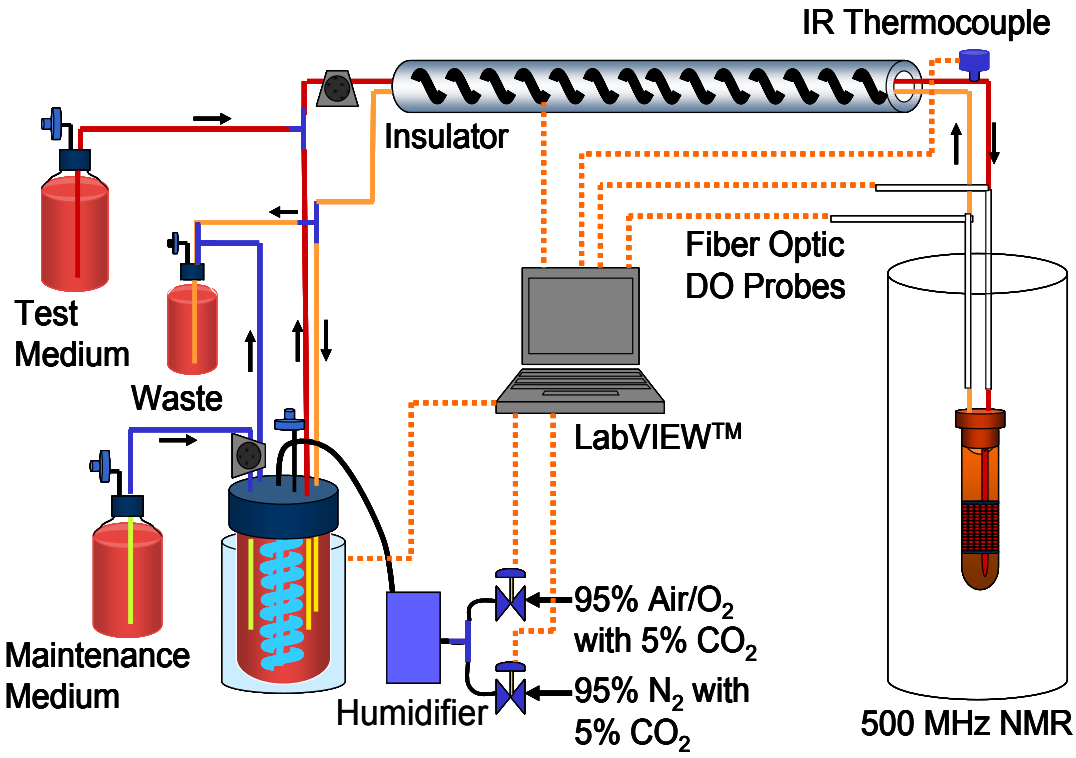

Figure 4.1 Schematic of the NMR-compatible perfusion bioreactor and support system used to control the temperature and DO concentration in the medium entering the bioreactor.

The medium within the perfusion loop circulated continuously at 8 mL/min from the medium reservoir to the bioreactor and back to the medium reservoir. At this flow rate, the bioreactor operated differentially, allowing the DO concentration to drop across the cell bed by no more than 0.025 mM, as evaluated by calculations and confirmed experimentally. The differential operation of the bioreactor made certain that the conditions for the cells at the outlet of the bioreactor were similar to the inlet, which ensured that no macroscopic heterogeneities with respect to cell viability and metabolic activity were present in the bed. On the other hand, heterogeneities of cell density and DO profiles within beads were present, and these are discussed below.

Dissolved oxygen was measured using fiber optic dissolved oxygen sensors (Ocean Optics, Dunedin, FL) both upstream and downstream of the bioreactor. The upstream dissolved oxygen probe provided the most critical measurement, henceforth referred to as DOin, since this was the DO level in the medium immediately before entering the bioreactor. The DO sensors were calibrated in the perfusion loop, first at 0.20 mM using medium equilibrated with air, and then at 0 mM using medium supplemented with 20 mM sodium hydrosulfite (Sigma). Perfusion with sodium hydrosulfite was performed single-pass, from a bottle labeled "Test Medium" in Figure 4.1 to a waste bottle. Following calibration of the sensors, the perfusion loop was purged with medium in preparation for introducing the cell-loaded bioreactor in the system.

For the monitoring and control of the perfusion circuit, a Dell Inspiron 2650 (Dell, USA) laptop computer with LabVIEW™ Full Development software (National Instruments, Austin, TX) was implemented. A constant temperature (37°C) was maintained in the medium entering the bioreactor using a 10 W/m^2 output heating tape

wrapped around foam insulation that covered the tubing both to and from the medium reservoir; a second piece of foam insulation covered the heating tape. The heating tape maintained the desired temperature via a duty cycle, which was dictated by a proportional-integral feedback loop from an infrared (IR) thermocouple placed immediately before the NMR magnet bore entrance. The temperature in the medium reservoir and at the (IR) thermocouple were kept at 38°C to account for an experimentally measured temperature drop of approximately 1°C from the NMR bore entrance to the bioreactor inlet.

Control of DO in the medium was accomplished with a control loop similar to the temperature control loop. A proportional-integral-derivative block was then connected to the DO probe upstream of the bioreactor. The algorithm controlled both the flow of air (5% CO_2, balanced with air) and nitrogen (5% CO_2, balanced with nitrogen) into the humidifier via solenoid valves (Omega Engineering, Inc., Stamford, CT) that worked in an on/off fashion. The humidifier consisted of a glass container filled with water and a glass tube with a fritted end, in which the gas entered and was dispersed into the water. The water was held at 37°C by a heating mat. An air filter was placed between the humidifier and the headspace of the medium reservoir, which was heated to 45°C to prevent condensation in the filter.

The bioreactor was designed to accommodate approximately 1.7 mL of beads. It consisted of a 10 mm diameter quartz NMR tube (Wilmad-Lab Glass, Buena, NJ) fitted with a custom-made glass cap. With the glass cap secured to the NMR tube by a compression fitting, medium entered the bioreactor through a 2 mm, outer diameter, capillary tube that ran down the center of the 10 mm NMR tube to 4 mm below the

sample at the bottom of the tube. The medium then passed through the packed bed of beads and exited through the top, returning to the medium reservoir. Beads were held in place with cotton plugs. The bioreactor was positioned in the magnet so that the beads were placed within the RF antenna of the NMR probe.

4.3.3 Dissolved Oxygen versus T_1 Relaxation Calibration Curves

The correlation between DO concentration and the T_1 relaxation time of perfluorocarbons was assessed at two different magnetic field strengths. Calibration curves were generated at 11.7 and 4.7 Tesla (T) for use at subsequent *in vitro* and *in vivo* studies, respectively.

4.3.3.1 Calibration Curve in 11.7 T Magnet

Cell-free alginate beads containing 4µl/ml of PFTBA or PFCE emulsion were loaded into the bioreactor and perfusion system. ^{19}F NMR spectra were acquired on an 11.7 T vertical bore magnet equipped with a Bruker Avance console (Bruker, Billerica, MA) using a 10 mm broadband probe equipped with a ^{1}H decoupling channel. T_1 relaxation measurements of these perfluorocarbons (with the CF_3 and the CF_2 resonance used for the PFTBA and PFCE, respectively) were made at 4 or more DO concentrations, ranging from 0 to 0.2 mM, using a standard inversion recovery pulse sequence provided by the Bruker operating software. The choice of resonances was based on literature reports demonstrating that they had the greatest sensitivity for their individual perfluorocarbon to changes in DO concentration [20]. For each T_1 measurement, 14 delay times were obtained ranging from 0.040s to 2s. Additional key acquisition parameters were: sweep width = 2.8 kHz, number of transients = 1. The T_1 relaxations were calculated using Bruker Avance software. Since beads did not contain cells, the

intrabead DO concentration was set equal to the DO concentration at the inlet of the bioreactor. The linear correlation between the inverse of the T_1 relaxation and DO is described by the following equation:

$$\frac{1}{T_1} = M \cdot DO + I$$

where *DO* is the concentration of dissolved oxygen in the aqueous phase [mM], *M* is the slope [$s^{-1}mM^{-1}$] of the $1/T_1$ vs. *DO* line, and *I* is the anoxic, y-intercept [s^{-1}].

4.3.3.2 Calibration Curve in 4.7 T Magnet:

A 4.7 T horizontal bore magnet equipped with a Varian Inova console (Varian, Palo Alto, CA) was utilized for all *in vivo* experiments; calibration curves between DO and perfluorocarbon T_1 were constructed at this magnetic field as well. The protocol described above for the 11.7 T was also used for the 4.7 T, except that the PFC concentrations were 50 µl/ml and the beads were not perfused. Instead, beads were placed in buffer equilibrated with pure nitrogen or air and sealed in a 50 ml Falcon tube. The tube was then placed on a surface coil and heated by a water bath that pumped 37°C water through tubing wrapped around the tube.

4.3.4 *In Vitro* DO Step Change Experiment

4.3.4.1 ^{19}F NMR

A total of 4-5 consecutive T_1 relaxations were acquired at the beginning and end of each DOin concentration setpoint in the 11.7 T Bruker magnet. Since each T_1 measurement took 4.34 minutes to complete, 20 to 30 minutes at the beginning and end of the DOin setpoint were used to acquire the T_1 relaxations.

4.3.4.2 ^{31}P NMR

Using the same 10 mm broadband probe that was used for the acquisition of the ^{19}F NMR spectra, ^{31}P NMR spectra were acquired on the 11.7 T Bruker magnet at each DO concentration immediately following the acquisition of ^{19}F NMR spectra. A total of six to nine ^{31}P NMR spectra were acquired at each DOin concentration, except for 0.12 mM, where a total of 27 spectra were acquired overnight, as manual switching back to ^{19}F NMR was required. Each spectrum consisted of 343 scans and a spectral width of approximately 16 kHz. Other key parameters were TR = 3 s and tip angle = 45°. Spectra were processed using MestReC Software (Mestrelab Research, A Caruña, Spain). The MestReC software was specifically used to integrate the β-NTP and inorganic phosphate (P_i) peaks. The β-NTP peak integral was then normalized to the P_i peak.

4.3.5 Mathematical Modelling

Previously a mathematical model was developed, which describes experimentally the observed cell rearrangement in capsules as a result of cell growth and death processes in alginate beads (CHAPTER 3). The cellular growth and death at specific locales within the beads were dictated by an interplay between spatial constraints and the DO concentration at each radial position [144]. To provide an initial validation, the model was used to compute the intrabead radial cellular and DO distributions vs. time. In these calculations, the model inputs were the intrinsic parameters for βTC-tet cells in APA beads [144] and the measured DOin during the *in vitro* experiment. The model output was the time-dependent cell and DO distributions, from which the total viable cell number and a volume-average intrabead DO were calculated and compared against experimental results.

4.3.6 *In Vivo* Study

Two groups of cell-free alginate beads were fabricated as described in the *Cell encapsulation* section of Materials and Methods. The first set of beads contained 50 µl/ml of PFTBA emulsion, while the second contained 50 µl/ml of PFCE emulsion and was coated with a layer of PLL to induce an inflammatory response upon implantation [145]. PFCE represented an optimal second PFC due to the small 9 ppm difference in chemical shift from PFTBA; thus, allowing for simultaneous acquisition of the T_1 relaxation from both PFCs. To ensure that any effects observed were not due to the type of PFC emulsion used, in a second experiment the PFC emulsions were switched in the two types of beads.

Eight C57BL/6J mice age 8-13 weeks were acquired from Jackson Labs (Bar Harbor, ME). On Day 0, mice were anesthetized using a chamber that contained isofluorane gas. A 1 ml, 50:50 mixture of the alginate only beads (containing PFTBA) and alginate-PLL beads (containing PFCE) were injected into the peritoneal cavity of six mice following a small incision to facilitate injection. The last two mice also received a 1 ml, 50:50 mixture of beads, in which the PFC emulsions were switched – alginate only beads contained PFCE and alginate-PLL beads contained PFTBA. On days 0, 1, 2, 6, and 7, three to six mice were anesthetized initially with 2.5% and then maintained with 1.5% isofluorane gas mixed with 95% O_2 and 5% CO_2. The mice were positioned on a rectangular saddle shape (30mm x 23.7 mm) surface coil that was attached on the outer surface of a 32 mm OD polycarbonate tube. This assembly was placed into a 4.7 T horizontal bore Varian magnet and four to six T_1 relaxation measurements were acquired from both PFC emulsions using an adiabatic inversion. A total of 23 delay times were

used ranging from 0.005s to 7s. Other acquisition parameters included acquisition time = 0.205s, TR = 12.0 s, and the number of transients = 1. The T_1 relaxation was calculated using Varian software. Standard tuning and matching were used. All T_1 measurements were then converted into DO concentrations using the previously established calibration curves.

After T_1 measurements were acquired on Day 7, mice were euthanized by CO_2 asphyxiation. Beads were collected via a peritoneal cavity lavage with 0.9% NaCl. Harvested beads were washed with 1.1% $CaCl_2$ and fixed with 3% gluteraldehyde for histological processing. Beads were embedded into paraffin blocks, sectioned, and stained with hematoxylin/eosin (H/E).

4.3.7 Statistical Methods

The differences of average intrabead DO concentrations measured via T_1 relaxation at various external DO levels (*in vitro*) studies were evaluated by two-tail t-tests. The differences in DO concentration measurements (*in vivo*) over time and between beads containing PFCE and beads containing PFTBA were evaluated using an ANOVA two-factor with replication.

4.4 Results

4.4.1 Calibration Curves

The relationship between the inverse of T_1 relaxation of the encapsulated PFTBA emulsion and the DO concentration in the perfusion medium is shown in Figure 4.2. DO concentrations were measured via the DO sensors at the inlet of the bioreactor. The $1/T_1$ measurements correlated positively and linearly with the DO concentration ($R^2 = 0.9915$)

with slope and y-intercept values of 1.80 $(s \cdot mM)^{-1}$ and 1.12 s^{-1}, respectively. Each point on the graph is the average of at least five T_1 measurements at each DO concentration, and the error bars represent the standard deviation of the $1/T_1$ values. Additionally, the fully relaxed ^{19}F NMR spectrum of the PFTBA is given with the CF_3 peak noted by an asterisk.

Table I lists the parameters for the four calibration curves determined for the two PFCs in the two magnets used in this study. As T_1 relaxations increase with decreasing magnetic field, the anoxic y-intercept was lower for both PFCs in the 4.7 T. The slopes were comparable among all four PFC calibration curves.

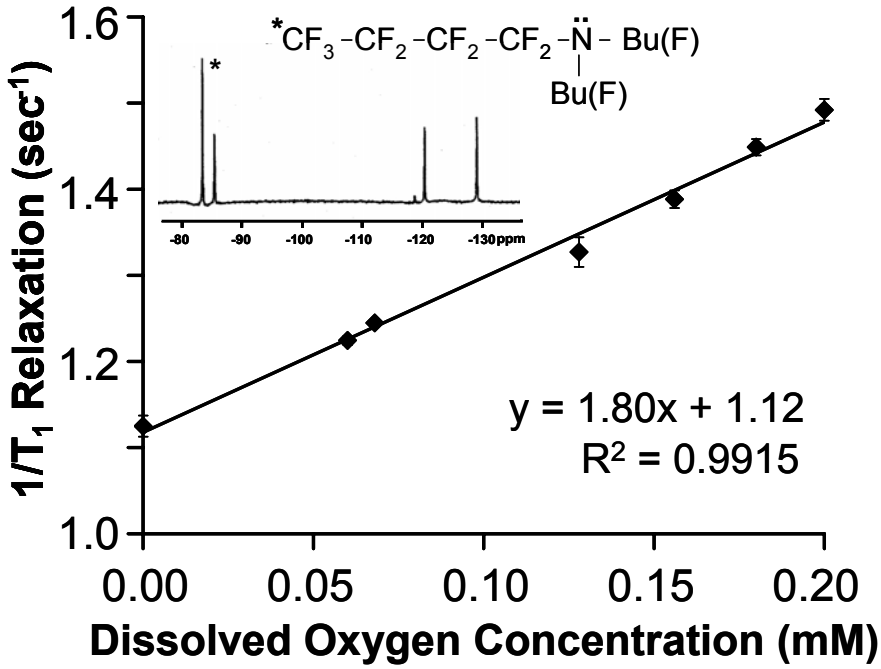

Figure 4.2 Calibration curve correlating the inverse T_1 relaxation of the encapsulated PFTBA emulsion to the dissolved oxygen concentration in the medium at 11.7 T. T_1 measurements were based on the CF_3 resonance of PFTBA. The insert displays the fully relaxed ^{19}F NMR spectrum of PFTBA as a reference. The resonance identified by an asterisk is the one used to generate the calibration curve.

Table 4.1 Slope (*M*) and y-intercept (*I*) of the linear calibration curves of $1/T_1$ vs. aqueous DO concentration. Calibrations were performed on a 11.7 T vertical bore Bruker magnet used for *in vitro* experiments and on a 4.7 T horizontal bore Varian magnet used for *in vivo* studies.

		M **[$s^{-1}mM^{-1}$]**	***I*** **[s^{-1}]**
PFTBA	***11.7 T***	1.80	1.12
	4.7 T	1.81	0.857
PFCE	***11.7 T***	1.84	0.611
	4.7 T	1.87	0.407

4.4.2 Inlet DO Concentration Effect on Intrabead Oxygenation

Figure 4.3 shows measurements from one of two independent studies that demonstrated similar trends. The DO concentration at the bioreactor inlet, DOin, was decreased in a stepwise fashion over a period of 30 hours, followed by a stepwise increase to the initial value. The oxygen consumption rate (OCR, normalized to an initial value of 100, Figure 4.3A) was measured by the sensors bracketing the bioreactor, whereas intrabead DO concentrations at the beginning and end of each DOin step were measured by ^{19}F NMR spectroscopy (AIDO start and AIDO end, connected by a solid line, Figure 4.3B). In this Figure, the DOin x-axis bar gives the duration over which the DOin concentration was held at a particular setpoint, while the y-axis bar is the standard deviation of the DOin measurements, which ranged from ±0.002 to ±0.008 mM. Each AIDO was lower than the corresponding DOin because of oxygen consumption by the cells. Changes in AIDO observed between the start and the end of a given DOin level

were not statistically significant, except at the initial DOin of 0.20 mM. However, the differences in AIDO when comparing the same DOin concentrations from the DOin decline phase and the DOin increase phase were statistically different ($p<0.05$) with the exception of the DOin at 0.08 mM. The lower AIDO values measured during the DOin increase phase were the result of a net cell growth in the beads, in accord with the uptrend of the OCR (Figure 4.3A). Similarly, the overall uptrend of the OCR, as denoted by the positive slope of the OCR regression line (Figure 4.3A), indicates a net cell growth during the experiment. However, as OCR is the product of the viable cell number and the specific consumption rate of the cells, changes in the latter caused by changes in DOin resulted in fluctuations of the OCR profile. The β-NTP/P_i integral ratios at each DOin setpoint are plotted in Figure 4.3C. At the initial high oxygen levels, the β-NTP/P_i increased from an average of 0.23 at a DOin = 0.20 mM to approximately 0.34 at a DOin = 0.12 mM. It is likely, however, that the initial β-NTP peaks were suppressed due to factors related to loading the bioreactor and incorporating it into the perfusion system. This is also evidenced by the dramatic reduction in AIDO from the start to the end of the DOin = 0.20 mM period. A regression line fitted to the points from the beginning of the DOin = 0.16 mM to the end of the DOin = 0.12 mM period indicates a specific cell growth rate of 0.21 day^{-1}, or a doubling time of 3.3 days, which is reasonable for encapsulated βTC-tet cells [51, 139, 144]. However, as the DOin was further decreased to hypoxic levels, the β-NTP/P_i also decreased, reaching a minimum of approximately 60% of the initial value. Increasing the DOin concentration from 0.05 to 0.08 mM caused the average β-NTP/P_i to increase from approximately 0.14 to 0.23 ($p<0.05$). Further increases in DOin resulted in statistically significant higher values of β-NTP/P_i,

which reached an average of 0.40 (173% of the initial or 154% of the β-NTP/P_i values at DOin = 0.16 mM). The overall increase in the β-NTP/P_i from the beginning to the end of the experiment is also indicative of the net cell growth that occurred in the system.

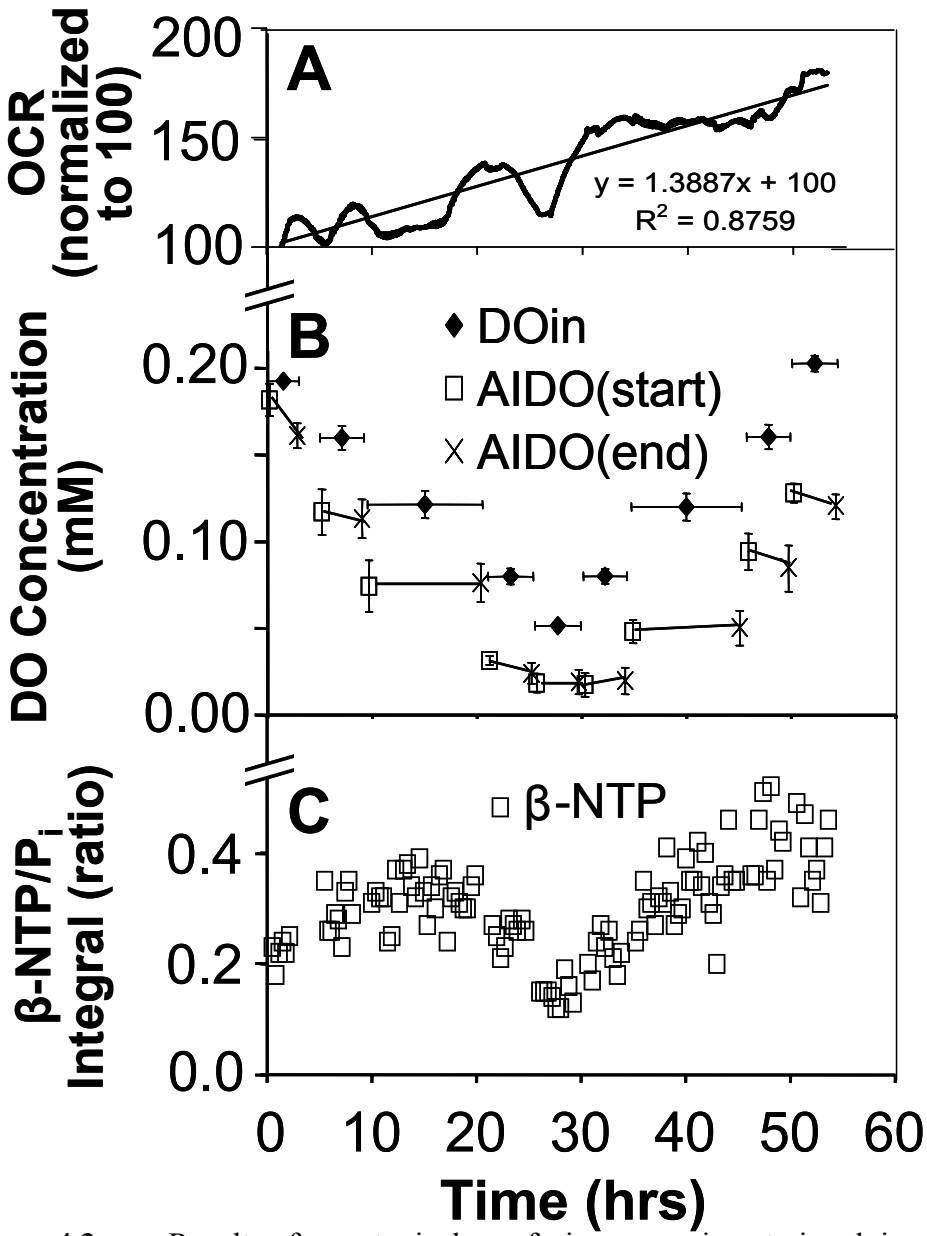

Figure 4.3 Results from typical perfusion experiment involving alginate-encapsulated βTC-tet cells. (A) Time profile of the overall oxygen consumption rate (OCR) normalized to an initial value of 100 over the course of the experiment (the actual initial value for the OCR was 1.5 mmole/(day · 10^9 cells)). A linear regression line through the OCR data and the corresponding equation are also given. (B) Prescribed changes in the DO concentration in the medium entering the bioreactor, DOin, and measured average intrabead dissolved oxygen concentrations (AIDO) in the aqueous phase. For each DOin value, the x- and y- error bars show the time period over which the DO was held at the setpoint and the standard deviation from the average DOin value, respectively. AIDO values were acquired at the very beginning (□) and end (x) of each constant DOin period; each pair of points is connected with a straight line. (C) β-NTP/P_i integral (□) plotted over the course of the experiment.

4.4.3 Simulated Cell Density and DO Profiles

A previously developed mathematical model of the encapsulated system [144] was used to simulate the results of Figure 4.3. The model used as input the DO concentration in the perfusion medium, averaged over the length of the bioreactor, and intrinsic parameters of the alginate-encapsulated βTC-tet cells to compute the cell density and DO distribution in beads. From those two, the total viable cell number in the bioreactor and the AIDO were calculated.

Comparisons of model simulations with experimental results are shown in Figure 4.4. Figure 4.4A shows the linear regression obtained from experimentally measured OCR and the model-predicted viable cell number, both normalized to an initial value of 100. The OCR regression line (solid line) closely matched the model-predicted viable cell number (dashed line). The experimentally acquired AIDOs are compared with the simulated AIDOs in Figure 4.4B. Simulations closely matched experimental data with few exceptions. Specifically, disparities were noted at the initial DOin of 0.20 mM and when DOin was increased from the minimum of 0.05 to 0.08 mM and from 0.08 to 0.12 mM. However, upon reaching 0.16 mM, the simulations again predicted the experimentally measured AIDO. At the initial 0.20 mM, the cause of the difference between the simulated and experimental AIDO is not entirely clear, but it is likely due to start up effects. Similar to the initially suppressed β-NTP/P_i peak, both the loading of the bioreactor, the brief period of no perfusion, and the initial connection to the perfusion system may have caused the cells to have a reduced oxygen consumption rate, which is manifested as a higher experimental than simulated AIDO.

To obtain insight into the β-NTP/P_i profile, the model was used to evaluate the fraction of cells exposed to DO concentration below 0.032 mM as a function of time. Previous studies with the βTC3 insulinoma line have shown that cells switch to a more anaerobic glycolytic metabolism as DO decreases below this value [8]. Results on the model-predicted fraction of cells below 0.032 mM DO are shown, along with the data on β-NTP/P_i and the simulated viable cell number, in Figure 4.4C. It can be seen that the decline in β-NTP/P_i correlates with the increase in the fraction of cells below 0.032 mM DO. When the fraction of hypoxic cells is negligible, as is the case prior to 20 and after 45 hours in the experiment, the β-NTP/P_i generally tracks the predicted viable cell number. The overall uptrend of β-NTP/P_i from the beginning to the end of the experiment correlates well with the simulated viable cell number.

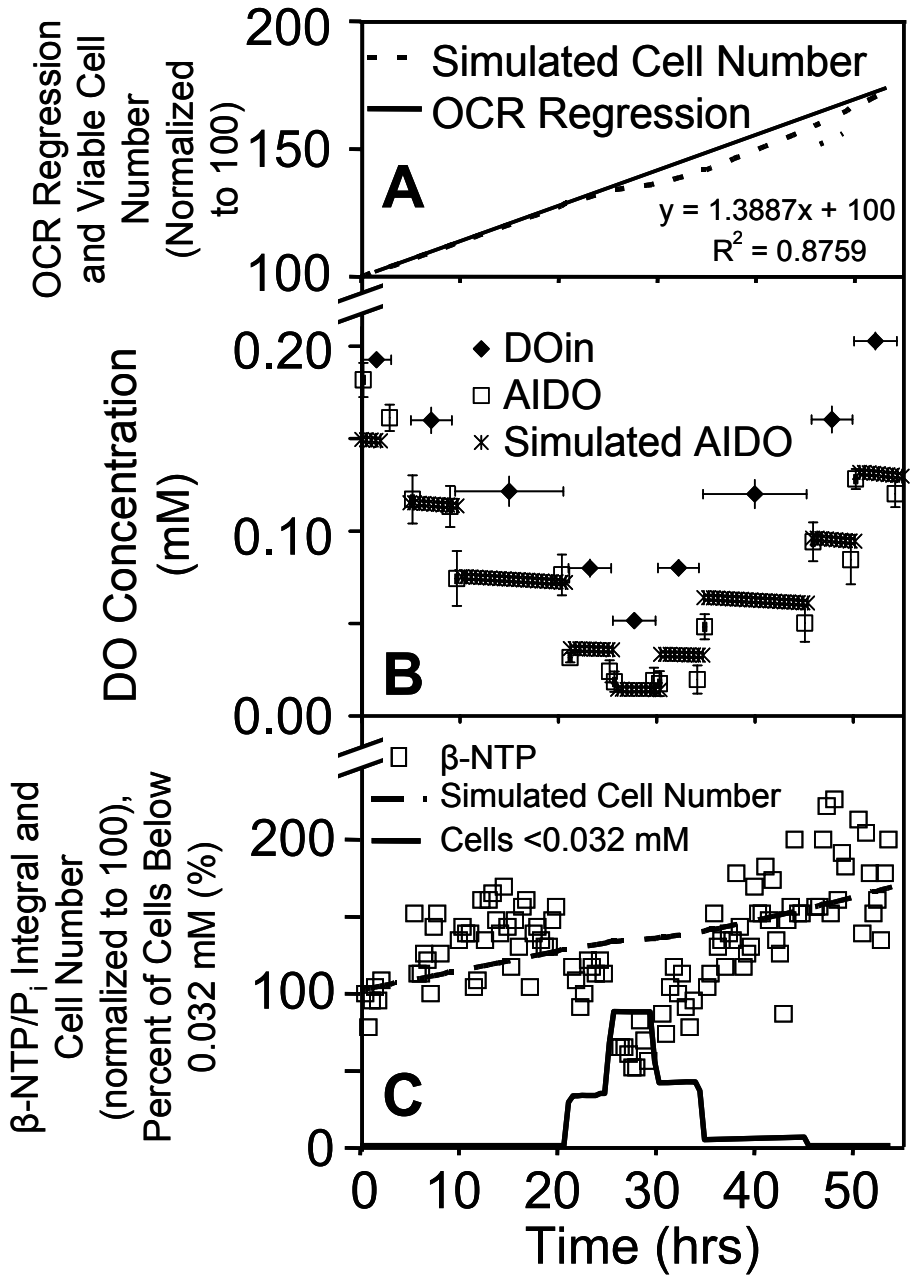

Figure 4.4 Comparison of experimental data with mathematical modelling results. (A) Comparison of the OCR regression line (solid line) with the model-predicted viable cell number (dashed line) over the course of the experiment; both initial values were normalized to 100 (actual value of the model-predicted viable cell density was 9.16×10^7 cells/ml). (B) Experimentally acquired AIDO concentrations compared with the simulated AIDO concentrations at each DOin concentration. (C) Change in the number of viable cells (dashed line), as calculated by the mathematical model and normalized to 100 at t = 0, compared against the experimentally measured change in the β-NTP/P_i integral (□), also with the initial value normalized to 100 (actual values reported in Figure 3C). The percent of viable cells exposed to less than 0.032 mM DO (solid line) is plotted for comparison against the β-NTP/P_i profile.

4.4.4 Two Perfluorocarbon System – *In Vivo*

The DO concentrations measured by ^{19}F NMR within implanted PLL and non-PLL coated alginate beads were compared between the two bead populations over the course of one week (Figure 4.5). Shortly after injecting the beads into the peritoneal cavity of six mice and on Day 1 post-implantation, measured DO concentrations in the coated and uncoated beads were statistically the same. However, on Day 2, the DO concentration in the PLL-coated beads was 0.03 mM lower than in the uncoated beads; this difference was statistically significant (ANOVA two-factor with replication). The DO concentration in the coated beads remained statistically lower than in the uncoated ones on Days 6 and 7, when the experiment was terminated. The range of DO concentrations within the peritoneal cavity over the course of the experiment was 0.02 to 0.27 mM. To verify that the above differences between the two bead populations were not PFC-specific, two mice received beads in which the PLL coating was switched to the PFTBA beads and indeed, the same trend was observed, i.e., the intrabead DO concentration became statistically lower in the PLL-coated beads relative to the uncoated ones on Day 2 post-implantation (results not shown). The Day 0 to 2 decline of intrabead DO could be the result of numerous factors that were either physiologic (e.g. heart rate and respiration rate) and/or experimental in nature (e.g. recovery from surgery and depth of anesthesia), making an explanation of the time profiles speculative and outside the scope of the study.

Histological sections of beads harvested from the peritoneal cavity of mice on Day 7 are displayed in Figure 4.5B. Approximately half of the beads exhibited fibrotic

overgrowth. A control experiment determined that alginate-only beads did not exhibit any fibrotic growth (results not shown).

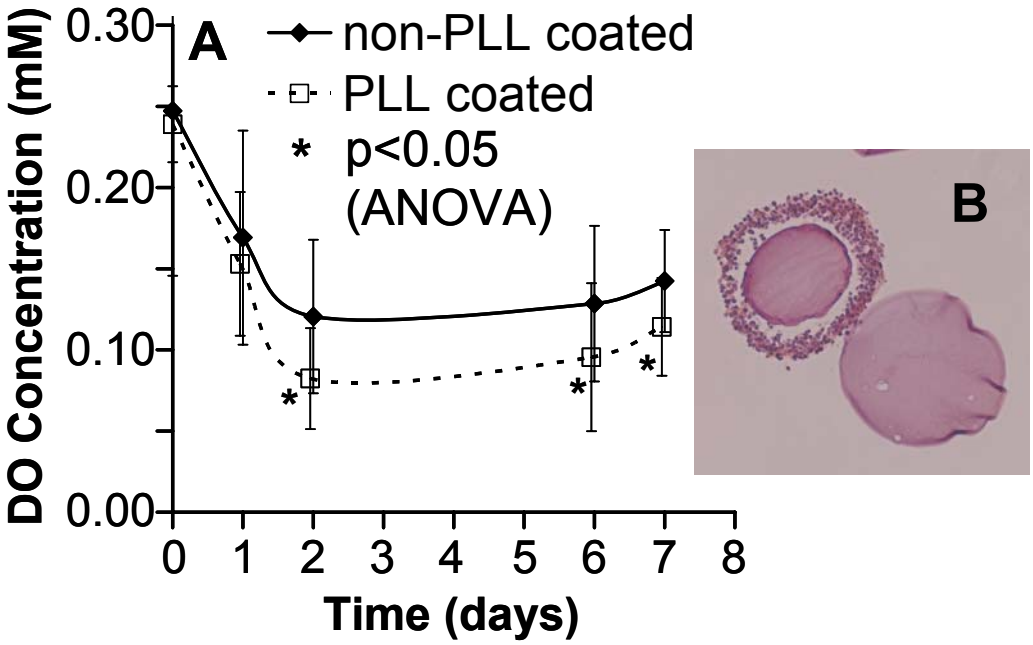

Figure 4.5 Dissolved oxygen concentrations measured within poly-L-lysine (PLL)-coated and uncoated alginate beads implanted into the peritoneal cavity of mice. PLL is known to induce an inflammatory response). (A) DO concentration in uncoated beads (♦) and in PLL-coated beads (□); the points for the uncoated (coated) beads are connected with a solid (dashed) line. (B) Histological image of representative beads harvested from mice containing a 50:50 mixture of PLL-coated and uncoated beads. A clear ring of fibrosis is seen around one of the beads.

4.5 Discussion

Nuclear magnetic resonance (NMR) imaging and spectroscopy allow non-invasive monitoring of tissue constructs and other implants for both *in vitro* and *in vivo* studies. In this work, ^{19}F and ^{31}P NMR spectroscopy in combination with mathematical modeling was used to track viable cell number and cellular physiology in a pancreatic

substitute consisting of encapsulated, insulin-secreting cells. Additionally, we demonstrated the ability to utilize ^{19}F NMR *in vivo* to measuring the DO concentration within two distinct bead populations in the mouse peritoneal cavity. Given that the ultimate success of a tissue substitute depends upon many factors that are intrinsic, i.e., inherent to the construct design, or extrinsic to the construct, including supply of nutrients and oxygen and the *in vivo* immune response towards the implant, monitoring the structural integrity of a construct, as well as the viability and function of the cells, could aide in understanding mechanisms of failure and improving functionality of the implant. *In vitro*, NMR monitoring has been used to study the biochemistry (water-suppressed ^{1}H) [141], bioenergetics (^{31}P) [9, 16] and metabolic fluxes (^{13}C) [139, 140] of the cells within alginate-based beads. *In vivo*, imaging has proven useful for monitoring structural integrity, and localized, water-suppressed ^{1}H NMR spectroscopy for monitoring viable cell number in a construct [112, 113]. However, *in vivo* ^{31}P and ^{13}C studies of encapsulated systems are very challenging due to the low NMR sensitivity of these nuclei and the relatively small number of cells within a construct. To monitor cellular physiology, we thus opted for an indirect approach that uses a low concentration of PFC emulsion in the encapsulated cell system to monitor the DO concentration in beads. Results demonstrate that ^{19}F NMR can effectively monitor an average intrabead DO concentration *in vitro* and *in vivo*. Preliminary data (not shown) indicate that incorporation of the PFC emulsion in the capsules at a low concentration of 0.4% does not affect the viability and function of βTC-tet cells.

Obtaining accurate DO concentration measurements from the sequestered PFTBA and PFCE emulsions is critical to tracking the pancreatic substitute and determining the

bioenergetic status of encapsulated cells. Since the DO values depend on the calibration curves, the slopes and intercepts of the calibration lines obtained in this study were compared to published values. The PFTBA slopes found in the 4.7 and 11.7 T magnets (1.81 $s^{-1}mM^{-1}$ and 1.80 $s^{-1}mM^{-1}$, respectively) were comparable to the value reported by Shukla et al. [26] at 7.05 T (1.85 $s^{-1}mM^{-1}$). However, due to the dependence of the T_1 relaxation on magnet strength, the y-intercept reported by Shukla et al. was comparable only to the y-intercept obtained in the 4.7 T magnet (0.852 s^{-1} vs. 0.857 s^{-1}, respectively). Similarly, the slope (1.865 $s^{-1}mM^{-1}$) and the y-intercept (0.407 s^{-1}) of the PFCE calibration curve at 4.7 T fell within the range observed by Noth et al. (2.127 $s^{-1}mM^{-1}$ and 0.346 s^{-1}, at 1.9 T) and Fan et al. (1.485 $s^{-1}mM^{-1}$ and 0.375 s^{-1}, at 4.7 T) [25, 143].

Dissolved oxygen concentration is an extrinsic factor that significantly influences both cellular bioenergetics and viability. In this study, the DO concentration entering the bioreactor was decreased stepwise from 0.20 to 0.05 mM and then subsequently returned to 0.20 mM stepwise, and the cell number and cellular responses were studied experimentally and modeled mathematically. The effect of short and long-term hypoxia on the biochemistry of encapsulated βTC mouse insulinomas has been extensively studied in the past. Using perfused alginate-encapsulated βTC3 cells, Papas et al. [15] observed that short-term (up to 24 hours) hypoxia always resulted in a decrease of NTP, measured by ^{31}P NMR spectroscopy, although the effects on insulin secretion varied depending on the rearrangement that the encapsulated cells had undergone due to growth. In longer-term (3-4 days) hypoxic episodes conducted with the same experimental system [9], the levels of NTP and phosphorylcholine were reduced, whereas inorganic phosphate exhibited a transient increase. Upon restoring the DO concentration in the perfusion

medium, all parameters returned to their pre-hypoxic levels either via gradual unidirectional changes or, for OCR, via an abrupt initial rise followed by a gradual increase to the pre-hypoxic level. This pattern of OCR increase is compatible with an initial adjustment of viable cells to the higher DO concentration followed by a net cell growth to the pre-hypoxic level. In the present study, NTP increased to approximately 170% of the initial level upon restoration of the oxygen level in the perfusion medium. This is likely due to the fact that experiments were performed shortly after the preparation of beads with an initial cell density below that supported in medium in equilibrium with air; hence, net cell growth during the experiment occurred. It can be reasonably expected that if the experiment was started with beads containing cells at the density supported under 0.20 mM dissolved oxygen, no net cell growth would have occurred over the duration of the experiment.

A previously developed mathematical model [144] simulates the changes in the distribution of cells and DO, which occur over time in a system of encapsulated βTC-tet cells. The model could also be used to provide information on the viable cell number and the cell and DO distributions in beads based on measured AIDO and the DO concentration in the surrounding milieu. Therefore, a method in which the DO concentration could be determined simultaneously from two distinct bead populations *in vivo* was explored. The method involved placing PFTBA and PFCE emulsions, which chemical shifts are only separated by 9 ppm, into two types of beads, allowing for simultaneous T_1 relaxation measurements. The beads containing PFTBA emulsion were coated with PLL, while the no additional coating was placed on beads containing PFCE. Thus, it is reasonable to assume that the lower DO concentrations measured by beads

with PFTBA were due to a fibrotic overgrowth induced by the PLL. Although in this study both bead types did not contain cells, one of the PFC emulsions could be encapsulated with cells, while the second PFC emulsion would be encapsulated in cell-free beads. The cell-free population of beads is then used to measure the DO concentration at the implantation site, as equilibration of the intrabead and the external DO is rapidly accomplished. It should also be noted that the DO level at various anatomic locales changes significantly with conditions, as was also noted in this study. For instance, Noth et al. [24] reported a -0.007 mM to 0.24 mM DO concentration range in the peritoneal cavity of rats, which is comparable to the range measured in this study (0.02 to 0.27 mM). However, in contrast to the single perfluorocarbon (F-44E) emulsion used by Noth et al. [24], the dual PFC system developed in this study allows for accurate comparisons of an experimental implant vs. a control measuring the implantation site DO. The dual PFC system could potentially also be used in biocompatibility studies addressing the inflammatory response towards various implanted materials. In this, a material that induces inflammation would rapidly develop a lower DO concentration within its volume relative to a control, non-inflammatory implant, as was observed with the PLL-coated and uncoated beads in this study.

In summary, we have shown that incorporation of a low concentration of PFC emulsion in an encapsulated cell system allows for the rapid, non-invasive measurement of the average intrabead DO concentration by ^{19}F NMR. A system of alginate-encapsulated mouse insulinomas was subjected to changes in external DO in a perfusion bioreactor and studied by following intrabead DO and cellular β-NTP by NMR spectroscopy, and by measuring the oxygen consumption rate of the culture by dissolved

oxygen sensors. Using a mathematical model of the encapsulated cells can significantly assist the tracking of this system on the basis of a limited amount of rapidly obtained experimental data. *In vivo* experiments demonstrated the feasibility of measuring simultaneously the intrabead DO in two different bead populations in the peritoneal cavity of mice. The developed experimental and mathematical modeling methodologies are expected to enable the non-invasive tracking of the dynamic changes in encapsulated cell systems post-implantation *in vivo*.

CHAPTER 5

MONITORING A PANCREATIC SUBSTITUTE DURING TRANSIENT HYPOXIA AND CELL DEATH

5.1 Abstract

Upon implantation, tissue engineered substitutes are subject to a variety of conditions that could ultimately lead to the loss of function. In this work, we have investigated the utility of a previously established non-invasive monitoring method in tracking pancreatic substitutes exposed to two mimicked *in vivo* scenarios – specifically, fluctuations in dissolved oxygen (DO) due to an inflammatory response and a cytokine attack due to a biocompatibility issue with the substitute. To mimic the changes in DO levels, encapsulated βTC-tet cells were placed in an NMR-compatible perfusion circuit and the medium DO concentration perfusing the bioreactor was declined stepwise from 0.20 to 0.04 mM and then returned in the same increments to 0.20 mM. During the study, the cellular metabolic activity and bioenergetics were evaluated by measuring the oxygen consumption rate (OCR) (via DO sensors) and nucleotide triphosphate levels (via ^{31}P NMR). The average intrabead DO (AIDO) concentration was also acquired using a PFC emulsion sequestered within the pancreatic substitute and ^{19}F NMR. AIDO measurements were converted to an estimate of cell density using a mathematical model (CHAPTER 3) over the course of the study, and the AIDO-based estimates were compared to those based on OCR. In the second study, the ability to track cell death (induced by puromycin) using AIDO measurements and the mathematical model was evaluated. Again, OCR and AIDO-estimated changes in cell density were compared. It was found that, in both studies, the AIDO measurement, which can be performed non-

invasively *in vitro* and *in vivo*, was indeed capable of tracking a pancreatic substitute. The use of this method in distinguishing between modes of tissue substiute failure upon *in vivo* implantation is discussed.

5.2 **Introduction**

The engineering of living tissues, also known as tissue engineering, has shown tremendous promise in replacing or repairing normal body functions that have been lost due to injury or disease [4]. Typically, cells are manipulated external to the body through either their environment or genetic engineering and then joined with an appropriate scaffold to allow for handling and proper function. Prior to transplantation, this tissue substitute is often cultured, manipulated, and monitored *in vitro* until the desired properties are achieved with the most critical properties being cell viability and proper function. Numerous methods are available for the *in vitro* assessment of these construct properties. However, upon implantation such parameters prove difficult to track, leaving physicians and researchers to rely on indirect methods of monitoring. Such indirect monitoring methods are non-ideal as they typically only show a substitute is not functioning properly when it is too late to provide any adjustments to reverse the course of malfunction. Therefore, a method that can directly monitor a tissue substitute *in vivo* would be valuable.

Nuclear magnetic resonance (NMR) imaging and spectroscopy have been shown to be robust non-invasive monitoring techniques by our group and others [9, 16, 112, 113, 120, 139, 142, 146]. ^{1}H NMR imaging and spectroscopy have been used to monitor structural features and the number of viable cells, respectively, within pancreatic

substitutes both *in vitro* and *in vivo* [112, 113]. Specifically, the pancreatic substitute consisted of βTC3 mouse insulinoma cells encapsulated in alginate/poly-L-lysine/alginate (APA) beads or agarose disks and either maintained in a long-term perfusion system or implanted into the peritoneal cavity of mice, respectively. ^{13}C NMR and ^{31}P NMR have also been used to assess the metabolic fluxes and the bioenergetic status of cells contained in pancreatic substitutes *in vitro* [16, 123, 126, 142]. However, given the especially low sensitivity of these NMR nuclei, *in vivo* utilization is not currently plausible; thus, a non-invasive method that directly or indirectly monitors the physiologic status of cells *in vitro* and *in vivo* would be highly beneficial.

The dissolved oxygen (DO) concentration is known to have an impact on both cell viability and function [6, 7, 9, 15, 17]. This impact has been demonstrated in pancreatic substitutes involving islets of Langerhans and the βTC3 mouse insulinoma cell line [5, 9, 15, 18, 124], where islets were shown to have diminished insulin secretion below a DO concentration of 60 mmHg and βTC3 cells below 7 mmHg. It should be noted that the effect of DO on viability and function is not always proportional, as cellular function is often diminished at higher DO concentrations than that which would cause cellular apoptosis and death [7, 8]. This becomes increasingly important in tissue substitutes, where dissolved oxygen gradients are created due to oxygen consumption by cells at the periphery and the low solubility of oxygen in water. In tissue substitutes in which continuous cell lines are used, these DO gradients change with time due to cell growth and death processes. Additionally, upon implantation, many *in vivo* factors cause constantly changing DO concentrations immediately external to the tissue substitutes. For example, Noth et al [24] and Gross et al [43] (CHAPTER 4) reported that the DO

concentration varied widely over time in the peritoneal cavity of rats and mice, ranging from -0.007 to 0.24 mM and 0.02 to 0.25 mM, respectively

Given the strong dependence of cellular viability and function on DO concentrations, our group, as well as others, has been developing NMR-based methods for assessing the DO concentration within tissue constructs [24, 32, 102]. Specifically, the inverse T_1 relaxation of perfluorocarbon emulsions sequestered in hydrogels has a linear relationship with the DO concentration in the surrounding aqueous solution. The T_1 relaxation rate is measured using ^{19}F NMR spectroscopy, which should be noted as the second most sensitive NMR nucleus and is not found naturally *in vivo*. Therefore, one could quantify the oxygen profiles within an implanted tissue substitute by performing two or three dimensional localized spectroscopy. However, such a three-dimensional reconstruction of oxygen profiles would require high concentrations of perfluorocarbon emulsion and may prove impractical due to the long anesthesia time that would be required. Alternatively, one DO concentration measurement can be acquired from the entire construct, representing a volume-averaged value of the entire construct; a mathematical model can then be used to assess the cellular and oxygen spatial profiles within the construct, which would greatly increase the speed of acquisition.

In CHAPTER 4, we demonstrated the ability to track cellular growth and oxygen profiles using ^{19}F NMR and a mathematical model. In these experiments, freshly encapsulated βTC-tet mouse insulinoma cells were placed into an automated long-term perfusion system and subjected to DO concentration step changes over the course of 50 hours. During the study, ^{19}F NMR was used to measure the volume averaged intrabead dissolved oxygen (AIDO) concentration within the pancreatic substitutes, whereas the

bioenergetic status of the cells was monitored using ^{31}P NMR, and the oxygen consumption rate of the cells was monitored using two DO sensors bracketing the bioreactor. Mathematical simulations of cell growth and AIDO were in good agreement with experimental data. In addition, the study demonstrated the ability to acquire DO concentration information from two distinct constructs *in vivo* via a dual perfluorocarbon system.

This chapter augments the above work by implementing the method to two mimicked *in vivo* scenarios. First, the ability of the mathematical model and ^{19}F NMR to track cell growth in alginate beads that were cultured for one week prior to being placed in the NMR-compatible perfusion system and then subjected to DO concentration step changes is evaluated. This study is designed to reproduce monitoring that may occur during *in vivo* experiments, where parameters influencing cell function and viability are not continuously monitored and the DO concentration can vary widely from day to day. The second scenario is designed to study the ability of the system to monitor cell death if a cytotoxic immune response occurs after such a pancreatic substitute is implanted. Specifically, the AIDO and medium DO concentration are used to assess the cell density within alginate beads after the addition of puromycin, a toxic antibiotic. The translation and importance of these studies to *in vivo* monitoring of implanted pancreatic substitutes are discussed.

5.3 Materials and Methods

5.3.1 Cells and Cell Encapsulation

βTC-tet cells [67] were obtained from the laboratory of Shimon Efrat, Albert

Einstein College of Medicine, Bronx, NY. Cells were cultured as monolayers in T-flasks with culture medium changed every 2-3 days. Culture medium consisted of Dulbecco's Modified Eagle's Medium (DMEM, Sigma Chemical Co., St. Louis MO) with 25 mM glucose, supplemented with 10% fetal bovine serum, 1% penicillin-streptomycin and L-glutamine to a final concentration of 6 mM. Cell monolayers that reached 80% to 90% confluence were trypsinized with 0.05% trypsin-EDTA (Sigma) and split at a 1:5 ratio; passage number increased by one at each splitting. Cells of passage number 36-40 were used in this study.

Cells were harvested by trypsin-EDTA and encapsulated at a density of $7x10^7$ cells/ml alginate in 2% w/v low viscosity high mannuronic content alginate (product LVM, NovaMatrix, Drammen, Norway) containing 4 μl/ml of perfluorotributylamine (PFTBA) emulsion (see below). Using an electrostatic droplet generator (Nisco Engineering Inc., Zurich, Switzerland), cells were encapsulated according to the procedure of Stabler et al [51], except that a PLL and a final alginate layer were not added. The final bead size was 925±52 μm in diameter.

The PFTBA was prepared following a protocol adapted from Joseph et al [23] and previously described by Gross et al [43] (CHAPTER 4).

5.3.2 Perfusion System

The NMR-compatible perfusion system and bioreactor utilized in this study has been fully described previously [43] (CHAPTER 4). In brief, the perfusion system consisted of a perfusion, a replenishing, and a switching medium circulation loop. For the purpose of these experiments, the perfusion loop was used exclusively, which allowed for continuous delivery of nutrients and dissolved oxygen (DO) to the cells located in the

bioreactor. The DO concentration at the bioreactor inlet and the medium temperature were maintained at user defined set-points via computer directed proportional-integral control loops, DO sensors bracketing the bioreactor, and an infrared T thermocouple.

5.3.3 DO Step Change Experiment

βTC-tet cells were encapsulated in alginate beads and cultured in a 37°C incubator for one week. At the start of the study, approximately 2 mls of beads were loaded into the bioreactor and attached to the perfusion system. The bioreactor was placed into a 11.7 T vertical bore magnet equipped with a Bruker Avance console (Bruker, Billerica, MA) and a 10 mm broadband probe. The DO concentration entering the bioreactor was initially set to 0.20 mM, after which the DOin setpoint was decreased by increments of 0.04 mM approximately every 4 hours. Upon reaching 0.04 mM, the DOin was then returned to 0.20 mM using the same increments as during the decline phase. It should be noted that during both the decline and incline phase, the DOin setpoint of 0.12 mM was maintained for approximately 10 hours overnight. To assess the intrabead DO concentration, a total of 4-5 consecutive T_1 relaxations were acquired by ^{19}F NMR (see parameters below) at the beginning and end of each DOin concentration setpoint. Since each T_1 measurement took 4.34 minutes to complete, 20 to 30 minutes at the beginning and end of the DOin setpoint were used to acquire the T_1 relaxations. The T_1 relaxation rates were converted into DO concentrations using a previously established calibration curve [43] (CHAPTER 4). ^{31}P NMR spectra were acquired (see parameters below) at each DO concentration immediately following the acquisition of ^{19}F NMR spectra for T_1 determination. A total of six to nine ^{31}P NMR spectra were acquired at

each DOin concentration, except for 0.12 mM, where a total of 27 spectra were acquired overnight.

5.3.3.1 ^{31}P NMR

Each ^{31}P NMR spectrum consisted of 344 scans and a spectral width of approximately 16 kHz. Other key parameters were TR = 3 s and tip angle = 45°. Spectra were processed using MestReC Software (Mestrelab Research, A Caruña, Spain). The MestReC software was specifically used to integrate the β-NTP and inorganic phosphate (P_i) peaks. The β-NTP peak integral was then normalized to the P_i peak.

5.3.3.2 ^{19}F NMR

For each T_1 measurement, 14 delay times were obtained ranging from 0.040s to 2s. Additional key acquisition parameters were as follows: sweep width = 2.8 kHz, number of transients = 1. The T_1 relaxations were calculated using Bruker Avance software.

5.3.4 Toxicity Experiment

One day after encapsulation, approximately 2 ml of beads were loaded into the bioreactor, at which point the bioreactor was attached to the perfusion system. The bioreactor was placed into the 11.7 T vertical bore magnet, as described above. The DOin was set to 0.14 mM and maintained at this concentration for the remainder of the study. With the DOin stabilized at the desired value, three ^{31}P NMR spectra were acquired over the course of one hour (see parameters and processing in previous section), serving as the pre-stressed condition of the cells. The ^{31}P NMR spectra were followed by 5 T_1 relaxation measurements of the immobilized PFTBA emulsion acquired by ^{19}F NMR (see parameters and processing in previous section) over 30 minutes. At the 2 hour mark,

puromycin (Sigma) was added to the system at a final concentration of 10μg/ml – preliminary tests showed that an approximately 40% reduction in viable cell number occurred in 24 hrs at this concentration (data not shown). Puromycin is an antibiotic that interferes with protein synthesis by ending mRNA translation prematurely [147]. For the next hour, several T_1 relaxation measurements by were taken for an hour followed by T_1 measurements being acquired every 55 minutes. Approximately 11 hours after the addition of puromycin, ^{31}P NMR spectra were acquired again amongst intermittent T_1 relaxation measurements for the remainder of the experiment. The entire study lasted approximately 48 hrs.

5.4 Results

5.4.1 Monitoring Cell Growth

Figure 5.1, A and B, shows measurements from one of two independent studies that demonstrated similar trends, while Figure 5.1 C included data from both studies to demonstrate the reproducibility. The DO concentration entering the bioreactor (DOin) was decreased stepwise from 0.20 mM to 0.042 mM and then returned to 0.20 mM (Figure 5.1 B). During the experiment, the oxygen consumption rate (OCR), the average intrabead DO (AIDO) concentration, and the β-NTP/P_i integral ratio were monitored (Figure 5.1 A, B, and C, respectively). During the first 8 hours, the measured OCR– determined by DO sensors bracketing the bioreactor –increased from an initial value of 1.9 to approximately 2.5 mmole/(day·10^9 cells). The OCR then remained between 2.4 and 2.7 mmole/(day·10^9 cells) until the DOin was changed from 0.08 mM to 0.042 mM, at which point the OCR dropped by almost 50% to 1.3 mmole/(day·10^9 cells). The OCR

quickly returned to 2.4 mmole/(day·10^9 cells) when the DOin was increased back to 0.08 mM. For the remainder of the DOin step increases, the OCR remained essentially constant with only a slight increase observed going from a DOin of 0.12 mM to 0.16 mM. The small difference in OCR from the DOin decline phase to the incline phase indicates that there was little to no net cellular growth over the 55 hours. Likewise, little difference was observed in the AIDOs (Figure 5.1 B) when comparing values from the DOin decline to incline phase. However, a statistical difference ($p<0.05$) was observed in the β-NTP/P_i integral ratios (Figure 5.1 C) when comparing ratios from the start of the experiment (100) to ratios at the end of the study (53 ± 6 in Exp-1 and 65 ± 8 in Exp-2). As expected, the lowest integral ratios were observed at a DOin of 0.042 mM, where the ratios were 31 ± 6 and 43 ± 14 for Exp-1 and Exp-2, respectively.

OCR and AIDO measurements were converted into cell density estimates and plotted in Figure 5.2. The OCR measurements were converted to cell densities based on a previously published specific oxygen consumption rate, q_O, of encapsulated βTC-tet cells (1.65 mmole/(day•10^9cells)) [43] (CHAPTER 4), which was comparable to previously published q_O of βTC3 cells (1.63 mmole/(day•10^9cells)) [125]. The AIDOs were converted using a previously established mathematical model [148] (CHAPTER 3). It should be mentioned that using a constant q_O value to convert the OCR measurements to cell densities scales the former linearly; hence, the OCR-estimated cell density profile in Figure 5.2 is identical to that of the OCR profile in Figure 5.1 A. However, the cell density estimates based on AIDO may be more accurate, as this conversion accounts for the reduction in oxygen consumption rates at lower oxygen levels. Nonetheless, the initial OCR and AIDO-estimated cell densities were approximately the same at 8.15 and

7.48 x 10^7 cells/ml, respectively (Figure 5.2). The change in estimated cell densities were in general agreement for the remainder of the study with each indicating a significant drop from hour 25 to 29, corresponding to the DO concentration drop in the surrounding medium. It should be pointed out that AIDOs are the only measurements of the two that can be acquired non-invasively and *in vivo*.

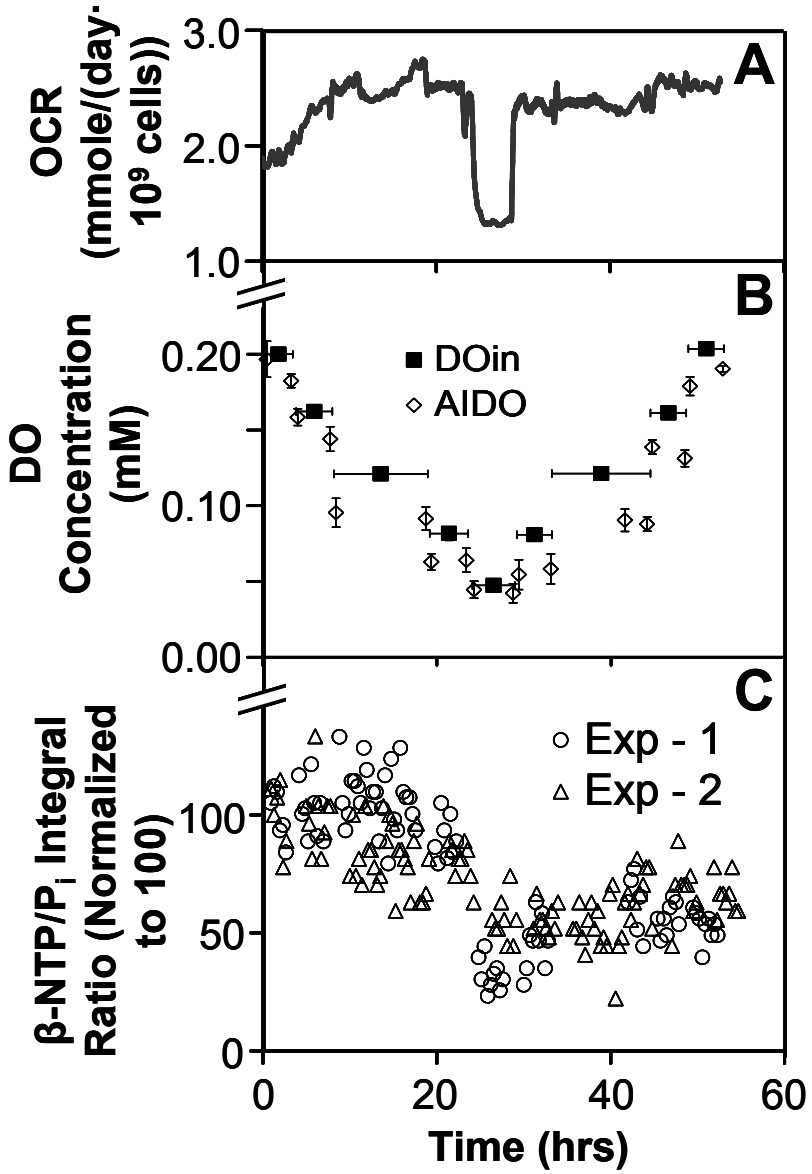

Figure 5.1 Results from a typical perfusion experiment involving alginate-encapsulated βTC-tet cells. (A) Time profile of the overall oxygen consumption rate (OCR) over the course of the experiment. (B) Prescribed changes in the DO concentration in the medium entering the bioreactor, DOin, and measured average intrabead dissolved oxygen concentrations (AIDO) in the aqueous phase. For each DOin value, the x- and y- error bars show the time period over which the DO was held at the setpoint and the standard deviation from the average DOin value, respectively. The AIDO y-error bars represent the standard deviation of the measurements. (C) β-NTP/P_i integral ratios normalized to 100 from two separate experiments plotted over the course of the experiment.

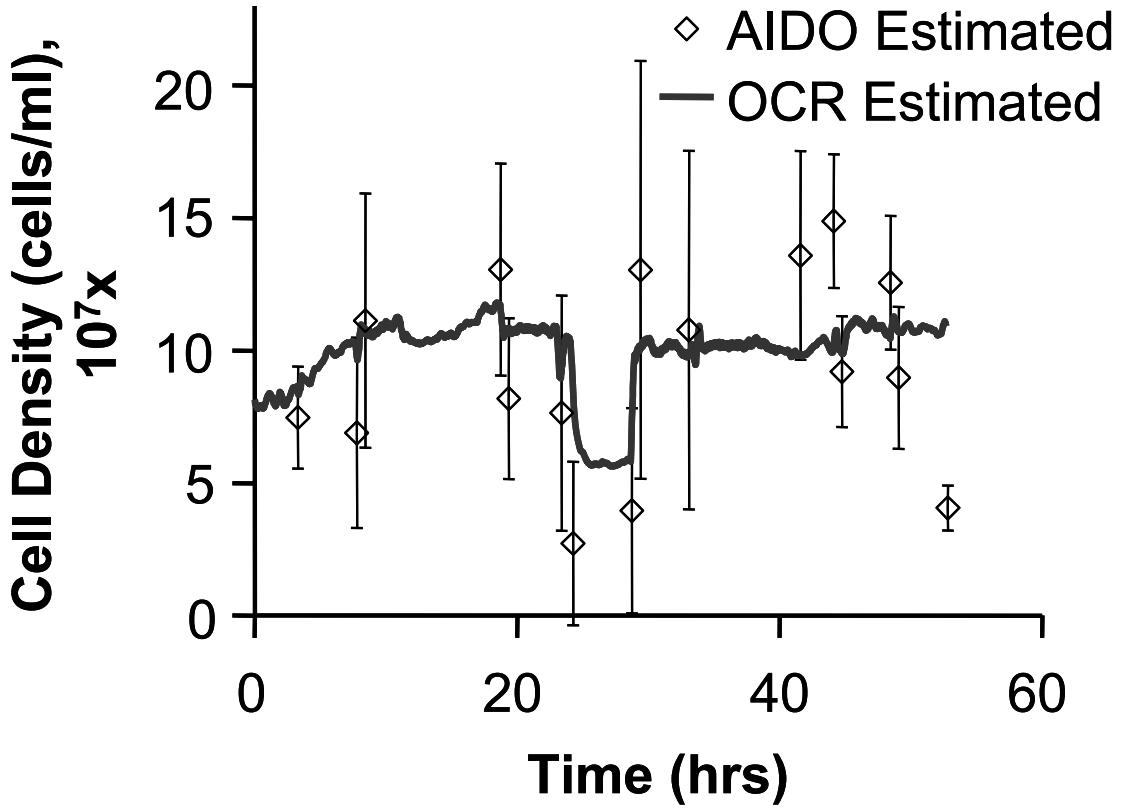

Figure 5.2 Estimated cell densities based on OCR measurements acquired from DO sensors bracketing the bioreactor and AIDO measurements acquired by ^{19}F NMR. OCR-based estimates used a previously measured value of the oxygen consumption rate of encapsulated βTC-tet cells (1.65 mmole/(day•10^9cells)) [148]. AIDO-based estimates were determined from a previously established mathematical model. Vertical bars indicate the standard deviation from the average.

5.4.2 Monitoring of Cell Death

The status of encapsulated cells immediately prior and after being exposed to 10 μg/ml puromycin was tracked for over 45 hours (Figure 5.3). Specifically, the OCR, the AIDO, and the β-NTP/P_i integral ratios were monitored (Figure 5.3 A, B, and C, respectively). During the first 2 hours, the OCR increased from 1.8 to 2.1 mmole/(day·10^9 cells). However, upon the addition of puromycin, the OCR reached a

temporary plateau at approximately 1.9 mmole/(day·10^9 cells) and by hour 5 (3 hours after the addition of puromycin), the OCR began a steady descent. The final OCR value was approximately 0.9 mmole/(day·10^9 cells), 50% below the starting value. A quick response to the addition of puromycin was also observed in the change of AIDO (Figure 5.3 B). Initially, the AIDO was approximately 0.08 mM, 0.06 mM below the DOin concentration of 0.14 mM. It should be noted that the difference between the AIDO and DOin is due to the DO concentration profiles created by the cellular oxygen consumption; thus, a smaller difference is the result of fewer viable cells. Like the OCR, the AIDO began to increase at hour 5, which was quick and pronounced, reaching 0.12 mM by hour 12. The AIDO then fluctuated between 0.11 and 0.136 mM for the remainder of the study. Unlike the relatively quick response of the OCR and AIDO to the addition of puromycin, the β-NTP/P_i integral ratios remained at approximately 100 for the first 13 hours of the study (Figure 5.3 C). Approximately 11 hours after the addition of puromycin to the medium, the β-NTP/P_i integral ratio began to decrease. Initially, the decrease occurred rapidly, dropping from 100 to 50 in 14 hours. The rate of decrease then slowed for the remainder of the study (27 to 48 hours), reaching an ultimate value of approximately 25.

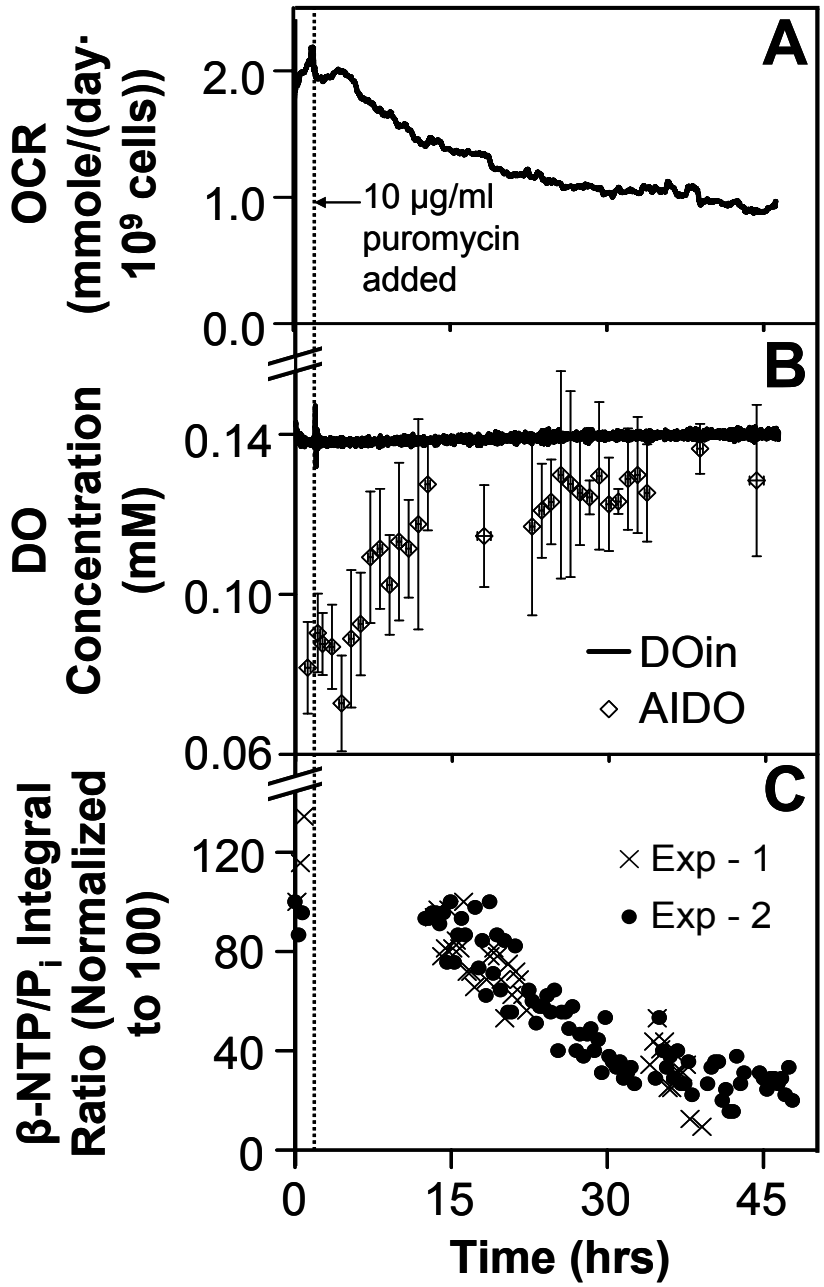

Figure 5.3 Results from a typical toxicity experiment involving alginate-encapsulated βTC-tet cells. (A) Time profile of the oxygen consumption rate (OCR) over the course of the experiment. (B) The DO concentration in the medium entering the bioreactor, DOin, and measured average intrabead dissolved oxygen concentrations (AIDO) in the aqueous phase. Vertical AIDO bars are the standard deviation of five contiguously measured AIDO concentrations. (C) β-NTP/P_i integral ratios normalized to 100 from two separate studies plotted over the course of the experiment. The gap in β-NTP/P_i integral from 2 to 13 hours is due to continuous AIDO measurements during this time period. The dashed line stretching through the three panels at 2 hours is the time point at which the 10 µg/ml puromycin was added.

As in the previous study (Figure 5.2), OCR and AIDO measurements were converted into cell density estimates and plotted in Figure 5.4. Initially, the AIDO predicted a higher density than the OCR, 13.3 x 10^7 cells/ml vs 7.5 x 10^7 cells/ml, respectively. However, this difference was within one standard deviation of the AIDO measurement and by hour 7, the AIDO-estimated cell densities closely matched the OCR-based cell density estimates. Both AIDO and OCR-based estimates exhibited a steady decline for the remainder of the study, reaching a final value of approximately 3.8 x 10^7 cells/ml.

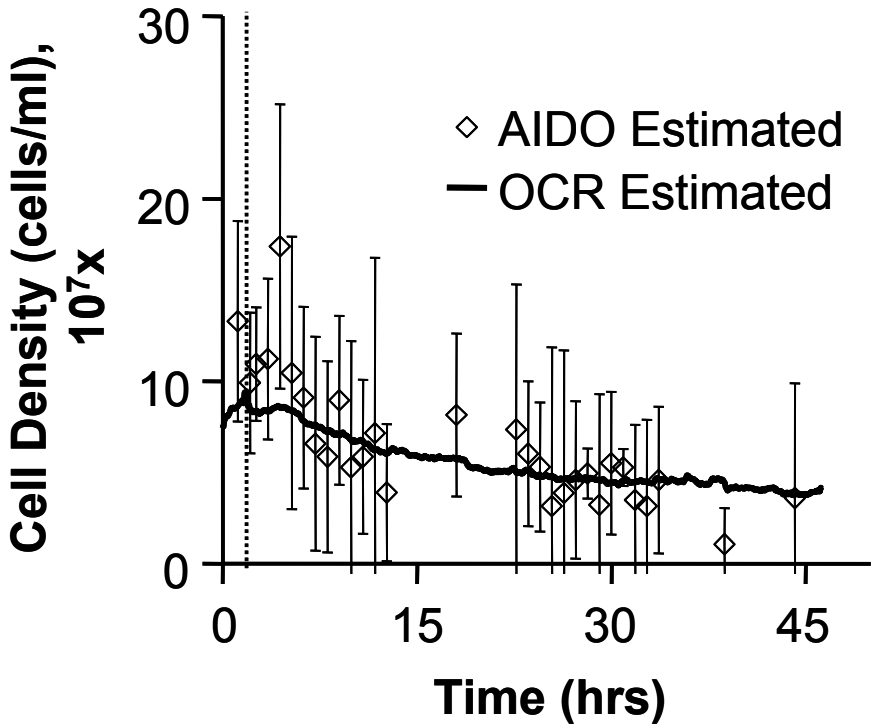

Figure 5.4 Estimated cell densities based on OCR measurements acquired from DO sensors bracketing the bioreactor and AIDO measurements acquired by ^{19}F NMR. The vertical bars of the AIDO-based estimates represent the standard deviation of five or more AIDO measurements. The dashed line at hour 2 is the point at which puromycin was added to a concentration of 10 µg/ml.

5.5 Discussion

Cell-based pancreatic substitutes have the potential of becoming a treatment option for insulin-dependent diabetics, as the need for insulin injections would decrease and the long-term complications would likely be mitigated as the substitute could provide near physiologic control of blood sugar. However, upon *in vivo* implantation, these substitutes can be subjected to an array of conditions that could ultimately be detrimental to the function and viability of the sequestered cells. Hence, non-invasive methods that are capable of monitoring an implanted pancreatic substitute are essential. Nuclear magnetic resonance (NMR) imaging and spectroscopy allow non-invasive monitoring of tissue constructs and other implants for both *in vitro* and *in vivo* studies. Previously, we established a method – consisting of DO measurements obtained by ^{19}F NMR and a mathematical model – that enabled the tracking the DO concentrations within the capsules and the bioenergetic status of freshly encapsulated βTC-tet cells. In this CHAPTER, we performed two studies to test the ability of the method to monitor βTC-tet cells (encapsulated in alginate) that were cultured for one week *in vitro* and that were subjected to changes in medium DO concentration and to the addition of puromycin, a potent antibiotic. These two *in vitro* studies were designed to mimic potential *in vivo* scenarios that occur upon implantation.

The first study tested the ability to monitor encapsulated cells that were subjected to changing DO concentrations. Specifically, the DO concentration of the medium entering the bioreactor was decreased stepwise from 0.20 to 0.042 mM and then returned to 0.20 mM, while the OCR was monitored by DO sensors bracketing the bioreactor, AIDO concentrations were measured by ^{19}F NMR, and the β-NTP/P_i integral ratio was

determined by ^{31}P NMR. Such changes in the DO concentration at the surface of implanted beads could occur *in vivo* due to normal DO fluctuations or from an induced fibrotic response to the tissue substitute – each of these two scenarios were noted during the *in vivo* study in CHAPTER 4. In this study, beads were cultured in an incubator for one week prior, since such encapsulated cell systems potentially have more pronounced DO gradients due to a net increase in viable cell number from the time of encapsulation and may more closely represent the type of bead that would be implanted. Additionally, the more pronounced DO gradients of beads cultured for longer periods may make the higher viable cell number within such beads more susceptible to hypoxic environments compared to freshly encapsulated βTC-tet cells that have relatively shallow DO gradients from the bead periphery to the center [148] (CHAPTER 3). However, upon measuring the OCR and the AIDO of the encapsulated cells, it was noted that over the one week of culture only a minimal net cell growth had occurred within the beads. Indeed, the initial encapsulation cell density was 7×10^7 cells/ml and both OCR and AIDO measurements estimated the starting cell density to be approximately 8×10^7 cells/ml. In addition, over the 55 hours of the study, little change was observed in the cell density. This minimal net cell growth over the one week of culture and during the 55 hours of the study was unexpected, as encapsulated βTC-tet cells in CHAPTER 4 almost doubled in 4 days. However, the purpose of this experiment was not to evaluate the underlying cause of the behavior of the encapsulated cells, rather to use the measurements and the model to track the system, and in this the objectives of the experiment were met. In particular, OCR, AIDO and the β-NTP/P_i integral ratio were tracked non-invasively, and the mathematical model was in general agreement with experimental results. An exception was the

deviation of AIDO and OCR measurements from the β-NTP/P_i integral ratio during the DOin incline. However, this lag in β-NTP changes compared to changes in OCR has been shown previously in studies of hypoxia on βTC3 cells by Papas et al. [9, 15].

The second study performed in this CHAPTER investigated the ability of the AIDO measurement and the mathematical model to detect a net loss of viable βTC-tet cells within an encapsulated cell system. The study was designed to mimic an *in vivo* immune cytokine attack against an implanted pancreatic substitute. Such an immunological attack has been noted by Safley et al [149], where increased amounts of inteleukin-5 (IL-5), IL-12, TGF-β, and IL-1β were found within the peritoneal cavity of mice after encapsulated islets were transplanted to this site. Mimicking such an immune response was accomplished by the addition of puromycin to the perfusing medium. Prior to the addition of the puromycin, baseline values for the OCR, AIDO, and β-NTP/P_i integral were acquired by DO sensors bracketing the bioreactor, ^{19}F and ^{31}P NMR, respectively. Within a few hours after the addition of puromycin, the OCR began to decrease and the AIDO increased, approaching that of the external DO concentration. Both of these changes indicated a loss in cell number and thus demonstrated the ability of the AIDO to detect a loss in viable cell number.

In summary, the combination of ^{19}F NMR measured average intrabead DO concentrations and a mathematical model was capable of estimating the cell densities within pancreatic substitutes during two *in vitro* conditions. The *in vitro* conditions were designed to mimic changes in the DO concentration – due to either natural fluctuations or an inflammatory response – and a cytotoxic immune response – due to a biocompatibility issue with a pancreatic substitute. Given the validation provided in this CHAPTER, it is

likely that the methodology of using ^{19}F NMR to measure AIDO, enabled by the mathematical model, could distinguish between various modes of failure upon *in vivo* implantation.

CHAPTER 6

EFFECT OF PFC EMULSIONS ON ENCAPSULATED CELLS

6.1 Abstract

Perfluorocarbon (PFC) emulsions have been indicated to improve oxygenation within tissue substitutes and consequently increase cell viability and function. In this paper, we investigated the effect of PFC emulsions on encapsulated βTC-tet cells both experimentally and through mathematical simulations. In the experiment, βTC-tet cells were encapsulated in alginate beads that contained 0%, 5%, or 10% v/v PFC emulsion. The viability and insulin secretion rates (ISR) of these cells were assessed during 16 days of culture. In these studies, the addition of PFC emulsions to the alginate beads had no effect on viability or rate of insulin secretion of the cells. These findings were corroborated through simulations by a mathematical model that was developed. Additional simulations that investigated the effect that PFC emulsions would have during constant hypoxia or transient hypoxic episodes were then performed. These simulations found that indeed PFC emulsions do have the capacity to buffer encapsulated cells from hypoxic episodes, however, the effect on the viable cell density is only small and thus not expected to influence the function of the construct in a major way. The implications of these findings, in regards to *in vivo* applications, are discussed.

6.2 Introduction

Tissue engineered substitutes are designed to repair or replace the function of damaged tissue within the body [4]. The design often consists of cells, from an appropriate source (autologous, allogeneic, or xenogeneic), sequestered in a hydrogel

matrix (e.g. collagen, alginate, or agarose) that provides a three-dimensional architecture for maintenance of cell function and ease of handling. For proper function, the construct must be designed to provide adequate nutrients and oxygen to all the cells within. However, a problem that has been a challenge in the design of tissue engineered substitutes, is the inability to effectively oxygenate tissues or cell-constructs greater than several hundred microns in size due to the low solubility of oxygen in medium [17, 38, 148, 150-152]. Thus, a method that increases the amount of dissolved oxygen (DO) by either increasing the solubility of DO or by increasing the effective diffusivity of DO within a substitute is highly beneficial and desirable in tissue engineered constructs.

The unique properties of perfluorocarbon (PFC) emulsions have led investigators to explore their use in tissue engineered devices, in blood substitutes, and oxygen monitoring [33, 38, 43, 76, 77, 153-155]. Specifically, PFC emulsions are known to have an oxygen solubility that is 15-20 fold higher than that of water [35]; they are non-toxic [31, 102]; and the $1/T_1$ relaxation – a nuclear magnetic resonance parameter – correlates linearly with the surrounding DO concentrations [19, 20, 23]. Given the inherent high solubility of oxygen in PFC emulsions, several groups of researchers have studied the effect of incorporating these emulsions into perfusing medium and/or sequestering the emulsion directly into tissue engineered substitutes [33, 38, 102]. Radisic et al. [38] demonstrated through experimentation and a mathematical model that adding the PFC emulsion, Oxygent, to medium perfusing a parallel plate cardiac bioreactor increases the DO concentration throughout the bioreactor and consequently supports a greater density of cardiomyocytes. It should be noted that in the study by Radisic et al., the medium DO concentration entering the bioreactor was kept constant at 160 Torr using a gas

exchanger, thereby reloading PFC emulsions with oxygen after each pass through the bioreactor. In a study by Khattak et al. [33], the presence of sequestered PFC emulsions in alginate capsules caused an enhanced proliferation of HepG2 cells compared to beads without PFC over two weeks. Additionally, improved metabolic activity of the HepG2 cells was also demonstrated at the physiologically relevant DO concentration of 20% air saturation.

In organ transplantation, PFCs have been used to increase organ preservation times. Specifically, the development of the two-layer method, in which a pancreas is suspended between oxygenated PFCs and University of Washington (UW) solution, increased the preservation of canine pancreata from up to 24 hours to up to 96 hours [84]. Additionally, the use of PFCs has been shown to improve survival of pancreata after transplantation and to increase the yield of purified islets [37, 39, 40]. Without the addition of PFCs, a 50% to 75% early graft loss is typically observed upon intraportal islet engraftment [156]. It is believed that a major contributing factor to the graft loss is the hypoxic environment experienced by the islets, as there is no immediate revascularization [157]. A recent study showed that intraperitoneal injection of PFCs after intraportal islet transplantation in rats increased the success rate from 1/6 to 5/6 [40]; thus, it is reasonable to assume that the incorporation of PFCs transiently buffered the islets from the hypoxic episode. Bergert et al [87], further characterized of the effect of PFCs on cultured islets, assessing parameters such as cell death, apoptosis, mRNA levels of insulin, insulin content and stimulated insulin secretion. The results of this detailed study indicated that the two-layer method, despite having significant benefit in transportation and relatively no effect on numerous other islet parameters, compromised

stimulated islet insulin secretion in the presence of PFCs [87]. Thus, it is essential that the effect of PFCs on the viability and, perhaps, more importantly the stimulated insulin secretion of cells be evaluated prior to implementation in a pancreatic substitute.

In this Chapter, we study the effect of an alginate encapsulated PFC emulsion, perfluorotributylamine, on the viability and function βTC-tet cells sequestered in alginate beads. Over the 16 day study, cell viability was assessed by alamarBlue®, a metabolic indicator, while function was monitored by stimulated insulin secretion tests every four days. A mathematical model of the alginate-PFC-cell system was developed and simulations are compared with the experimentally acquired data. The model was also used to simulate the effect of having a PFC emulsion sequestered in a pancreatic substitute subjected to a constant, moderately hypoxic DO concentration of 0.04 mM, as well as switched from incubator conditions (DO of 0.20 mM) to a severely hypoxic environment (0.01 mM), and then to moderately hypoxic conditions (0.04 mM). The implications of the modeling results and the potential uses for the model are discussed.

6.3 Materials and Methods

6.3.1 PFTBA Effect on Encapsulated Cells

6.3.1.1 Cells and Cell Encapsulation

βTC-tet cells [67] were obtained from the laboratory of Shimon Efrat, Albert Einstein College of Medicine, Bronx, NY. Cells were cultured as monolayers in T-flasks with culture medium changed every 2-3 days. Culture medium consisted of Dulbecco's Modified Eagle's Medium (DMEM, Sigma Chemical Co., St. Louis MO) with 25 mM glucose, supplemented with 10% fetal bovine serum, 1% penicillin-streptomycin and L-

glutamine to a final concentration of 6 mM. Cell monolayers that reached 80% to 90% confluence were trypsinized with 0.05% trypsin-EDTA (Sigma) and split at a 1:5 ratio; passage number increased by one at each splitting. Cells of passage number 36-40 were used in this study.

Cells were harvested by trypsin-EDTA and encapsulated at a density of $3.5x10^7$ cells/ml alginate in 2% w/v low viscosity high mannuronic content alginate (product LVM, NovaMatrix, Drammen, Norway) containing the appropriate concentration of PFTBA emulsion (0%, 5%, or 10% v/v) (see below). Using an electrostatic droplet generator (Nisco Engineering Inc., Zurich, Switzerland), cells were encapsulated according to the procedure of Stabler et al [51], except that a PLL and a final alginate layer were not added. The final bead size was 900±42 μm in diameter.

The PFTBA was prepared following a protocol adapted from Joseph et al [23] and previously described by Gross et al [43] (CHAPTER 4).

Alginate encapsulated βTC-tet cells were placed into T-75 flasks and cultured on a rocking platform in a 37°C, 5% CO_2 incubator. The medium was replaced every 2-3 days for the duration of the study.

6.3.1.2 Viability Assessment – AlamarBlue

On Days 1, 4, 8, 12, and 16 after encapsulation, three 0.1 ml samples were taken from the control and PFC groups. The beads were placed in the wells of a 24-well plate and mixed with 1 ml of medium and 0.1 ml of alamarBlue® reagent (Invitrogen Corp, Carlsbad, CA). The samples were placed on a rocking platform located in a 37°C incubator with 5% CO_2 for 2.5 hours. After the incubation, a 0.1 ml medium sample was taken from each well and quantified with a Spectra Max Gemini Plate Reader (Molecular

Devices, Sunnyvale, CA) using an excitation wavelength of 544 nm and an emission wavelength of 590 nm. Relative intensity units (RIUs) were normalized to the RIUs of the Day 1 control sample and to the aqueous bead volume.

6.3.1.3 Insulin Secretion Assessment

On Days 4, 8, 12, and 16 after encapsulation, three 0.1 ml samples were taken from the control and PFC groups. The beads placed into 6-well dishes, washed twice with 4 ml of 0 mM glucose DMEM, and incubated in 4 ml of unsupplemented, 0 mM glucose DMEM on a rocking platform at 37°C. After one hour, the 0 mM glucose DMEM was replaced with 3 ml of 16 mM glucose DMEM and incubated on a rocking platform at 37°C for 20 min. At the start and end of the 20 min, 0.3 ml medium samples were acquired and frozen for later assay of insulin. Insulin in collected samples was assayed by rat insulin radioimmunoassay (Linco Research, St Charles, MI).

6.3.2 Statistical Analysis

Viability and insulin secretion results were evaluated using a two tail t-test. Statistical significance was defined as $p<0.05$.

6.4 Mathematical Model and Assumptions

The assumptions used to build the model are listed below. These are based on a previously developed mathematical model [148] (CHAPTER 3) with some additional assumptions to accommodate the incorporation of a perfluorocarbon emulsion.

1. DO is the only nutrient that limits cell proliferation (ie, all other essential nutrients are assumed to be in excess throughout the construct)

2. Spatial constraints are the only other factor besides DO concentration that limits the rate and extent of cell proliferation within the construct.
3. Cells do not migrate within the matrix, hence the observed remodeling in cell distribution is due entirely to cellular growth and death at each locale.
4. The PFC emulsion is homogeneously distributed through the alginate matrix.
5. Equilibration of dissolved oxygen between the aqueous and PFC phases at each locale is instantaneous.
6. The values of the model parameters, including the effective diffusivity of DO through the encapsulated system, remain constant over the time period of the simulations.
7. The concentration gradient within the aqueous phase is the only driving force for oxygen diffusion (Figure 6.1).
8. There is no external boundary layer effect when modeling the beads placed on a rocking platform, as performed in this paper. This is a reasonable assumption for systems in which there is significant velocity of the medium relative to the surface of the beads.

The model equations describing DO diffusion for spherical geometry are as follows (see also Figure 6.1).

$$\frac{\partial\left(V_T C_T(r,t)\right)}{\partial t} = V_{aq} D_{eff}\left(\frac{\partial^2 C_{aq}(r,t)}{\partial r^2} - \frac{2}{r}\frac{\partial C_{aq}(r,t)}{\partial r}\right) - V_{aq} S(r) \tag{1}$$

$$V_T \cdot C_T(r,t) = V_{aq} \cdot C_{aq}(r,t) + V_p \cdot C_p(r,t) \tag{2}$$

$$S(r,t) = X(r,t) \cdot \frac{\nu_{\max} C_{aq}(r,t)}{K_m + C_{aq}(r,t)} \tag{3}$$

where, t is time and r is radial position in the construct; $C_T(r,t)$, $C_{aq}(r,t)$, and $C_p(r,t)$ are the concentrations of dissolved oxygen in the total volume (V_T), aqueous phase (V_{aq}), and PFC phase (V_p) volume, respectively, as functions of radial position and time; D_{eff} is the effective oxygen diffusivity through the alginate/PFC matrix; V_T, V_{aq}, and V_p are the total, aqueous, and PFC volume; $S(r,t)$ is the rate of oxygen consumption per unit volume of aqueous phase as a function of radial position and time, which is based on a Monod model with kinetic parameters ν_{max} (maximum oxygen consumption rate) and K_m (Monod model parameters); $X(r,t)$ is the cell density as a function of radial position and time. These equations were solved using finite differences, as diagrammed in Figure 6.1.

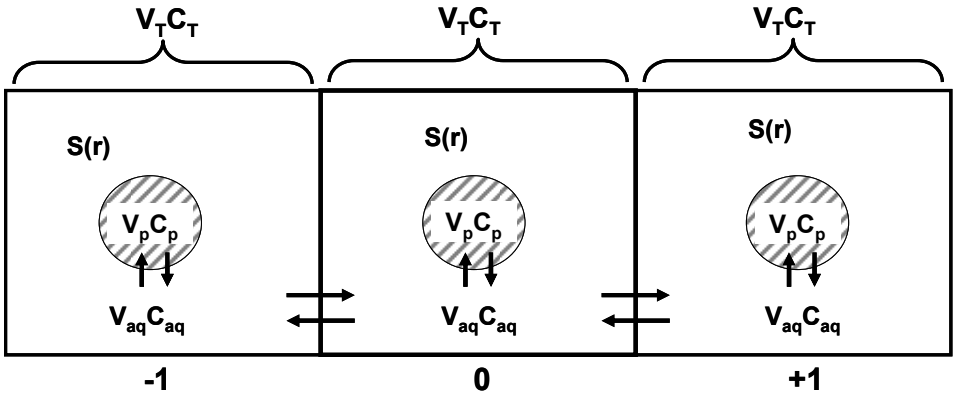

Figure 6.1 Schematic illustrating the method used to solve the DO concentration profile. In solving for the total (aqueous plus PFC phases) DO concentration (C_T) at compartment '0', diffusional transport occurs by the DO concentration differences in the aqueous phase (C_{aq}) between compartment '0' and the neighboring compartments. Additionally, the DO in the PFC and aqueous phase are always in equilibrium based on the partition coefficient. *S(r)* is the oxygen consumption rate by the cells per unit volume of aqueous phase, as described in Equation 3.

The effective diffusivity was calculated using the equation given by Radisic et al. [38], describing D_{eff} in a two phase system.

$$D_{eff} = D_{aq}\left[1+3\left(\frac{\gamma-1}{\gamma+2}\right)\phi\right] \tag{4}$$

$$\gamma = \frac{K \cdot D_p}{D_{aq}} \tag{5}$$

D_{aq} and D_p are the diffusivities of oxygen through alginate-only and PFC; K is the partition coefficient of oxygen in PFC vs. the aqueous phase; φ is the volume fraction of the PFC emulsion (V_p/V_T).

The equations used for determining the growth and death of cells radially through the alginate matrix over time are the same as reported in Gross et al [148] (CHAPTER 3) and are listed below.

$$\frac{dX_{aq}(r,t)}{dt} = X_{aq}(r,t)\left(\mu_g - \mu_d\right) \quad (6)$$

$$\mu_g = \frac{\mu_{g,\max} C_{aq}(r,t)}{K_g + C_{aq}(r,t)}\left(1 - \frac{X_{aq}(r,t)}{X_{\max}}\right) \quad (7)$$ (Monod's model with kinetic parameters $\mu_{g,max}$ and K_g, accounting for spatial constraints)

$$\mu_d = \mu_{d,\max} - \left(\mu_{d,\max} - \mu_{d,\min}\right)\frac{C_{aq}(r,t)}{K_d + C_{aq}(r,t)} \quad (8)$$ (modified Monod's model maximizing the cell death rate at C=0 and minimizing it at $C>>K_d$)

In the above equations, μ_g and μ_d are the specific cell growth and death rates, respectively; $\mu_{g,max}$ and $\mu_{d,max}$ are the maximum specific growth and death rates, respectively; $\mu_{d,min}$ is the minimum death rate, which prevails under an abundance of oxygen; K_g and K_d are Monod model parameters; and X_{max} in the maximum cell density that can be accommodated in the construct. The ratio X/X_{max} is thus the fractional maximum occupancy at a particular locale in the construct.

6.4.1 Boundary Conditions

$C_{aq}\big|_{t=0} = C_o$ (9) (the initial concentration of oxygen is constant throughout the spherical construct and known)

$X_{aq}\big|_{t=0} = X_o$ (10) (the cells are initially distributed homogeneously throughout the construct at a known density)

$$\frac{\partial C_{aq}}{\partial r}\Big|_{r=0} = 0 \quad (11)$$ (symmetry condition for oxygen concentration at the center of the sphere)

Mathematical simulations of alginate encapsulated cells with an infinite volume outside the bead – e.g. simulating beads in T-flasks in a large volume of medium on a rocking platform – used Equation 12. To simulate conditions in which encapsulated cells are placed into a finite volume (e.g. beads implanted into a confined space *in vivo*), Equation 13 was used.

$$C_{aq}\big|_{r=R} = C_b \quad (12)$$ (the concentration of oxygen at the surface of the construct is equal to the concentration in the surrounding medium, which is known)

$$A\frac{\partial C_{aq}}{\partial r}\bigg|_{r=R} = V_b \frac{dC_b}{dt} \quad (13)$$ (the change in oxygen concentration in the surrounding medium is dependent on the flux of oxygen in/out across the bead surface)

6.4.2 Baseline Parameters

Parameters used in the simulations were obtained from Gross et al [148] (CHAPTER 3). In addition, the diffusivity of oxygen in perfluorotributylamine (D_p) is 2.59 cm^2/day [158] and the partition coefficient for oxygen in the PFC phase vs. the aqueous phase (K) is 16 [34, 35].

6.5 Results

6.5.1 PFC Effect on Cell Viability

The viability of alginate encapsulated βTC-tet cells with 0%, 5%, or 10% v/v PFC emulsion was assessed by the metabolic indicator alamarBlue® (Figure 6.2). The data were normalized to the aqueous volume of the alginate beads, as this is the volume in which cells reside, and to Day 1 control beads (0% PFC emulsion), which was set at 100. On Day 1, the cell number within the aqueous phase of the three alginate bead types was approximately equal, as they were encapsulated at the same initial cell density. Four days after encapsulation, beads containing PFC emulsion tended have a slightly higher viable cell number in a concentration dependent manner with 5% PFC beads increasing by 10% and 10% PFC beads increasing by 20%, while beads containing no PFC showed only a small reduction. On day 8, a statistically significant increase in viable cell number was observed in the 10% PFC beads compared to day 1. However, the average viable cell density among the three bead types on day 8 remained was statistically significant. From day 8 to 12 in the study a decrease in viable cell number was observed, which was statistically significant ($p<0.05$) in beads with 10% PFC emulsion. Again, there was no detectable difference between the three bead types on Days 12 and 16.

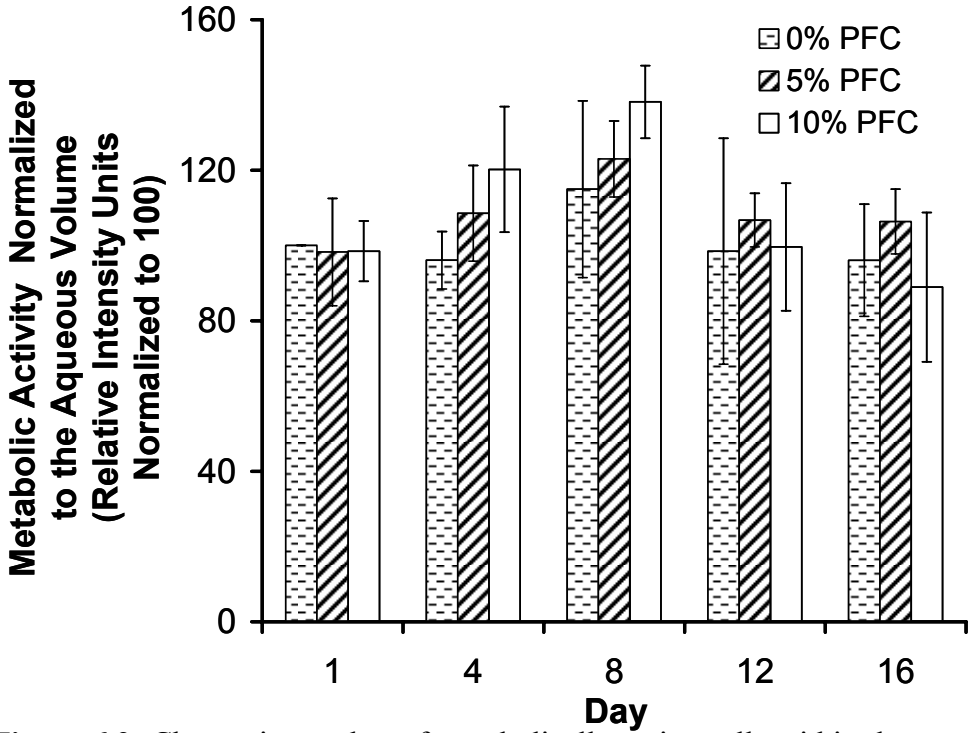

Figure 6.2 Change in number of metabolically active cells within the aqueous phase of alginate beads containing either 0% (Control), 5%, or 10% PFC emulsion.

6.5.2 PFC Effect on Stimulated Insulin Secretion

The stimulated insulin secretion rates (ISRs) of the encapsulated βTC-tet cells (normalized to Day 1 cell numbers) are given in Figure 6.3. On Day 4, the three groups of beads all secreted insulin at approximately 215 pmole/(hr•10^8cells). By Day 8, the alginate beads containing 10% v/v PFC emulsion had statistically significant ($p<0.05$) lower ISR (148±9 pmole/(hr•10^8cells)) compared to the 0% (261±46 pmole/(hr•10^8cells)) and 5% (254±15 pmole/(hr•10^8cells)) PFC beads. However, this difference was not observed for the remainder of the study, as all beads increased to a secretion rate between 656 and 731 pmole/(hr•10^8cells) on Day 12. This increase on Day 12 was statistically significant compared to Day 8 in all three beads ($p<0.05$). On the last day (Day 16), the ISR of the three bead types decreased to approximately 400 pmole/(hr•10^8cells). However, this decrease was only statistically significant in the 10% v/v PFC beads.

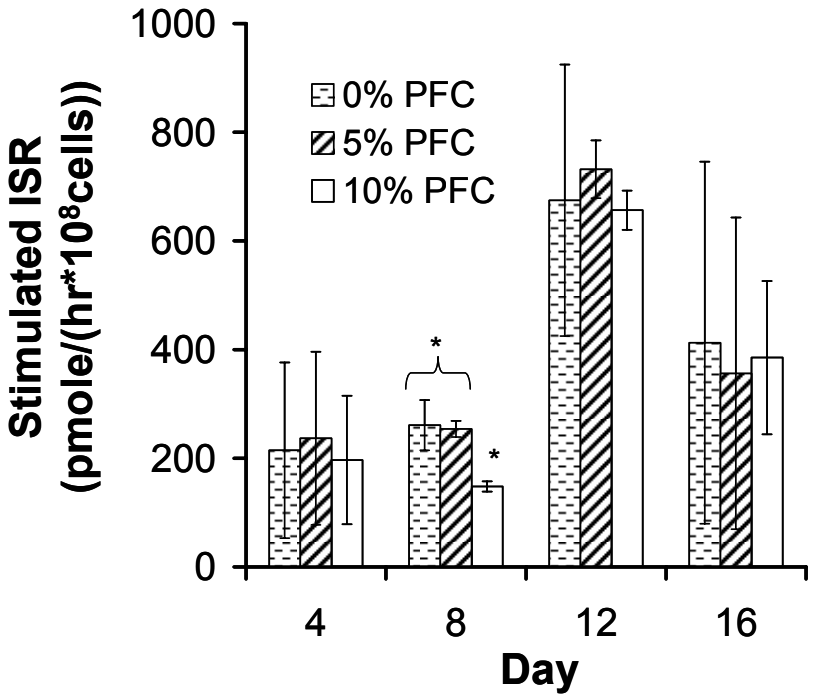

Figure 6.3 Stimulated insulin secretion rates of alginate encapsulated βTC-tet cells containing 0%, 5%, or 10% PFC emulsion. The '*' indicates statistical significance ($p<0.05$).

6.5.3 Mathematical Simulation – Incubator Conditions (DO of 0.20 mM)

The changes in average intrabead DO (AIDO) concentration in the aqueous phase and in cell density (normalized to the aqueous volume fraction within a bead) were simulated for 16 days (Figure 6.4, A and B, respectively), using the parameters listed in Table 3.1 of CHAPTER 3 and the PFC parameters given in Section 6.4.2. The effective diffusivities for the no PFC, 5%, and 10% PFC beads were calculated (Equation 4) to be 1.4, 1.6, and 1.8 cm^2/day, respectively. Due to the increased effective diffusivity, the AIDO concentrations in the three simulated beads started at different values – 0.179, 0.180, and 0.181 mM, respectively (Figure 6.4 A). As the cell density increased within the beads, the AIDO dropped accordingly, since more cells increase the total oxygen consumption within the bead. However, the decrease in AIDO was less severe in beads containing 5% and 10% PFC emulsion. On day 16, the AIDO concentrations within the no PFC, 5% and 10% PFC beads were 0.075, 0.079, and 0.083 mM, respectively.

The cell densities in the alginate beads start at $3.5x10^7$ cells/ml. It should be noted that when cell densities were calculated using the volume of the bead as a reference point, the beads containing PFC had lower cell densities than that of the bead with no PFC. Over the initial 8 days, no significant difference was observed between the three bead types, each reaching 2.75×10^8 cells/ml (Figure 6.4 B). From day 8 to 16, however, the cell densities within beads containing PFC departed from the no PFC beads. The maximum difference was attained on day 16, when the 0% and 10% PFC beads had cell densities of 6.01 and 6.44×10^8 cells/ml, respectively.

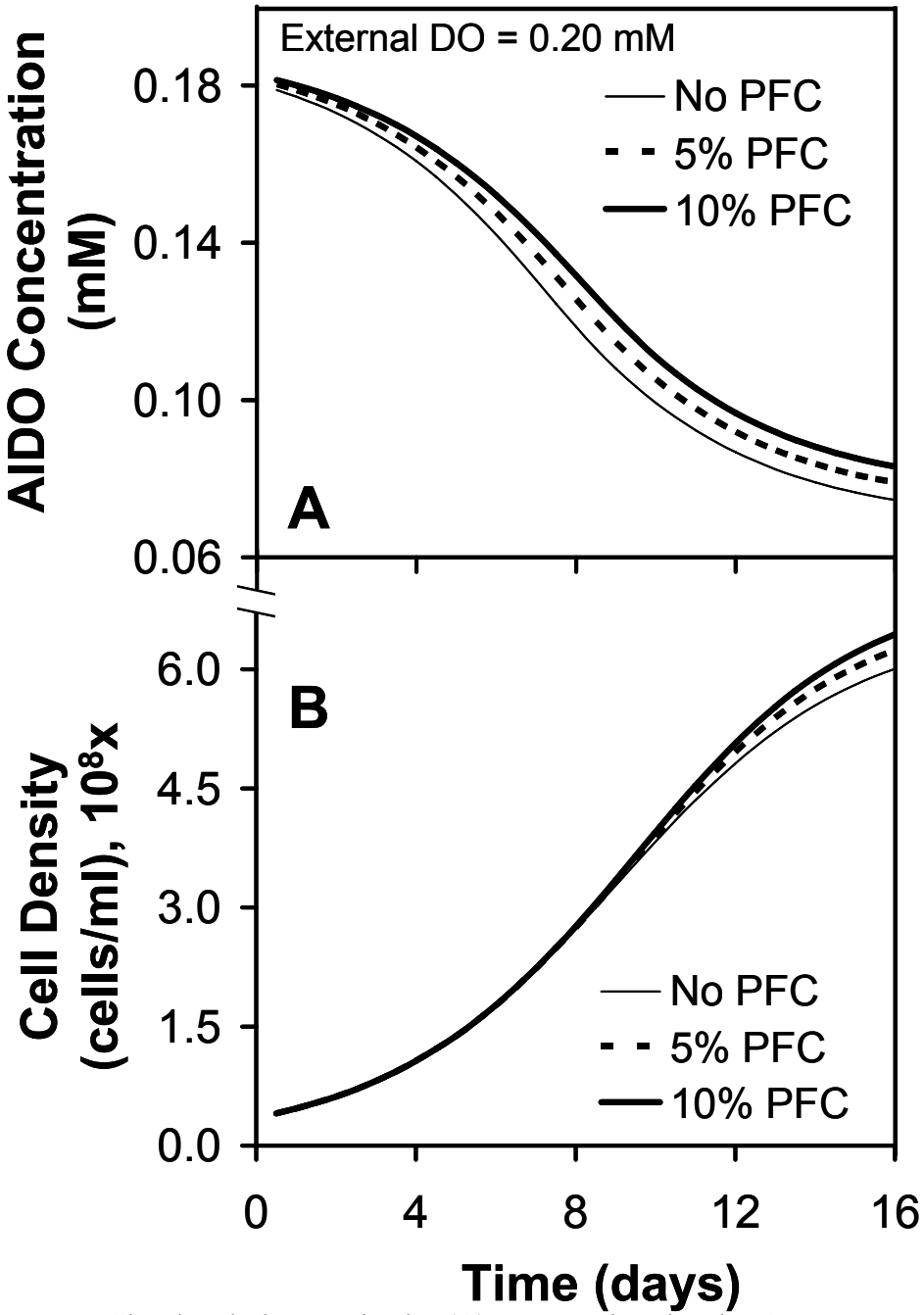

Figure 6.4 Simulated changes in the (A) average intrabead DO concentrations and (B) cell densities of alginate beads containing no PFC, 5%, and 10% PFC emulsion. The DO concentrations are values within the aqueous phase. In addition, cell densities are normalized to the aqueous bead volume.

6.5.4 Mathematical Simulations – Reduced and Transient DO Concentrations

6.5.4.1 Reduced DO Concentration (0.04 mM)

The benefit of incorporating PFC emulsions into encapsulated cells systems was explored under additional conditions that may be experienced by such systems upon *in vivo* implantation. Figure 6.5, A and B, show simulated changes in AIDO concentrations and cell densities within alginate beads that are placed into a reduced oxygen environment (0.04 mM). As in the previous simulations, increasing concentrations of PFC emulsion resulted in higher AIDOs at time 0, which ranged from 0.031 to 0.033 mM (Figure 6.5 A). The difference between the AIDO concentrations remained fairly constant while the concentrations dropped due to increasing cell densities over the 16 days. The final AIDO concentrations were 0.0154, 0.0160, and 0.0165 mM for the 0%, 5%, and 10% PFC beads, respectively. Unlike the simulated incubator conditions in the previous section where cell density differences did not appear until after day 8, the simulated cell densities at the reduced DO concentration began to deviate depending on PFC concentration on day 4 (Figure 6.5 B). Beads containing 10% PFC emulsion had the highest cell density at the end of 16 days, at 2.73 x 10^8 cells/ml, followed by 5% and 0% PFC, at 2.61 and 2.48 x 10^8 cells/ml, respectively.

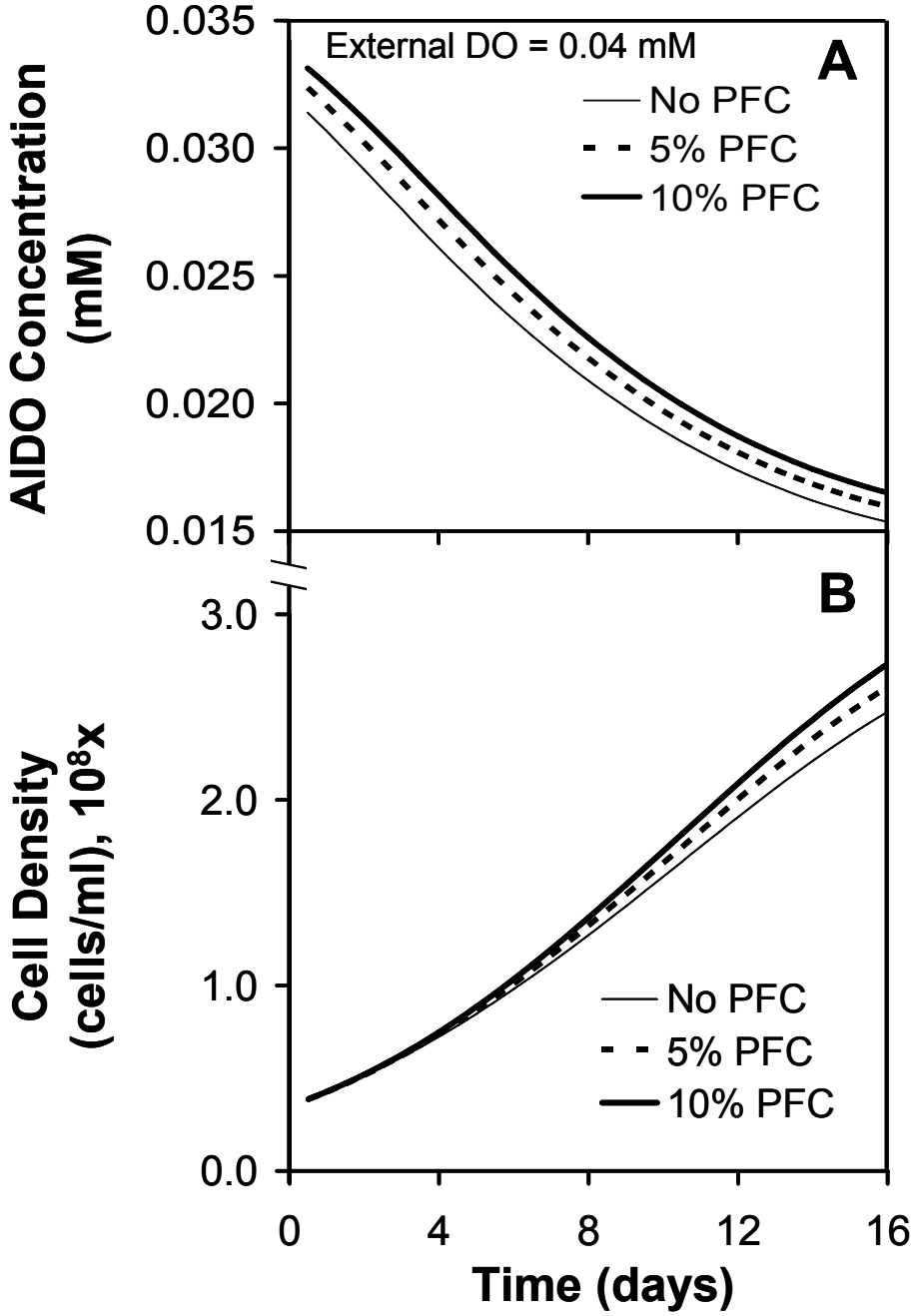

Figure 6.5 Simulated changes in the (A) average intrabead DO concentrations and (B) cell densities of alginate beads containing no PFC, 5%, and 10% PFC emulsion at a surrounding DO concentration of 0.04 mM. The DO concentrations are values within the aqueous phase. In addition, cell densities are normalized to the aqueous bead volume.

6.5.4.2 Transient DO Concentration – Infinite and Finite External Volumes

6.5.4.2.1 Infinite Surrounding Medium Volume

The DO concentration surrounding encapsulated cells often changes dramatically upon *in vivo* implantation. To determine if the incorporation of a PFC emulsion into an encapsulated cell system would aide in buffering cells from a hypoxic episode, a simulation was run in which the surrounding DO concentration was held at 0.20 mM for 24 hours and subsequently decreased to 0.01 mM and then increased to 0.04 mM. Figure 6.6 A-C simulates the changes in the surrounding DO concentration, cell density, and the AIDO concentration upon implementing the change in surrounding DO concentration (i.e. after the 24 hour incubation at 0.20 mM), while assuming that the volume in which the bead resides is infinitely large. As one would expect, the surrounding DO concentration (Figure 6.6 A) is unaffected by the diffusion of oxygen out of the bead upon a step down in the surrounding DO. The AIDO concentration quickly drops in both the 0% and 10% PFC beads (Figure 6.6 B). However, the incorporation of 10% PFC appeared to buffer the decrease slightly, which was expected given the higher oxygen concentrations within the PFC phase. Upon increasing the surrounding DO concentration to 0.04 mM, the AIDO concentration within both beads increased at the same rate with the 10% PFC beads reaching a slightly higher end value of 0.030 mM versus the 0% PFC beads that ended at 0.028 mM. A decrease in the cell density was observed shortly after lowering the surrounding DO concentration in the 0% and 10% PFC beads (Figure 6.6 C), which paralleled the decrease in AIDOs in the respective beads. Nonetheless, the cell density change in both bead types was small.

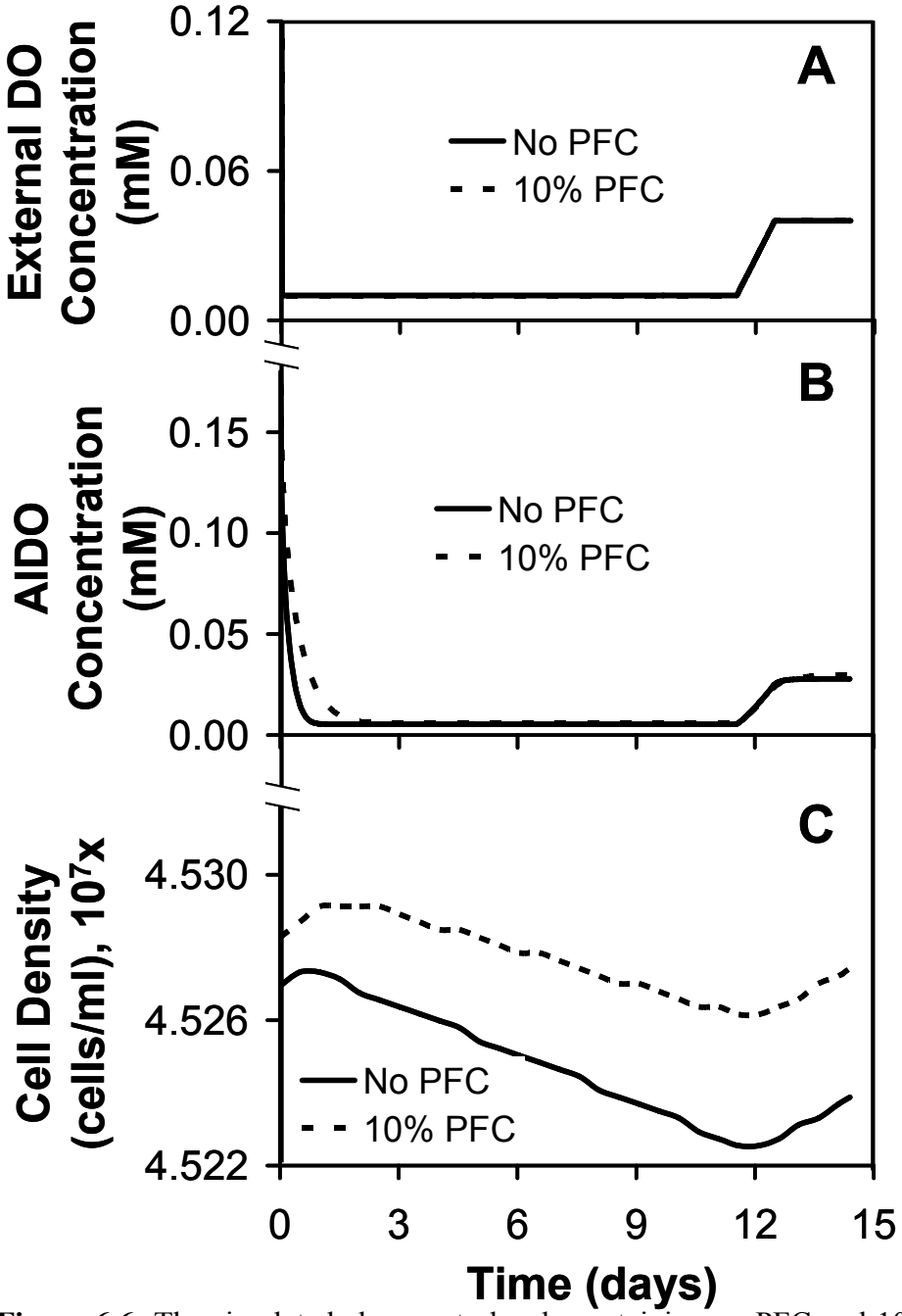

Figure 6.6 The simulated changes to beads containing no PFC and 10% PFC emulsion upon (A) changing the DO concentration surrounding such beads from 0.20 to 0.01 to 0.04 mM and assuming an infinite surrounding volume. (B) Changes in the average intrabead DO concentration. (C) Changes in the cell density.

6.5.4.2.2 Finite Surrounding Medium Volume

The change in surrounding DO concentration, AIDO, and cell density was simulated as described above with the exception that the volume in which the bead resided was only twice as large as the bead (Figure 6.7 A-C). Again, at time equals zero, the DO concentration was switched from 0.20 to 0.01 mM in the surrounding volume. The diffusion of oxygen out of the bead and into the surrounding volume is observed in Figure 6.7 A. Specifically, the DO concentration quickly rises from 0.01 to 0.057 mM in beads containing 0% PFC and from 0.01 to 0.10 mM in beads containing 10% PFC. The point of inflection in the surrounding DO concentration – i.e., where the DO concentration changes from a positive to a negative slope – corresponds to the time at which the AIDO concentration (Figure 6.7 B) drops below that of the surrounding DO concentration. The change of oxygen diffusion direction is due to the oxygen consumption of the cells within the bead; hence, the surrounding DO concentration continues to decrease until reaching the imposed lower limit of 0.01 mM. Upon increasing the surrounding DO concentration to 0.04 mM, the AIDO concentration in both bead types increases likewise and again, the 10% PFC bead reaches a slightly elevated concentration compared to the 0% PFC bead (0.30 and 0.28 mM, respectively). The ability of the 10% PFC bead to buffer the AIDO during the decreased surrounding DO concentration had the added benefit of minimizing cell death within the bead and thus only a small change in cell density was observed (Figure 6.7 C).

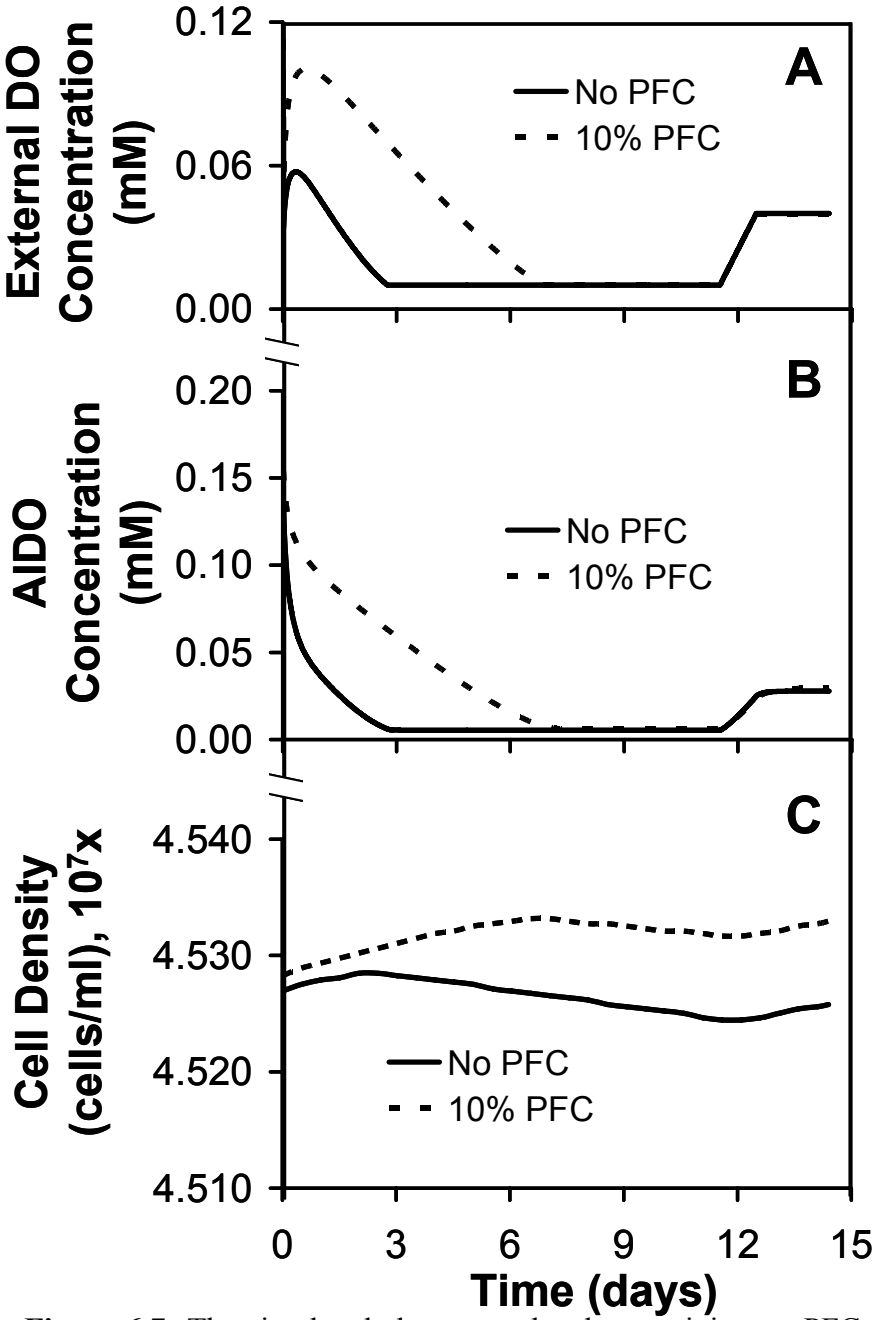

Figure 6.7 The simulated changes to beads containing no PFC and 10% PFC emulsion upon (A) changing the DO concentration surrounding such beads from 0.20 to 0.01 to 0.04 mM and assuming a surrounding volume two fold greater than the bead volume. (B) Changes in the average intrabead DO concentration. (C) Changes in the cell density.

6.6 Discussion

The incorporation of perfluorocarbon (PFC) emulsions into tissue engineered substitutes has garnered the interest of researchers that face the difficult challenge of maintaining sufficiently high DO concentrations within tissue substitutes – either due to large diffusion distances or high cell densities. PFC emulsions have an oxygen solubility that is 16-20 fold higher than that of water; thus, they can act as a large oxygen reservoir within tissue engineered devices. In addition, the incorporation of PFC emulsions holds the added benefit of increasing the diffusivity of oxygen through the matrix. This Chapter investigated the benefit of sequestering the PFC emulsions perfluorotributylamine (PFTBA) into pancreatic substitutes through experimentation and mathematical modeling. As a model system, βTC-tet cells were encapsulated into an alginate hydrogel that contained 0%, 5%, or 10% v/v PFC emulsion. Over the course of 16 days, the cell viability and the stimulated insulin secretion were assessed in beads to determine if the incorporation of PFCs enhanced viability or function. In the second portion of this paper, a mathematical model was then used to simulate the growth of cells within such an encapsulated cell system under various conditions that mimicked both *in vitro* and *in vivo* environments.

The first study found that there was no statistical difference in βTC-tet cell growth when PFTBA was added to the alginate beads. During the first eight days, it appeared as though the beads containing PFC emulsion had a slight enhancement over beads that did not have PFC. However, this difference was not statistically significant and by day 12, the difference had waned. This finding is unlike an earlier publication by Khattak et al [33] where a statistically significant increase in cell growth was observed in a HepG2

alginate encapsulated system that incorporated 10% perfluorooctylbromide (PFOB). The difference in observations could be due to the use of two different PFCs, as PFOB has a higher oxygen solubility than PFTBA (44.0 vs. 35.2 mM, at standard temperature and pressure [35]). In addition, the higher oxygen partition coefficient of PFOB would increase the effective diffusivity of oxygen through the alginate matrix to a level slightly beyond that of PFTBA (1.788 vs. 1.780 cm^2/day, respectively). However, the difference made by such a small change in the effective diffusivity would not significantly change the simulations presented here.

The stimulated insulin secretion from the βTC-tet cells within the three bead types also showed no advantage through the incorporation of PFC emulsion. If there was any effect, the PFCs were detriment to the insulin secretion. This finding is consistent with that of Bergert et al [87], in which the insulin secretion of islets was compromised after being cultured by the two-layer method (TLM), which consists of placing islets at the interface between University of Washington solution and PFC. Specifically, Bergert et al found that the stimulation index (relation between the fraction of total insulin secreted after stimulation vs. the fraction of total insulin secreted at basal conditions) was approximately 55% of control (no PFC) on day 1 and 38% of the control on day 7 [87] after TLM. However, a study by Brandhorst et al [88] found that there was no statistical difference in the stimulation index if islets were cultured by a one-layer method of PFC (i.e. islets were completely submerged in PFC). Given this variability, further investigation is needed as to the effect of PFCs on insulin-secreting cells.

In the second portion of this paper, a mathematical model that was capable of simulating changes in cell growth based on the incorporation of PFC emulsions was used

to investigate several *in vitro* and *in vivo* environments. The first study simulated the experiment performed in this paper, in which beads were cultured at a DO concentration of 0.20 mM with 0%, 5%, or 10% v/v PFC emulsion added to the matrix. During the simulated initial 8 days, there was no discernable difference in cell densities between the various bead types. This was expected since beads that have a low initial cell density do not create large DO concentration gradients, which would inhibit cellular growth at the center of such beads where DO levels are the lowest. From day 8 to 16, the cell densities in the PFC containing beads increased slightly above that of beads with no PFC. Nevertheless, the difference was very slight and would be difficult to discern experimentally. In addition, the slight benefit only remained as long as cell densities were normalized to the aqueous volume phase of the beads. If cell densities were normalized to the bead volume, beads containing PFC would have lower cell densities than beads that had no PFC, since a portion of the bead volume is taken by the PFC phase.

There are several conditions or environments in which one could imagine the incorporation of PFC emulsions would have an added benefit in maintaining viable cells within encapsulated cell systems. One such condition that was simulated using the mathematical model is beads placed in a more hypoxic oxygen environment. Beads cultured with 10% PFC emulsion at a constant DO concentration of 0.04 mM indeed maintained a somewhat higher viable cell density than beads that had no PFC, due to the increased average intrabead DO concentration within these beads.

To determine if the incorporation of PFC emulsions buffers encapsulated cells from hypoxic episodes, the model was used to simulate beads that had been cultured for

24 hrs at 0.20 mM, subsequently placed into a hypoxic environment (0.01 mM) for 12 min and finally returned to a moderately hypoxic DO concentration of 0.04 mM. This study of transient DO concentrations was first simulated assuming that the volume surrounding the bead was infinite and then assuming that the volume was of a finite size – specifically, 2 fold greater than the bead volume. In the simulation that assumed an infinite surrounding volume, the incorporation of the PFC emulsion offered only a very small buffer, as the 10% PFC bead AIDO reached the final value approximately 45 seconds after the bead without PFC. However, upon simulating the change in AIDO when beads were assumed to be within a finite volume, a greater buffering capacity of the PFC was noted. Specifically, the 10% PFC bead AIDO took 3 minutes longer than the bead without PFC to reach the final DO concentration. The buffering capacity of the 10% PFC beads was due to the increase in the surrounding DO concentration that resulted from oxygen leaving the alginate/PFC beads and diffusing into the surrounding volume.

In summary, the addition of PFC emulsions to pancreatic substitutes that consisted of βTC-tet cell entrapped in alginate did not have a statistically significant benefit to cell growth, nor did it show a benefit to the stimulated insulin-secretion. This finding was supported by mathematical simulations that noted only a small increase in cell density due to the incorporation of PFC. An investigation of additional scenarios revealed through mathematical simulations that PFC emulsions indeed are beneficial at low oxygen concentrations and provide a slight buffering effect from hypoxic episodes. Additional studies investigating the use of other PFC emulsions and various DO

concentrations are needed to fully characterize the benefit of incorporating PFCs into tissue engineered substitutes.

CHAPTER 7

CONCLUSIONS AND FUTURE DIRECTIONS

7.1 Conclusions

Dissolved oxygen concentrations within a pancreatic substitute influence the viability and function of insulin-secreting cells. In this thesis, we have contributed to the field by developing a method that is capable of assessing the oxygenation of a tissue engineered construct non-invasively, which additionally could be used to evaluate viable cell number, DO and cell density profiles, and potentially the mode of an implant failure. A major limitation to assessing the DO concentrations within a construct containing a continuous cell line was that the DO profiles changed over time as the cells proliferated and remodeled. *In vitro* this limitation could be overcome by using chemical shift imaging; however, the long acquisition times associated with such methods are problematic upon moving to an *in vivo* model. In Chapter 3, this caveat was circumvented by the development of a mathematical model that simulated the changes in cell density and DO concentrations within an alginate bead construct. Simulations using the model revealed that one could acquire a single average intrabead DO (AIDO) concentration measurement and uniquely identify the viable cell number, as well as cell density and oxygen distribution at a given external DO. Indeed, at a certain DO concentration, this relationship was maintained regardless of the initial cell density.

In the second part of this thesis, the ability to track a pancreatic substitute using the mathematical model along with NMR measurements was demonstrated. During these studies, a custom built computer controlled NMR-compatible perfusion system and bioreactor maintained alginate encapsulated βTC-tet cells for 50 hours, over which the

DO concentration was changed stepwise from 0.20 to 0.05 mM and returned to 0.20 mM. The temporal changes in the medium DO concentration caused typical bioenergetic and metabolic changes in the sequestered cells; specifically, hypoxic DO concentrations caused a reduction in nucleotide triphosphates (NTPs) and oxygen consumption. AIDO concentrations acquired during the experiment were then compared against simulations based on the external DO concentration and time. The observed changes in both the experimentally acquired and simulated AIDOs closely matched. Additionally, the experimentally observed reduction in NTP paralleled the percentage of cells calculated by the model to be below a critical DO concentration value. From this validation we concluded that the mathematical model was indeed able to track a pancreatic substitute over time *in vitro*.

Chapter 5 investigated the mathematical model and AIDO measurements as an evaluation tool, assessing viable cell number under two conditions that often occur *in vivo*. The ability to monitor constructs non-invasively *in vivo* can provide valuable information regarding the effect of construct integration and the biocompatibility of a substitute. The activation of an inflammatory response or cytokine attack by the host immune system are two typical issues relating to an implanted tissue substitute. In Chapter 5, these two *in vivo* scenarios were simulated *in vitro* by the NMR perfusion circuit and bioreactor. The inflammatory response was mimicked via changes in the medium DO concentration entering the bioreactor. During this study, the estimated cell density was tracked using the measured AIDO, the external DO concentration and the mathematical model developed in CHAPTER 3. To mimic a cytokine attack, a cytotoxic dose of puromycin was added to perfusing medium. Again, the estimated cell density

was tracked using the AIDO, surrounding DO concentration, and the mathematical model. Estimated cell densities during both scenarios paralleled the cell density estimated by oxygen consumption rates that were acquired by bracketing DO sensors. Again, it should be noted that upon *in vivo* implantation, DO sensors cannot be used to measure OCRs, but the AIDO and surrounding DO concentrations could be acquired. From these studies, we concluded that the AIDO and external DO concentration measurements would indeed allow the tracking of cell densities during an inflammatory response or cytokine attack and could distinguish between these two modes of implant failure.

Bridging the gap from employing the monitoring method *in vitro* to utilization *in vivo* was the development of a novel dual-PFC system that could be used to acquire simultaneous DO concentrations from two distinct bead populations. Such a system was needed, as the mathematical model developed in CHAPTER 3 requires that both the AIDO and external DO concentrations be known. The dual-PFC system was demonstrated by incorporating perfluoro-15-crown-5-ether (PFCE) emulsion into cell-free alginate beads and perfluorotributylamine (PFTBA) emulsion into cell-free alginate/poly-l-lysine (AP) beads. Implanted into the peritoneal cavity of mice, the AP beads elicited a strong inflammatory response, while no observable response was seen against alginate-only beads. Given the fibrotic layer surrounding AP beads, it was expected that the DO concentration would be lower in these beads compared to beads with no fibrosis. Indeed, through the acquisition of T_1 relaxation measurements from PFCE and the PFTBA, a statistically significant lower DO concentration was quantified in AP beads versus alginate-only beads. Therefore, we have developed a system of

acquiring DO concentrations from two distinct constructs simultaneously, meeting the requirements of the mathematical model *in vivo*. Additionally, the dual PFC system has further reaching applicability in tissue engineering, as researchers studying biocompatibility of new materials could use the system to assess the degree to which a material elicits an inflammatory response.

As reported in APPENDIX I, the low concentrations of PFTBA used in the monitoring studies had no impact on cell viability or function. Additionally, we showed that there was no detectable leak of the PFC emulsion from the alginate beads after 5 days of perfusion and that the T_1 relaxation rates changed rapidly in response to changes in surrounding DO concentrations. In the final portion of this thesis, the effect of incorporating higher concentrations of PFCs on the viability and function of encapsulated βTC-tet cells was evaluated (experimentally and through modeling), as increasing concentrations could have an effect on the oxygen buffering capacity and diffusivities. We found that incorporating PFC emulsions up to 10% v/v in alginate beads did not increase the viable cell number nor did it have any effect on stimulated insulin secretion of βTC-tet cells. This was corroborated by a mathematical model we developed that simulated the increased oxygenation within a substitute of spherical geometry that had a PFC emulsion incorporated. From the model we concluded that a slight benefit in cell proliferation occurs when incubator DO concentrations (0.20 mM) are used. However, the benefit is small and would be challenging to distinguish experimentally. It should also be noted that the total number of viable cells within a bead that contained PFC emulsion was lower than beads that did not contain PFC, which was due to the reduced aqueous volume fraction that cells could occupy. Additional mathematical simulations

found that PFCs incorporated into alginate beads provided an oxygen buffering capacity when the DO concentration in the external environment decreased rapidly to hypoxic levels. We concluded that such a capacity may be beneficial to pancreatic substitutes upon *in vivo* implantation, as such transient hypoxic episodes have been noted in the literature [157]. It was also found experimentally that the addition of PFC emulsions had no impact on cell function, as the insulin secretion rates of the β cell line in PFC-containing beads were comparable to the PFC-free control.

7.2 Future Directions

7.2.1 Pancreatic Substitute Tracking Studies

The foundation of using a mathematical model and ^{19}F NMR to track βTC-tet cells encapsulated in alginate beads has been established by this thesis. To further develop this method, improvements that could be made have been broken down into the following five areas: (1) validation of the mathematical model, (2) tracking of pancreatic substitutes *in vitro*, (3) improvements to the NMR-compatible perfusion system, (4) move to *in vivo* monitoring, and (5) expanding to additional cell lines and geometries. These improvements are discussed in further detail below.

The NMR magnet used in this thesis studies to develop the tracking system did not have spatial gradients and for this reason, the DO concentration profiles created within the alginate beads could not be discerned directly. This forced the use of more indirect methods to validate the model. Therefore, a more robust model validation could be obtained through the use of an NMR magnet with such gradients. Specifically, gradients would be used to perform ^{19}F NMR chemical shift imaging, which would

quantify the DO concentrations at distinct voxels within the alginate beads, allowing reconstruction of DO profiles. The DO profile reconstruction would have to be performed while the DO concentration external to the beads was held constant. In addition, the viable cell number could be ascertained through ^{1}H NMR spectroscopy, which has been demonstrated previously by Stabler et al. [112, 113], where the total-choline peak was shown to correlate with the number of viable cells. Utilizing the combined measurements of DO concentration profiles and viable cell number, enhanced correlations could be made to the model. Additionally, such studies would provide a greater understanding of the alginate bead microenvironment.

Improvements to the system of tracking pancreatic substitutes *in vitro* could be accomplished by studying the insulin secretion rates of the encapsulated cells and investigating the substitutes at a lower, more physiologic, range of DO concentrations. By comparing the ^{1}H NMR and AIDO measurements with the function (insulin secretion) of the pancreatic substitute, a more thorough understanding could be attained as to the effect of DO gradients on insulin secretion characteristics. In regards to studies at lower oxygen concentrations, a study of cell viability and function at DO concentrations below 0.04 mM (the lowest DO concentration used in this thesis) is warranted, as studies by Gross et al. [43] and Noth et al. [24] found the DO concentration within the peritoneal cavity of mice and rats, respectively, in the 0 to 0.04 mM range. In these studies, ^{1}H NMR spectroscopy could be used as described above to determine viable cell number and compared with AIDO predicted oxygen gradients. This comparison would be useful in determining the number of cells that are in hypoxic regions of the substitute and consequently have switched to a more anaerobic metabolism. Adding to a more complete

picture, ^{13}C NMR studies could also be implemented to assess metabolic pathways being used.

The experiments described above would also require an NMR-compatible perfusion system that had several design improvements, as this system was designed specifically for the 500 MHz NMR magnet used in this thesis. To accommodate a stronger NMR magnet that had gradients, distances from the medium reservoir to the bioreactor would have to be increased without compromising oxygen and temperature control of the system. In addition to the changes made to the perfusion circuit's specifications to accommodate a new magnet, the system must also be improved by increasing the range of control at low dissolved oxygen levels, as such a design change would enable the experiments proposed in the previous paragraph. Currently, a concentration of 0.04 mM is the lowest DO concentration that can be attained by the present design. System parameters such as choice of tubing, breaks in the perfusion loop, and distances between the medium reservoir and bioreactor have all been optimized and implemented in the current design; therefore, a perfusion system with the capacity of delivering a lower DO concentration would require the addition of a gas exchanger placed at the opening of the NMR bore. Each of the changes mentioned above would impact the DO concentration proportional-integral controller parameters, as the increased distance would create additional lag times and a second gas exchanger would add a layer of complexity to the system. Hence, reprogramming of the LabVIEW™ automation software would also be required.

Another aspect for future study is the move from *in vitro* to *in vivo* development of the monitoring system. To accomplish this objective, the dual PFC system that was

established in this thesis should be first investigated with encapsulated cells *in vitro*. In these studies, the βTC-tet cells would be encapsulated in alginate beads containing PFTBA, while a second group of cell-free beads would be made containing PFCE. A mixture of the two bead groups would be placed into the bioreactor and DO concentrations from each bead population would be acquired. Proof-of-concept studies have been performed using this system, but a more detailed investigation is needed prior to *in vivo* implementation. Upon establishing the method *in vitro*, cell-free and cell-containing beads with the two PFC emulsions would then be implanted into the peritoneal cavity of mice and the ability to monitor these two bead populations would be assessed. Once the system has been fully characterized and established, a study investigating the ability of the pancreatic substitute to maintain normoglycemia with measures of AIDO and the DO concentration within the peritoneal cavity could be performed.

Lastly, the monitoring methods developed in this thesis are general enough to be applied to other cell types and construct types and geometries. Making the transition to new cell lines and construct materials would require a change of the baseline parameters and assumptions used to run the mathematical simulations, as well as additional validations studies. New cell types would likely have different oxygen consumption rates, in addition to distinct grow and death kinetics. Given that biomaterials used in tissue engineered devices have various characteristics in regard to permissiveness (i.e. the degree to which the material impedes cell growth) and the ability of cells to adhere, model assumptions in regards to cell migration and growth would need change. However, utilizing systems with permissive hydrogels similar to alginate in different

geometries would require only slight variation in the model equations. For example, disk-shaped agarose constructs that have been used previously by our laboratory, have already been modeled by changing the equations to account for slab geometry.

7.2.2 Perfluorocarbon Studies

The benefit of incorporating PFC emulsions into tissue engineered substitutes warrants further investigation. Given that DO concentrations have been reported to vary widely within a specific locale, a detailed study as to the buffering capacity of PFCs against hypoxia should be studied, as mathematical simulations suggest there is a benefit in using the emulsions as a temporary oxygen reservoir. Such experiments would require careful design that closely mimicked an *in vivo* environment, in which boundary layer effects are created within a finite volume. Finally, upon establishing a greater understanding in regards to PFC benefit to cell viability, buffering against hypoxia, DO concentration monitoring, and effects on tissue function, concentration optimization could be established for various tissue substitutes based on oxygen demand, cell type, construct geometry, and location of implantation. For example, during islet transplantation a transient hypoxic episode typically occurs immediately upon implantation. The incorporation of PFC emulsions into alginate beads containing islets may both buffer the oxygen within the construct and allow for non-invasive monitoring of these pancreatic substitutes.

APPENDIX I

PERFLUOROCARBON CHARACTERIZATION

A1.a Distribution of PFC Emulsion within Beads

The PFC emulsion must be homogeneously distributed throughout the alginate beads to accurately assess the available oxygen in the encapsulated cell system. To determine the distribution of the emulsion, the PFC surfactant, lecithin, was tagged with fluorescent compounds. The two lecithin tags used were 2-(6-(7-nitrobenz-2-oxa-1,3-diazol-4-yl) amino)hexanoyl-1-hexadecanoyl-sn- glycero-3-phosphocholine (460 excitation/534 emission) and 2-(3-(diphenylhexatrienyl)propanoyl)-1- hexadecanoyl-sn-glycero-3- phosphocholine (362 excitation/433 emission). The tagged lecithin compounds were mixed with untagged lecithin at a ratio of 1mg/94mg, respectively, and were then used to create the emulsion according to the previously described protocol. The alginate beads containing a 50/50 mixture of the two tagged emulsions were then imaged using confocal microscopy, shown in Figure A1. If the emulsions were not homogeneously distributed, clusters of green or blue would be found in the bead. As it is shown in Figure A1, the blue/green fluorescence is seen throughout the bead and not concentrated in any specific region. It should also be noted that this was further validated using NMR micro-imaging (data not shown).

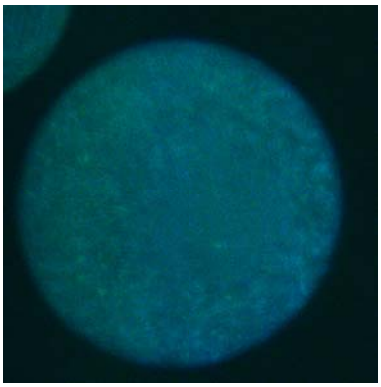

Figure A1 Distribution of PFC emulsion through an alginate bead.

A1.b Leak of PFC Emulsion from Alginate Beads

The amount of PFC emulsion that would leak out of the alginate beads was assessed in a small perfusion system. Cell-free alginate beads were created that contained 4% v/v PFTBA. A total of 3 mls of beads were placed into bioreactors that were identical to those used in the long-term perfusion studies (CHAPTER 4). The beads were then perfused for 5 days with approximately 10 mls of saline solution. As a positive control, saline was replaced with a solution containing 200 mM sodium citrate with 0.85% NaCl, which dissolved the beads over the 5 days and thereby releasing all the PFTBA into the solution. The perfusing solutions were collected at the end of the study for NMR analysis. To each sample, perfluoro-15-crown-5-ether (PFCE) was added at a concentration of 20 µl per ml of solution. ^{19}F NMR spectra were then acquired on a 500MHz Bruker magnet. Figure A2, A and B, show the results of the positive control and experimental groups, respectively. No detectable amount of PFTBA could be found in the experimental samples, while in the positive control group PFTBA was easily detected.

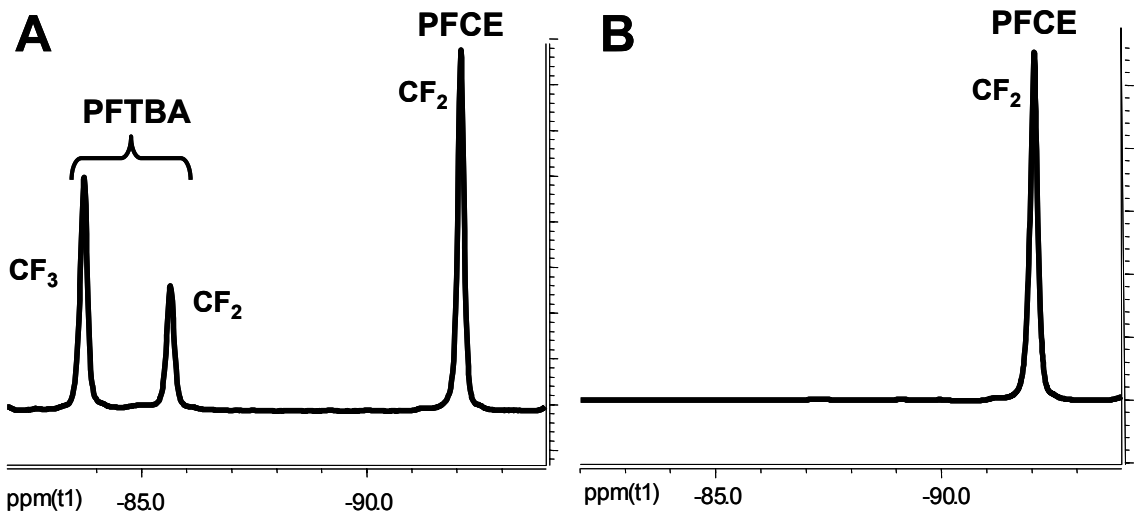

Figure A2 ^{19}F NMR spectra from samples assessing the leak of PFTBA from alginate beads. (A) In the positive control, where beads were dissolved and PFTBA was released, the PFTBA is detectable along with the added PFCE emulsion. (B) A representative sample from the experimental group shows no detectable amounts of PFTBA, only the added PFCE.

A1.c PFC Monitoring of Rapid Changes in DO Concentrations

To quantify the rate at which T_1 relaxations change with changes in surrounding DO concentrations, cell-free alginate beads containing PFTBA were loaded into a bioreactor, attached to the NMR-compatible perfusion system and placed in a 500MHz NMR magnet. The DO concentration of the medium entering the bioreactor was switched between the following user-defined setpoints: 0.20 to 0.16 mM; 0.16 to 0.12 mM; and 0.04 to 0.08 mM. During the DO concentration switches, T_1 relaxation measurements were acquired by inversion recovery experiments that lasted approximately 5 minutes. Figure A3 plots both the medium DO concentration – as quantified by a DO sensor placed immediately before the bioreactor – and DO

concentrations within the alginate beads – as quantified by ^{19}F T_1 relaxation measurements. As can be seen in Figure A3, T_1 relaxation measured DO concentrations closely paralleled those measured by the DO sensors, thus validating their quick response.

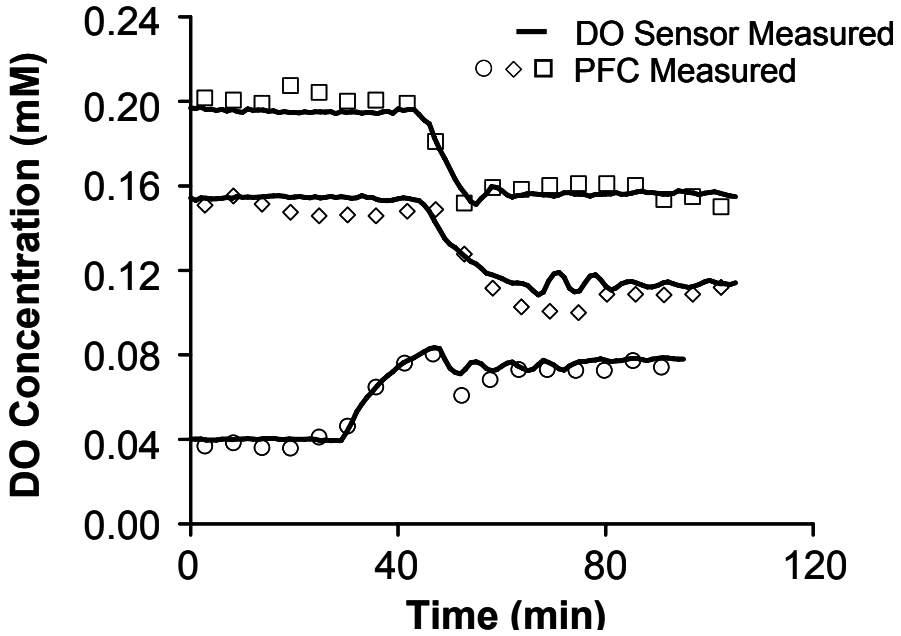

Figure A3 Data comparing the rate at which T_1 relaxation measurements change in response to changes in external DO concentrations.

A1.d PFC Effect on Cell Viability and Insulin Secretion

The effect of PFTBA on alginate encapsulated βTC-tet cells was evaluated at a concentration of 0.4% v/v PFC to alginate, as this was the concentration used in monitoring studies. Specifically, the cell viability was assessed on Days 1, 3, and 7. On these days, three 0.1 ml samples were taken from the control and PFC groups. The beads were placed in the wells of a 24-well plate and mixed with 1 ml of medium and 0.1 ml of alamarBlue® reagent (Invitrogen Corp, Carlsbad, CA). The samples were placed on a rocking platform located in a 37°C incubator with 5% CO_2 for 2.5 hours. After the incubation, a 0.1 ml medium sample was taken from each well and quantified with a Spectra Max Gemini Plate Reader (Molecular Devices, Sunnyvale, CA) using an excitation wavelength of 544 nm and an emission wavelength of 590 nm. Relative intensity units (RIUs) were normalized to the RIUs of the Day 1 control sample and to the aqueous bead volume. The insulin secretion rate of encapsulated βTC-tet cells was assessed by taking three 0.1 ml samples from the control and PFC groups on Day 1. The beads were placed into 6-well dishes, washed twice with 4 ml of 0 mM glucose DMEM, and incubated in 4 ml of unsupplemented, 0 mM glucose DMEM on a rocking platform at 37°C. After one hour, the 0 mM glucose DMEM was replaced with 3 ml of 3 mM glucose DMEM and incubated on a rocking platform at 37°C for 20 min. At the end of the 20 minutes, the 3 mM glucose DMEM was replaced with 3 ml of 16 mM glucose DMEM and incubated on a rocking platform at 37°C for an additional 20 min At the start and end of the 20 min, 0.3 ml medium samples were acquired and frozen for later assay of insulin. Insulin in collected samples was assayed by rat insulin radioimmunoassay (Linco Research, St Charles, MI).

Results from the cell viability and insulin secretion tests are shown in Figure A4 and A5, respectively. It was determined that the presence of PFC had no effect on cell viability or insulin secretion.

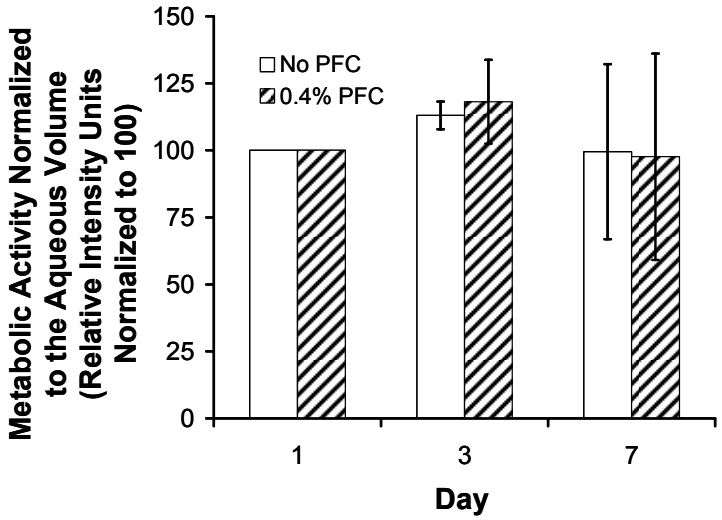

Figure A4 Change in number of metabolically active cells within the aqueous phase of alginate beads containing no PFC or 0.4% v/v PFC

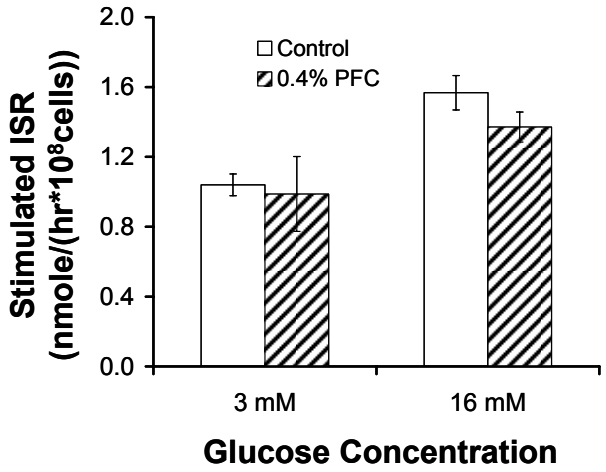

Figure A5 The Stimulated insulin secretion rates of alginate encapsulated βTC-tet cells containing no PFC or 0.4% v/v PFC emulsion.

APPENDIX II

TECHNOLOGICAL INNOVATION: GENERATING ECONOMIC RESULTS

1.1 A2.a TI:GER® Project

During my graduate career, I had the opportunity to participate in the two year NSF-sponsored IGERT TI:GER® program that spanned across Georgia Institute of Technology and Emory University. The program brought together Ph.D. candidates and M.B.A. students from Georgia Tech with two J.D. students from Emory University to learn about commercializing research. The technology worked on by my team was aimed at assessing the quality of islets destined for implantation – a brief description of this technology is given in section A2.b. My teammates and I developed a full commercialization and business plan based on this technology and competed in several business plan competitions, placing in the top three in two of the competitions. The Executive Summary from the business plan is given in section A2.c. In addition, it should be noted that a provisional patent on the technology has been filed.

A2.b Invention Description

A system has been designed to evaluate pancreatic islets or other insulin-secreting cells, free or encapsulated in hydrogels, for quantitative, objective assessment of their functionality in a perfusion apparatus prior to transplantation. The system evaluates both oxygen consumption and insulin secretion in response to prescribed glucose concentration profiles, at various dissolved oxygen concentrations. Flow of medium and dissolved oxygen concentration at the bioreactor input are automatically controlled. Upon loading a population of insulin-secreting cells, free or encapsulated, the automated

tabletop device starts the evaluation process. The measured oxygen consumption and insulin secretion profiles are compared to a pre-established database/algorithm and based on this comparison, a score is given to the tested sample, which reflects the overall health and quality of the cells and their capacity for secretion. The score given to the cells will act as a quality control system for the harvested sample and it is expected to reflect the probability that the graft will be functional in vivo following successful transplantation.

Figure A6 illustrates a simplified schematic of the perfusion system. Evaluation begins with basal glucose media being perfused through the bioreactor. Dissolved oxygen probes placed immediately before and after the bioreactor take oxygen measurements that are directly integrated with a laptop computer. The computer translates the measurements into oxygen consumption rates of the sample. Additionally, samples collected downstream of the reactor are subjected to an insulin assay to create an insulin secretion profile. Upon establishing the basal condition, the system switches to a stimulatory glucose media during which the oxygen consumption and insulin secretion are continuously monitored. The system then switches to the basal condition for secretion, and the process is repeated at a different dissolved oxygen concentration. Typically, the two dissolved oxygen concentrations used are representative of atmospheric oxygen and the oxygen concentration at the implantation site in vivo. At the end of the process, the computer compares the obtained profiles with established control profiles and gives a functional score to the sample.

The advantages of this system include:

(i) providing a well established functional score that is directly correlated with the functional quality of the insulin-secreting cells, free or encapsulated;

(ii) once the bioreactor is loaded, the machine is fully automated with flow, temperature and dissolved oxygen control.

(iii) ease of loading with free or encapsulated cells

(iv) expandability to other secretory cells

In its present form, the apparatus focuses on providing a thorough assessment of the quality of the insulin-secreting cells. The time period for the evaluation is determined by the time it takes for the collected fractions to be assayed for insulin. Currently, speed of analysis is not a critical factor, as there exists a time period between islet isolation and implantation in all clinical procedures. However, if speed of analysis becomes an issue, the device can be modified to accommodate a flow through insulin immunosensor, purchased commercially or licensed from another company.

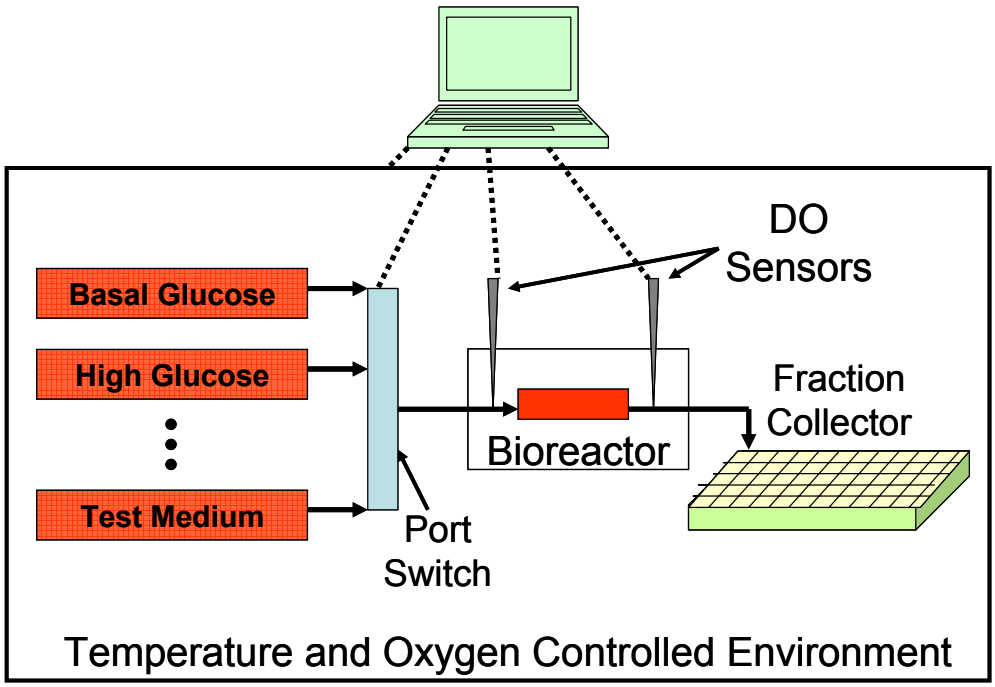

Figure A6 Simplified schematic of the quality control system. In addition to the glucose-containing medium, other 'Test Medium' could be used, as indicated.

A2.c Executive Summary

Diabetes is the fastest growing disease in both the United States and worldwide. Insulin dependant diabetes is the more severe type of the disease, and approximately 4 million Americans suffer from this form of diabetes. In the U.S. alone, 130,000 new cases of Type 1 diabetes (a subset of all insulin dependant diabetics) are diagnosed each year; a growth rate of 7.2%. There is no cure for diabetes in the conventional sense, only various treatment options.

In short, diabetics cannot produce insulin to regulate their blood sugar. The newest and most promising way to treat insulin dependant diabetics is islet transplantation. Islets are the cell clusters in the pancreas that produce insulin and control blood sugar. Islet transplantation involves implanting functioning islet cells from donors' pancreases into a diabetic to perform the vital process of regulating blood sugar. A critical step in an islet transplantation procedure is evaluating the donor's islet cells to test their functionality before implanting them. The dominant design is very subjective: looking at islet cells under a microscope and assessing their functionality based on the cells' appearance. The head of an islet transplant center recently told EvIslet that the current method of islet cell evaluation "is not terribly predictive or functional." This is not surprising; cell size and appearance does not equate with functionality.

As a result of this subjective proxy for testing functionality, transplants fail 42% of the time and four donors are needed for a single patient. Evaluating cells based on their size under a microscope is not much of an advance over the way that Galileo worked in the 16th century. EvIslet plans to revolutionize this methodology, bring new technology to the table, and take the guesswork out of islet evaluation. EvIslet gives

transplant centers better diagnostic tools; in turn, doctors are able to make better decisions about transplants before surgery. Better tools and better decisions translate into better quality of life for Type 1 diabetics, because successful transplants mean less pain and fewer procedures per patient.

EvIslet's technology is based on correlations between islets' functional characteristics. Through numerous *in vitro* and *in vivo* tests run in parallel, EvIslet has developed an algorithm that accurately assesses which islets are suitable for transplantation. The algorithm is the backbone software of a table-top diagnostic device that will house a bioreactor to accept small samples of islets, gather data from the islets through an automated system, and assess the functional characteristics against successful islet profiles to determine the donor's islets suitability for transplantation.

Three pieces of intellectual property have been generated by the EvIslet team: the correlative algorithm, the table-top device that houses the testing apparatus, and the database of test results. Both the algorithm and the table-top device will be protected with patents, and the database of clinical intelligence decisions will be held as a trade secret.

While today's initial market is admittedly small, it is artificially suppressed because the islet transplantation procedure itself is currently undergoing the final portion of its FDA approval process. EvIslet projects that the number of hospitals performing this procedure will increase once FDA approval is obtained. The number of transplants performed should be comparable to the annual number of kidney and liver transplants performed in the U.S. today: 15,000 and 6,000 respectively. EvIslet estimates the returns from the sales and licensing of this initial algorithm and device combination to be at or

over $50 million a year, recurring annually, after the first three years of commercialization. A tri-fold recurring revenue model for the algorithm, based on a per-use fee, a disposable bio-reactor component, and the device leasing program is anticipated. This will offer EvIslet a sustainable revenue stream with few additional annual costs.

EvIslet plans to offer the algorithm, and companion table-top device on which to run it, to islet transplantation centers, those research universities spending at least $5 million annually on scientific research, and various corporations in the cellular research industry. Our market research has shown us that our potential customers are willing to pay a "premium price" for a tool that would put quantifiable data assessing islet functionality into the hands of transplant surgeons and diabetes researchers.

EvIslet's direct customers are the transplant centers (TC) and research companies who serve the needs of diabetic patients, the indirect customer. The TC pain is rooted in the primitive evaluation methodology that wastes precious islets and valuable time, and often results in unsuccessful surgeries (further compounding the shortages of islets and time). By taking the guesswork out of cell evaluation, and providing a quantifiable functional test for viability, islet transplantation will become a more efficient and effective procedure by reducing patients' needs for a second, third, or even fourth transplant. At EvIslet we are helping hospitals and surgeons make better decisions about treating patients.

As the paragraphs above delineate, EvIslet's initial innovation is centered on the growing demands of the diabetes epidemic and focused on delivering a functional test for islet cell evaluation prior to transplantation. EvIslet's revenue stream for this initial

innovation will mainly come from three sources: machine rentals from transplant centers, machines sales from particular corporations and research institution customers, and recurring revenues of database service fees and bio-reactor sales. EvIslet is estimated to generate revenue of $11 million in 2011 to $53 million in 2014. Considering our relatively low fixed and variable costs, our gross margin is projected at near 99%; net profits are expected to be 57%. In addition, future markets may be developed around liver transplants and stem cell research. We believe that EvIslet's initial innovation will be the cornerstone/platform upon which to position the company as a medical device research and development company with a unique ability to develop diagnostic devices for cell implantation.

Over the next 4 to 5 years EvIslet will be seeking a total of $6.5 million in start up capital, which will cover continued research and development, clinical trials, legal and regulatory costs, patent costs, final prototype development, initial sales and marketing, and other business expenses associated with bringing our initial solution to the marketplace. EvIslet's start up capital fundraising will be done in phases. In the Initial phase EvIslet is seeking a first round investment of $3 million. This initial investment capital will take EvIslet through Developmental Stage 2. EvIslet will begin seeking the second round investment funding for the Clinical Trial Stage near the end of Developmental Stage 2. The desired $3.5 million second investment will carry EvIslet through clinical trials and well into the Full Adoption Stage and revenue generation. In exchange for these initial capital investments, at each investment phase, EvIslet is willing to negotiate stock offerings and board seats.

APPENDIX III

ADDITIONAL NMR DATA

A3.a Stability of the Inorganic Phosphate Peak

The inorganic phosphate (P_i) peak obtained during ^{31}P NMR acquisitions served as a standard to which the β-NTP peak was normalized. Given that the volume of the perfusion medium was much greater than the cell volume, it was assumed that the P_i peak was primarily attributed to the phosphates within the medium and that the P_i concentration within the medium did not change over time. Figure A7 plots the integral of the P_i over the course of the study performed in CHAPTER 4 (Figure 4.3). The P_i was normalized to the initial integral with the first integral set at 100. Indeed, the normalized P_i integral remained relatively constant over the study with an average value of 99.8 ± 7.1 (ave. ± std. dev.) over the 55 hours of the experiment. However, a trend in which the P_i integral increased to approximately 110 was noted at the time points associated with the lowest DOin (hours 25 to 30), which would lower the β-NTP/P_i ratio. Nevertheless, this would only change the ratio by a maximum of 10% of its reported value.

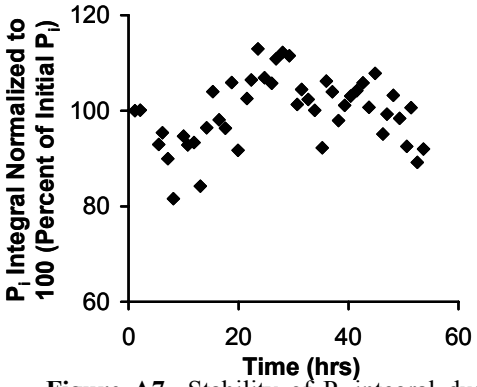

Figure A7 Stability of P_i integral during perfusion studies.

A3.b Change in β-NTP/P_i Integral and AIDO at a Constant DOin

In the data of CHAPTER 5, the β-NTP/P_i integral ratio decreased during the initial DOin step decreases. To determine if these decreases were the result of encapsulated cells equilibrating to the perfusion system and not the result of the DOin step changes, a study was performed in which the beads were perfused for 23 hours at a constant DOin. Specifically, beads cultured for one week were loaded into a bioreactor and perfused for 22 hours at DOin concentration of 0.20 mM. During this study, the β-NTP/P_i integral ratio was monitored by ^{31}P NMR and the AIDO concentration was monitored by ^{19}F NMR. Figure A8 demonstrates that there was little change of both of these parameters over the course of the study with an average β-NTP/P_i integral ratio of 97.4 ± 15.3 and an average AIDO of 0.168 ± 0.003 mM (ave. ± std. dev.).

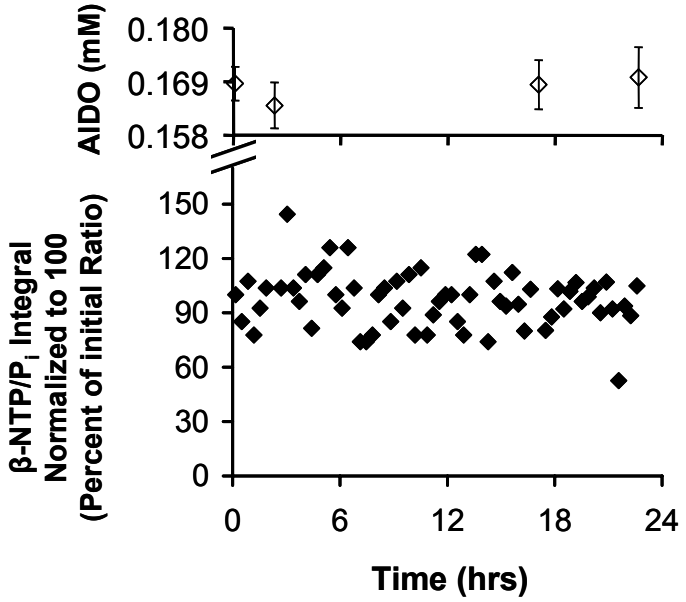

Figure A8 Transient changes in the β-NTP/P_i integral ratio (♦) and AIDO (◊) at a constant DOin. The DOin was maintained at 0.20 mM for approximately 23 hours while perfusing encapsulated βTC-tet cells.

REFERENCES

1. Accessed (11/2005): http://www.jdrg.org.

2. *The effect of intensive treatment of diabetes on the development and progression of long-term complications in insulin-dependent diabetes mellitus. The Diabetes Control and Complications Trial Research Group.* N Engl J Med, 1993. **329**(14): p. 977-986.

3. Shapiro, A.M., J.R. Lakey, E.A. Ryan, G.S. Korbutt, E. Toth, G.L. Warnock, N.M. Kneteman, and R.V. Rajotte, *Islet transplantation in seven patients with type 1 diabetes mellitus using a glucocorticoid-free immunosuppressive regimen.* N Engl J Med, 2000. **343**(4): p. 230-8.

4. Nerem, R.M. and A. Sambanis, *Tissue engineering: from biology to biological substitutes.* Tissue Engineering, 1995. **1**(1): p. 3-13.

5. Dionne, K.E., C.K. Colton, and M.L. Yarmush, *Effect of oxygen on isolated pancreatic tissue.* ASAIO Trans, 1989. **35**(3): p. 739-41.

6. Graeber, T.G., C. Osmanian, T. Jacks, D.E. Housman, C.J. Koch, S.W. Lowe, and A.J. Giaccia, *Hypoxia-mediated selection of cells with diminished apoptotic potential in solid tumours.* Nature, 1996. **379**(6560): p. 88-91.

7. Mercille, S. and B. Massie, *Induction of apoptosis in oxygen-deprived cultures of hybridoma cells.* Cytotechnology, 1994. **15**(1-3): p. 117-28.

8. Papas, K.K., R.C. Long, Jr., I. Constantinidis, and A. Sambanis, *Effects of oxygen on metabolic and secretory activities of beta TC3 cells.* Biochim Biophys Acta, 1996. **1291**(2): p. 163-6.

9. Papas, K.K., R.C. Long, Jr., A. Sambanis, and I. Constantinidis, *Development of a bioartificial pancreas: II. Effects of oxygen on long- term entrapped betaTC3 cell cultures.* Biotechnol Bioeng, 1999. **66**(4): p. 231-7.

10. Miller, W.M., C.R. Wilke, and H.W. Blanch, *Effects of dissolved oxygen concentration on hybridoma growth and metabolism in continuous culture.* J Cell Physiol, 1987. **132**(3): p. 524-30.

11. Ozturk, S.S. and B.O. Palsson, *Effects of dissolved oxygen on hybridoma cell growth, metabolism, and antibody production kinetics in continuous culture.* Biotechnol Prog, 1990. **6**(6): p. 437-46.

12. Murphy, C.L. and A. Sambanis, *Effect of oxygen tension and alginate encapsulation on restoration of the differentiated phenotype of passaged chondrocytes.* Tissue Eng, 2001. **7**(6): p. 791-803.

13. Lin, Q., Y.J. Lee, and Z. Yun, *Differentiation arrest by hypoxia.* J Biol Chem, 2006. **281**(41): p. 30678-83.

14. Ma, X.Q., R.F. Fu, G.Q. Feng, Z.J. Wang, S.G. Ma, and S.A. Weng, *Hypoxia-reoxygenation-induced apoptosis in cultured neonatal rat cardiomyocyets and the protective effect of prostaglandin E.* Clin Exp Pharmacol Physiol, 2005. **32**(12): p. 1124-30.

15. Papas, K.K., R.C. Long, Jr., I. Constantinidis, and A. Sambanis, *Effects of short-term hypoxia on a transformed cell-based bioartificial pancreatic construct.* Cell Transplant, 2000. **9**(3): p. 415-22.

16. Papas, K.K., R.C. Long, Jr., A. Sambanis, and I. Constantinidis, *Development of a bioartificial pancreas: I. Long-term propagation and basal and induced secretion from entrapped betaTC3 cell cultures.* Biotechnol Bioeng, 1999. **66**(4): p. 219-30.

17. Radisic, M., J. Malda, E. Epping, W. Geng, R. Langer, and G. Vunjak-Novakovic, *Oxygen gradients correlate with cell density and cell viability in engineered cardiac tissue.* Biotechnol Bioeng, 2006. **93**(2): p. 332-43.

18. Dionne, K.E., C.K. Colton, and M.L. Yarmush, *Effect of hypoxia on insulin secretion by isolated rat and canine islets of Langerhans.* Diabetes, 1993. **42**(1): p. 12-21.

19. Reid, R.S., C.J. Koch, M.E. Castro, J.A. Lunt, E.O. Treiber, D.J. Boisvert, and P.S. Allen, *The influence of oxygenation on the 19F spin-lattice relaxation rates of fluosol-DA.* Phys Med Biol, 1985. **30**(7): p. 677-86.

20. Shukla, H.P., R.P. Mason, D.E. Woessner, and P.P. Antich, *A comparison of three commerical perfluorocarbon emulsions as high-field 19F NMR probes of oxygen tension and temperature.* J Magn Reson, 1995. **106**: p. 131-141.

21. Constantinidis, I., I. Rask, R.C. Long, Jr., and A. Sambanis, *Effects of alginate composition on the metabolic, secretory, and growth characteristics of entrapped beta TC3 mouse insulinoma cells.* Biomaterials, 1999. **20**(21): p. 2019-27.

22. Stabler, C.L., A. Sambanis, and I. Constantinidis, *Effects of alginate composition on the growth and overall metabolic activity of betaTC3 cells.* Ann N Y Acad Sci, 2002. **961**: p. 130-3.

23. Joseph, P.M., J.E. Fishman, B. Mukherji, and H.A. Sloviter, *In vivo 19F NMR imaging of the cardiovascular system.* J Comput Assist Tomogr, 1985. **9**(6): p. 1012-9.

24. Noth, U., P. Grohn, A. Jork, U. Zimmermann, A. Haase, and J. Lutz, *19F-MRI in vivo determination of the partial oxygen pressure in perfluorocarbon-loaded alginate capsules implanted into the peritoneal cavity and different tissues.* Magn Reson Med, 1999. **42**(6): p. 1039-47.

25. Noth, U., L.M. Rodrigues, S.P. Robinson, A. Jork, U. Zimmermann, B. Newell, and J.R. Griffiths, *In vivo determination of tumor oxygenation during growth and in response to carbogen breathing using 15C5-loaded alginate capsules as fluorine-19 magnetic resonance imaging oxygen sensors.* Int J Radiat Oncol Biol Phys, 2004. **60**(3): p. 909-19.

26. Shukla, H.P., R.P. Mason, N. Bansal, and P.P. Antich, *Regional myocardial oxygen tension: 19F MRI of sequestered perfluorocarbon.* Magn Reson Med, 1996. **35**(6): p. 827-33.

27. Eidelberg, D., G. Johnson, D. Barnes, P.S. Tofts, D. Delpy, D. Plummer, and W.I. McDonald, *19F NMR imaging of blood oxygenation in the brain.* Magn Reson Med, 1988. **6**(3): p. 344-52.

28. Berkowitz, B.A., C.A. Wilson, and D.L. Hatchell, *Oxygen kinetics in the vitreous substitute perfluorotributylamine: a 19F NMR study in vivo.* Invest Ophthalmol Vis Sci, 1991. **32**(8): p. 2382-7.

29. Sotak, C.H., P.S. Hees, H.N. Huang, M.H. Hung, C.G. Krespan, and S. Raynolds, *A new perfluorocarbon for use in fluorine-19 magnetic resonance imaging and spectroscopy.* Magn Reson Med, 1993. **29**(2): p. 188-95.

30. Lowe, K.C. and F.H. Armstrong, *Oxygen-transport fluid based on perfluorochemicals: effects on liver biochemistry.* Adv Exp Med Biol, 1990. **277**: p. 267-76.

31. Lowe, K.C. and F.H. Armstrong, *Biocompatibility studies with perfluorochemical oxygen carriers.* Biomater Artif Cells Immobilization Biotechnol, 1992. **20**(2-4): p. 993-9.

32. Zimmermann, U., U. Noth, P. Grohn, A. Jork, K. Ulrichs, J. Lutz, and A. Haase, *Non-invasive evaluation of the location, the functional integrity and the oxygen supply of implants: 19F nuclear magnetic resonance imaging of perfluorocarbon-loaded Ba2+-alginate beads.* Artif Cells Blood Substit Immobil Biotechnol, 2000. **28**(2): p. 129-46.

33. Khattak, S.F., K.S. Chin, S.R. Bhatia, and S.C. Roberts, *Enhancing oxygen tension and cellular function in alginate cell encapsulation devices through the use of perfluorocarbons.* Biotechnol Bioeng, 2007. **96**(1): p. 156-66.

34. King, A.T., B.J. Mulligan, and K.C. Lowe, *Perfluorochemicals and cell culture.* Biotechnology, 1989. **7**: p. 1037-1042.

35. Lowe, K.C., M.R. Davey, and J.B. Power, *Perfluorochemicals: their applications and benefits to cell culture.* Trends Biotechnol, 1998. **16**(6): p. 272-7.

36. Matsumoto, S., *Clinical application of perfluorocarbons for organ preservation.* Artif Cells Blood Substit Immobil Biotechnol, 2005. **33**(1): p. 75-82.

37. Matsumoto, S. and Y. Kuroda, *Perfluorocarbon for organ preservation before transplantation.* Transplantation, 2002. **74**(12): p. 1804-9.

38. Radisic, M., W. Deen, R. Langer, and G. Vunjak-Novakovic, *Mathematical model of oxygen distribution in engineered cardiac tissue with parallel channel array perfused with culture medium containing oxygen carriers.* Am J Physiol Heart Circ Physiol, 2005. **288**(3): p. H1278-89.

39. Ramachandran, S., N.M. Desai, T.A. Goers, N. Benshoff, B. Olack, S. Shenoy, M.D. Jendrisak, W.C. Chapman, and T. Mohanakumar, *Improved islet yields from pancreas preserved in perflurocarbon is via inhibition of apoptosis mediated by mitochondrial pathway.* Am J Transplant, 2006. **6**(7): p. 1696-703.

40. Sakai, T., S. Li, Y. Tanioka, T. Goto, T. Tanaka, I. Matsumoto, T. Tsujimura, Y. Fujino, Y. Suzuki, and Y. Kuroda, *Intraperitoneal injection of oxygenated perfluorochemical improves the outcome of intraportal islet transplantation in a rat model.* Transplant Proc, 2006. **38**(10): p. 3289-92.

41. Spruell, R.D., E.R. Ferguson, J.J. Clymer, W.V. Vicente, C.P. Murrah, and W.L. Holman, *Perfluorocarbons are effective oxygen carriers in cardiopulmonary bypass.* Asaio J, 1995. **41**(3): p. M636-41.

42. Witkowski, P., Z. Liu, Q. Guo, E. Poumian-Ruiz, S. Cernea, K. Herold, and M.A. Hardy, *Two-layer method in short-term pancreas preservation for successful islet isolation.* Transplant Proc, 2005. **37**(8): p. 3398-401.

43. Gross, J.D., R.C. Long, I. Constantinidis, and A. Sambanis, *Monitoring of Dissolved Oxygen and Cellular Bioenergetics within a Pancreatic Substitute.* Biotechnol Bioeng, 2007. **In Press**.

44. http://www.jdrf.org. [cited.

45. Gaglia, J.L., A.M. Shapiro, and G.C. Weir, *Islet transplantation: progress and challenge.* Arch Med Res, 2005. **36**(3): p. 273-80.

46. Smidsrod, O. and G. Skjak-Braek, *Alginate as immobilization matrix for cells.* Trends Biotechnol, 1990. **8**(3): p. 71-8.

47. Draget, K.I., B.T. Stokke, Y. Yuguchi, H. Urakawa, and K. Kajiwara, *Small-angle X-ray scattering and rheological characterization of alginate gels. 3. Alginic acid gels.* Biomacromolecules, 2003. **4**(6): p. 1661-8.

48. Lim, F. and A.M. Sun, *Microencapsulated islets as bioartificial endocrine pancreas.* Science, 1980. **210**(4472): p. 908-10.

49. Ma, X., I. Vacek, and A. Sun, *Generation of alginate-poly-l-lysine-alginate (APA) biomicrocapsules: the relationship between the membrane strength and the reaction conditions.* Artif Cells Blood Substit Immobil Biotechnol, 1994. **22**(1): p. 43-69.

50. Leblond, F.A., J. Tessier, and J.P. Halle, *Quantitative method for the evaluation of biomicrocapsule resistance to mechanical stress.* Biomaterials, 1996. **17**(21): p. 2097-102.

51. Stabler, C., K. Wilks, A. Sambanis, and I. Constantinidis, *The effects of alginate composition on encapsulated betaTC3 cells.* Biomaterials, 2001. **22**(11): p. 1301-10.

52. Ramiya, V.K., M. Maraist, K.E. Arfors, D.A. Schatz, A.B. Peck, and J.G. Cornelius, *Reversal of insulin-dependent diabetes using islets generated in vitro from pancreatic stem cells.* Nat Med, 2000. **6**(3): p. 278-82.

53. Assady, S., G. Maor, M. Amit, J. Itskovitz-Eldor, K.L. Skorecki, and M. Tzukerman, *Insulin production by human embryonic stem cells.* Diabetes, 2001. **50**(8): p. 1691-7.

54. Santana, A., R. Ensenat-Waser, M.I. Arribas, J.A. Reig, and E. Roche, *Insulin-producing cells derived from stem cells: recent progress and future directions.* J Cell Mol Med, 2006. **10**(4): p. 866-83.

55. Efrat, S., S. Linde, H. Kofod, D. Spector, M. Delannoy, S. Grant, D. Hanahan, and S. Baekkeskov, *Beta-cell lines derived from transgenic mice expressing a hybrid insulin gene-oncogene.* Proc Natl Acad Sci U S A, 1988. **85**(23): p. 9037-41.

56. Olson, D.E., S.A. Paveglio, P.U. Huey, M.H. Porter, and P.M. Thule, *Glucose-responsive hepatic insulin gene therapy of spontaneously diabetic BB/Wor rats.* Hum Gene Ther, 2003. **14**(15): p. 1401-13.

57. Thule, P.M., J. Liu, and L.S. Phillips, *Glucose regulated production of human insulin in rat hepatocytes.* Gene Ther, 2000. **7**(3): p. 205-14.

58. Thule, P.M. and J.M. Liu, *Regulated hepatic insulin gene therapy of STZ-diabetic rats.* Gene Ther, 2000. **7**(20): p. 1744-52.

59. Efrat, S., M. Leiser, M. Surana, M. Tal, D. Fusco-Demane, and N. Fleischer, *Murine insulinoma cell line with normal glucose-regulated insulin secretion.* Diabetes, 1993. **42**(6): p. 901-7.

60. Efrat, S., S. Linde, H. Kofod, D. Spector, M. Delannoy, S. Grant, D. Hanahan, and S. Baekkeskov, *Beta-cell lines derived from transgenic mice expressing a hybrid insulin gene-oncogene.* Proc Natl Acad Sci U S A, 1988. **85**(23): p. 9037-41.

61. Knaack, D., D.M. Fiore, M. Surana, M. Leiser, M. Laurance, D. Fusco-DeMane, O.D. Hegre, N. Fleischer, and S. Efrat, *Clonal insulinoma cell line that stably maintains correct glucose responsiveness.* Diabetes, 1994. **43**(12): p. 1413-7.

62. Papas, K.K., R.C. Long, Jr., I. Constantinidis, and A. Sambanis, *Effects of oxygen on metabolic and secretory activities of beta TC3 cells.* Biochim Biophys Acta, 1996. **1291**(2): p. 163-6.

63. Papas, K.K., R.C. Long, Jr., I. Constantinidis, and A. Sambanis, *Role of ATP and Pi in the mechanism of insulin secretion in the mouse insulinoma betaTC3 cell line.* Biochem J, 1997. **326 (Pt 3)**: p. 807-14.

64. Papas, K.K., R.C. Long, Jr., A. Sambanis, and I. Constantinidis, *Development of a bioartificial pancreas: II. Effects of oxygen on long-term entrapped betaTC3 cell cultures.* Biotechnol Bioeng, 1999. **66**(4): p. 231-7.

65. Papas, K.K., R.C. Long, Jr., I. Constantinidis, and A. Sambanis, *Effects of short-term hypoxia on a transformed cell-based bioartificial pancreatic construct.* Cell Transplant, 2000. **9**(3): p. 415-22.

66. Mukundan, N.E., P.C. Flanders, I. Constantinidis, K.K. Papas, and A. Sambanis, *Oxygen consumption rates of free and alginate-entrapped beta TC3 mouse insulinoma cells.* Biochem Biophys Res Commun, 1995. **210**(1): p. 113-8.

67. Efrat, S., D. Fusco-DeMane, H. Lemberg, O. al Emran, and X. Wang, *Conditional transformation of a pancreatic beta-cell line derived from transgenic mice expressing a tetracycline-regulated oncogene.* Proc Natl Acad Sci U S A, 1995. **92**(8): p. 3576-80.

68. Cheng, S.-Y., I. Constantinidis, and A. Sambanis, *Insulin Secretion Dynamics of Free and Alginate-Encapsulated Insulinoma Cells.* Cytotechnology, 2006. **51**: p. 159-170.

69. Black, S.P., I. Constantinidis, H. Cui, C. Tucker-Burden, C.J. Weber, and S.A. Safley, *Immune responses to an encapsulated allogeneic islet beta-cell line in diabetic NOD mice.* Biochem Biophys Res Commun, 2006. **340**(1): p. 236-43.

70. Clark, L.C., Jr. and F. Gollan, *Survival of mammals breathing organic liquids equilibrated with oxygen at atmospheric pressure.* Science, 1966. **152**(730): p. 1755-6.

71. Hoke, J.F., W.R. Ravis, G.H. Hankes, and J. Spano, *Physiological effects of a perfluorochemical blood substitute in beagle dogs.* Res Commun Chem Pathol Pharmacol, 1991. **73**(3): p. 315-32.

72. Waxman, K., *Perfluorocarbons as blood substitutes.* Ann Emerg Med, 1986. **15**(12): p. 1423-4.

73. Rosen, N.A., H.W. Hopf, and T.K. Hunt, *Perflubron emulsion increases subcutaneous tissue oxygen tension in rats.* Wound Repair Regen, 2006. **14**(1): p. 55-60.

74. Dardzinski, B.J. and C.H. Sotak, *Rapid tissue oxygen tension mapping using 19F inversion-recovery echo-planar imaging of perfluoro-15-crown-5-ether.* Magn Reson Med, 1994. **32**(1): p. 88-97.

75. Gross, U., S. Rudiger, H. Reichelt, and J. Draffehn, *Phospholipid vesiculated fluorocarbons--promising trend in blood substitutes.* Biomater Artif Cells Immobilization Biotechnol, 1992. **20**(2-4): p. 831-3.

76. Guruge, K.S., S. Taniyasu, N. Yamashita, S. Wijeratna, K.M. Mohotti, H.R. Seneviratne, K. Kannan, N. Yamanaka, and S. Miyazaki, *Perfluorinated organic compounds in human blood serum and seminal plasma: a study of urban and rural tea worker populations in Sri Lanka.* J Environ Monit, 2005. **7**(4): p. 371-7.

77. Spahn, D.R. and R. Kocian, *Artificial O2 carriers: status in 2005.* Curr Pharm Des, 2005. **11**(31): p. 4099-114.

78. Abel, W.G., *Blood substitute oxygen carriers.* N Y State J Med, 1982. **82**(10): p. 1429-33.

79. Endrich, B., M.M. Newman, A.G. Greenburg, and M. Intaglietta, *Fluorocarbon emulsions as a synthetic blood substitute: effects on microvascular hemodynamics in the rabbit omentum.* J Surg Res, 1980. **29**(6): p. 516-26.

80. Motta, G., G.B. Ratto, A. De Barbieri, M. Tomellini, M. Rovatti, A. Sacco, and M. Castagnola, *An experimental study on fluorocarbons as blood substitutes.* Ital J Surg Sci, 1983. **13**(2): p. 89-93.

81. Rosoff, J.D., L.O. Soltow, C.R. Vocelka, G. Schmer, W.L. Chandler, R.P. Cochran, K.S. Kunzelman, and B.D. Spiess, *A second-generation blood substitute (perfluorodichlorooctane emulsion) does not activate complement during an ex vivo circulation model of bypass.* J Cardiothorac Vasc Anesth, 1998. **12**(4): p. 397-401.

82. Krafft, M.P. and J.G. Riess, *Highly fluorinated amphiphiles and colloidal systems, and their applications in the biomedical field. A contribution.* Biochimie, 1998. **80**(5-6): p. 489-514.

83. Freire, M.G., A.M. Dias, M.A. Coelho, J.A. Coutinho, and I.M. Marrucho, *Aging mechanisms of perfluorocarbon emulsions using image analysis.* J Colloid Interface Sci, 2005. **286**(1): p. 224-32.

84. Kin, S., E. Stephanian, P. Gores, A. Mass, H. Flores, I. Nakai, K. Tamura, R. Gruessner, and D.E. Sutherland, *96-hour cold-storage preservation of the canine pancreas with oxygenation using perfluorochemical.* Transplantation, 1993. **55**(1): p. 229-30.

85. Kuroda, Y., T. Kawamura, Y. Suzuki, H. Fujiwara, K. Yamamoto, and Y. Saitoh, *A new, simple method for cold storage of the pancreas using perfluorochemical.* Transplantation, 1988. **46**(3): p. 457-60.

86. Fujino, Y., Y. Kuroda, Y. Suzuki, H. Fujiwara, T. Kawamura, A. Morita, Y. Ku, and Y. Saitoh, *Preservation of canine pancreas for 96 hours by a modified two-layer (UW solution/perfluorochemical) cold storage method.* Transplantation, 1991. **51**(5): p. 1133-5.

87. Bergert, H., K.P. Knoch, R. Meisterfeld, M. Jager, J. Ouwendijk, S. Kersting, H.D. Saeger, and M. Solimena, *Effect of oxygenated perfluorocarbons on isolated rat pancreatic islets in culture.* Cell Transplant, 2005. **14**(7): p. 441-8.

88. Brandhorst, D., M. Iken, M.D. Brendel, R.G. Bretzel, and H. Brandhorst, *Long-term preservation of the pig pancreas by a one-layer method for successful islet isolation.* Transplant Proc, 2005. **37**(1): p. 229-30.

89. Xia, M., V. Kodibagkar, H. Liu, and R.P. Mason, *Tumour oxygen dynamics measured simultaneously by near-infrared spectroscopy and 19F magnetic resonance imaging in rats.* Phys Med Biol, 2006. **51**(1): p. 45-60.

90. McCoy, C.L., D.J. McIntyre, S.P. Robinson, E.O. Aboagye, and J.R. Griffiths, *Magnetic resonance spectroscopy and imaging methods for measuring tumour and tissue oxygenation.* Br J Cancer Suppl, 1996. **27**: p. S226-31.

91. Mason, R.P., P.P. Antich, E.E. Babcock, A. Constantinescu, P. Peschke, and E.W. Hahn, *Non-invasive determination of tumor oxygen tension and local variation with growth.* Int J Radiat Oncol Biol Phys, 1994. **29**(1): p. 95-103.

92. Raleigh, J.A., A.J. Franko, D.A. Kelly, L.A. Trimble, and P.S. Allen, *Development of an in vivo 19F magnetic resonance method for measuring oxygen deficiency in tumors.* Magn Reson Med, 1991. **22**(2): p. 451-66.

93. Fishman, J.E., P.M. Joseph, M.J. Carvlin, M. Saadi-Elmandjra, B. Mukherji, and H.A. Sloviter, *In vivo measurements of vascular oxygen tension in tumors using MRI of a fluorinated blood substitute.* Invest Radiol, 1989. **24**(1): p. 65-71.

94. Achermann, R.E., S.M. Ohlerth, C. Rohrer Bley, M. Gassmann, N. Inteeworn, M. Roos, M. Scharz, M.C. Wergin, and B. Kaser-Hotz, *Oxygenation of spontaneous canine tumors during fractionated radiation therapy.* Strahlenther Onkol, 2004. **180**(5): p. 297-305.

95. De Jaeger, K., F.M. Merlo, M.C. Kavanagh, A.W. Fyles, D. Hedley, and R.P. Hill, *Heterogeneity of tumor oxygenation: relationship to tumor necrosis, tumor size, and metastasis.* Int J Radiat Oncol Biol Phys, 1998. **42**(4): p. 717-21.

96. Morawski, A.M., G.A. Lanza, and S.A. Wickline, *Targeted contrast agents for magnetic resonance imaging and ultrasound.* Curr Opin Biotechnol, 2005. **16**(1): p. 89-92.

97. Wickline, S.A., A.M. Neubauer, P.M. Winter, S.D. Caruthers, and G.M. Lanza, *Molecular imaging and therapy of atherosclerosis with targeted nanoparticles.* J Magn Reson Imaging, 2007.

98. Winter, P.M., K. Cai, J. Chen, C.R. Adair, G.E. Kiefer, P.S. Athey, P.J. Gaffney, C.E. Buff, J.D. Robertson, S.D. Caruthers, S.A. Wickline, and G.M. Lanza, *Targeted PARACEST nanoparticle contrast agent for the detection of fibrin.* Magn Reson Med, 2006. **56**(6): p. 1384-8.

99. Lanza, G.M., K.D. Wallace, M.J. Scott, W.P. Cacheris, D.R. Abendschein, D.H. Christy, A.M. Sharkey, J.G. Miller, P.J. Gaffney, and S.A. Wickline, *A novel site-targeted ultrasonic contrast agent with broad biomedical application.* Circulation, 1996. **94**(12): p. 3334-40.

100. Lanza, G.M., X. Yu, P.M. Winter, D.R. Abendschein, K.K. Karukstis, M.J. Scott, L.K. Chinen, R.W. Fuhrhop, D.E. Scherrer, and S.A. Wickline, *Targeted antiproliferative drug delivery to vascular smooth muscle cells with a magnetic*

resonance imaging nanoparticle contrast agent: implications for rational therapy of restenosis. Circulation, 2002. **106**(22): p. 2842-7.

101. Pilatus, U., E. Aboagye, D. Artemov, N. Mori, E. Ackerstaff, and Z.M. Bhujwalla, *Real-time measurements of cellular oxygen consumption, pH, and energy metabolism using nuclear magnetic resonance spectroscopy.* Magn Reson Med, 2001. **45**(5): p. 749-55.

102. McGovern, K.A., J.S. Schoeniger, J.P. Wehrle, C.E. Ng, and J.D. Glickson, *Gel-entrapment of perfluorocarbons: A fluorine-19 NMR spectroscopic method for monitoring oxygen concentration in cell perfusion systems.* Magn. Reson. Med., 1993. **29**: p. 196-204.

103. McGovern, K.A., J.S. Schoeniger, J.P. Wehrle, C.E. Ng, and J.D. Glickson, *Gel-entrapment of perfluorocarbons: a fluorine-19 NMR spectroscopic method for monitoring oxygen concentration in cell perfusion systems.* Magn Reson Med, 1993. **29**(2): p. 196-204.

104. Jaeger, M., M. Soehle, M.U. Schuhmann, D. Winkler, and J. Meixensberger, *Correlation of continuously monitored regional cerebral blood flow and brain tissue oxygen.* Acta Neurochir (Wien), 2005. **147**(1): p. 51-6.

105. Vujaskovic, Z., E.L. Rosen, K.L. Blackwell, E.L. Jones, D.M. Brizel, L.R. Prosnitz, T.V. Samulski, and M.W. Dewhirst, *Ultrasound guided pO2 measurement of breast cancer reoxygenation after neoadjuvant chemotherapy and hyperthermia treatment.* Int J Hyperthermia, 2003. **19**(5): p. 498-506.

106. Wilson, D.F., *Oxygen dependent quenching of phosphorescence: a perspective.* Adv Exp Med Biol, 1992. **317**: p. 195-201.

107. Mik, E.G., T.G. van Leeuwen, N.J. Raat, and C. Ince, *Quantitative determination of localized tissue oxygen concentration in vivo by two-photon excitation phosphorescence lifetime measurements.* J Appl Physiol, 2004. **97**(5): p. 1962-9.

108. Fiat, D., J. Hankiewicz, S. Liu, S. Trbovic, and S. Brint, *17O magnetic resonance imaging of the human brain.* Neurol Res, 2004. **26**(8): p. 803-8.

109. O'Hara, J.A., H. Hou, E. Demidenko, R.J. Springett, N. Khan, and H.M. Swartz, *Simultaneous measurement of rat brain cortex PtO2 using EPR oximetry and a fluorescence fiber-optic sensor during normoxia and hyperoxia.* Physiol Meas, 2005. **26**(3): p. 203-13.

110. O'Hara, J.A., R.D. Blumenthal, O.Y. Grinberg, S. Grinberg, C. Wilmot, D.M. Goldenberg, and H.M. Swartz, *Tumor pO2 assessments in human xenograft tumors measured by EPR oximetry: location of paramagnetic materials.* Adv Exp Med Biol, 2003. **530**: p. 205-14.

111. Simpson, N.E., S.C. Grant, S.J. Blackband, and I. Constantinidis, *NMR properties of alginate microbeads.* Biomaterials, 2003. **24**(27): p. 4941-8.

112. Stabler, C.L., R.C. Long, Jr., I. Constantinidis, and A. Sambanis, *In vivo noninvasive monitoring of a tissue engineered construct using 1H NMR spectroscopy.* Cell Transplant, 2005. **14**(2-3): p. 139-49.

113. Stabler, C.L., R.C. Long, Jr., A. Sambanis, and I. Constantinidis, *Noninvasive Measurement of Viable Cell Number in Tissue-Engineered Constructs in Vitro, Using 1H Nuclear Magnetic Resonance Spectroscopy.* Tissue Eng, 2005. **11**(3-4): p. 404.

114. Newgard, C.B. and J.D. McGarry, *Metabolic coupling factors in pancreatic beta-cell signal transduction.* Annu Rev Biochem, 1995. **64**: p. 689-719.

115. Nerem, R.M., Sambanis, A., *Tissue engineering: from biology to biological substitutes.* Tissue Engineering, 1995. **1**(1): p. 3-13.

116. Stabler, C., K. Wilks, A. Sambanis, and I. Constantinidis, *The effects of alginate composition on encapsulated betaTC3 cells.* Biomaterials, 2001. **22**(11): p. 1301-10.

117. Burg, K.J., M. Delnomdedieu, R.J. Beiler, C.R. Culberson, K.G. Greene, C.R. Halberstadt, W.D.J. Holder, A.B. Loebsack, W.D. Roland, and G.A. Johnson, *Application of magnetic resonance microscopy to tissue engineering: a polylactide model.* J Biomed Mater Res, 2002. **61**: p. 380-390.

118. Constantinidis, I., R.C. Long, Jr., C. Weber, S. Safley, and A. Sambanis, *Non-invasive monitoring of a bioartificial pancreas in vitro and in vivo.* Annals New York Academy Sciences, 2001. **944**: p. 83-96.

119. Constantinidis, I. and A. Sambanis, *Non-invasive monitoring of tissue engineered constructs by nuclear magnetic resonance methodologies.* Tissue Engineering, 1998. **4**: p. 9-17.

120. Constantinidis, I., C.L. Stabler, R. Long, Jr., and A. Sambanis, *Noninvasive monitoring of a retrievable bioartificial pancreas in vivo.* Ann N Y Acad Sci, 2002. **961**: p. 298-301.

121. Stabler, C.L., R.C. Long, Jr., A. Sambanis, and I. Constantinidis, *In vivo noninvasive monitoring of a tissue engineered construct using 1H NMR spectroscopy.* Cell Transplant, 2005. **14**(2-3): p. 139-49.

122. Long, R.C., Jr., K.K. Papas, A. Sambanis, and I. Constantinidis, *In vitro monitoring of total choline levels in a bioartificial pancreas: ^{1}H NMR*

spectroscopic studies of the effects of oxygen level. Journal of Magnetic Resonance, 2000. **146**: p. 49-57.

123. Constantinidis, I. and A. Sambanis, *Towards the development of artificial endocrine tissues: 31P NMR spectroscopic studies of immunoisolated, insulin-secreting AtT-20 cells.* Biotechnol Bioeng, 1995. **47**: p. 431-443.

124. Dionne, K.E., C.K. Colton, and M.L. Yarmush, *A microperifusion system with environmental control for studying insulin secretion by pancreatic tissue.* Biotechnol Prog, 1991. **7**(4): p. 359-68.

125. Mukundan, N.E., P.C. Flanders, I. Constantinidis, K.K. Papas, and A. Sambanis, *Oxygen consumption rates of free and alginate-entrapped beta TC3 mouse insulinoma cells.* Biochem Biophys Res Commun, 1995. **210**(1): p. 113-8.

126. Papas, K.K., R.C. Long, Jr., I. Constantinidis, and A. Sambanis, *Role of ATP and Pi in the mechanism of insulin secretion in the mouse insulinoma betaTC3 cell line.* Biochem J, 1997. **326**(Pt 3): p. 807-14.

127. Noth, U., P. Grihn, A. Jork, U. Zimmermann, A. Haase, and J. Lutz, *^{19}F-MRI in vivo determination of the partial oxygen pressure in perfluorocarbon-loaded alginate capsules implanted into the peritoneal cavity and different tissues.* Magn. Reson. Med., 1999. **42**: p. 1039-1047.

128. Alsberg, E., K.W. Anderson, A. Albeiruti, R.T. Franceschi, and D.J. Mooney, *Cell-interactive alginate hydrogels for bone tissue engineering.* J Dent Res, 2001. **80**(11): p. 2025-9.

129. Rowley, J.A. and D.J. Mooney, *Alginate type and RGD density control myoblast phenotype.* J Biomed Mater Res, 2002. **60**(2): p. 217-23.

130. Efrat, S., *Genetically engineered pancreatic beta-cell lines for cell therapy of diabetes.* Ann N Y Acad Sci, 1999. **875**: p. 286-93.

131. Efrat, S., D. Fusco-DeMane, H. Lemberg, O. al Emran, and X. Wang, *Conditional transformation of a pancreatic beta-cell line derived from transgenic mice expressing a tetracycline-regulated oncogene.* Proc Natl Acad Sci U S A, 1995. **92**(8): p. 3576-80.

132. Tziampazis, E. and A. Sambanis, *Tissue engineering of a bioartificial pancreas: modeling the cell environment and device function.* Biotechnol Prog, 1995. **11**(2): p. 115-26.

133. Wohlpart, D., Kirwan, D., and Gainer, J., *Effects of cell density and glucose and glutamine levels on the respiration rates of hybridoma cells.* Biotechnol Bioeng, 1990. **36**: p. 630-635.

134. Sambanis, A., Tan, S.A., *Quantitative modeling of limitations caused by diffusion*, in *Methods in Molecular Medicine, Vol. 18: Tissue Engineering Methods and Protocols*, J.R. Morgan, and Yarmush, M.L., Editor. 1999, Humana Press, Inc.: Totowa, NJ.

135. Mehmetoglu, U., S. Ates, and R. Berber, *Oxygen diffusivity in calcium alginate gel beads containing Gluconobacter suboxydans.* Artif Cells Blood Substit Immobil Biotechnol, 1996. **24**(2): p. 91-106.

136. Kreyszig, E., *Advanced Engineering Mathematics*. 8th ed. 2003, New York: John Wiley & Sons, Inc. 1156.

137. Bassom, A.P., A. Ilchmann, and H. Voss, *Oxygen diffusion in tissue preparations with Michaelis-Menten kinetics.* J Theor Biol, 1997. **185**(1): p. 119-27.

138. Mikos, A.G., L.V. McIntire, J.M. Anderson, and J.E. Babensee, *Host response to tissue engineered devices.* Adv Drug Deliv Rev, 1998. **33**(1-2): p. 111-139.

139. Simpson, N.E., S.C. Grant, L. Gustavsson, V.M. Peltonen, S.J. Blackband, and I. Constantinidis, *Biochemical consequences of alginate encapsulation: a NMR study of insulin-secreting cells.* Biomaterials, 2006. **27**(12): p. 2577-86.

140. Constantinidis, I.a.S., A., *Noninvasive monitoring of tissue-engineered constructs by nuclear magnetic resonance methodologies.* Tissue Eng, 1998. **4**: p. 9-17.

141. Long, R.C., Jr., K.K. Papas, A. Sambanis, and I. Constantinidis, *In vitro monitoring of total choline levels in a bioartificial pancreas: (1)H NMR spectroscopic studies of the effects of oxygen level.* J Magn Reson, 2000. **146**(1): p. 49-57.

142. Constantinidis, I., N.E. Mukundan, M.P. Gamcsik, and A. Sambanis, *Towards the development of a bioartificial pancreas: a 13C NMR study on the effects of alginate/poly-L-lysine/alginate entrapment on glucose metabolism by beta TC3 mouse insulinoma cells.* Cell Mol Biol (Noisy-le-grand), 1997. **43**(5): p. 721-9.

143. Fan, X., J.N. River, M. Zamora, H.A. Al-Hallaq, and G.S. Karczmar, *Effect of carbogen on tumor oxygenation: combined fluorine-19 and proton MRI measurements.* Int J Radiat Oncol Biol Phys, 2002. **54**(4): p. 1202-9.

144. Gross, J.D., I. Constantinidis, and A. Sambanis, *Modeling of encapsulated cell systems.* J Theor Biol, 2006.

145. Johnson, R., D. Harrison, M. Tucci, A. Tsao, M. Lemos, A. Puckett, J.L. Hughes, and H. Benghuzzi, *Fibrous capsule formation in response to ultrahigh molecular weight polyethylene treated with peptides that influence adhesion.* Biomed Sci Instrum, 1997. **34**: p. 47-52.

146. Constantinidis, I., S.C. Grant, S. Celper, I. Gauffin-Holmberg, K. Agering, J.A. Oca-Cossio, J.D. Bui, J. Flint, C. Hamaty, N.E. Simpson, and S.J. Blackband, *Non-invasive evaluation of alginate/poly-l-lysine/alginate microcapsules by magnetic resonance microscopy.* Biomaterials, 2007.

147. Tabuchi, I., *Next-generation protein-handling method: puromycin analogue technology.* Biochem Biophys Res Commun, 2003. **305**(1): p. 1-5.

148. Gross, J.D., I. Constantinidis, and A. Sambanis, *Modeling of encapsulated cell systems.* J Theor Biol, 2007. **244**(3): p. 500-10.

149. Safley, S.A., J.A. Kapp, and C.J. Weber, *Proliferative and cytokine responses in CTLA4-Ig-treated diabetic NOD mice transplanted with microencapsulated neonatal porcine ICCs.* Cell Transplant, 2002. **11**(7): p. 695-705.

150. Malda, J., T.B. Woodfield, F. van der Vloodt, F.K. Kooy, D.E. Martens, J. Tramper, C.A. van Blitterswijk, and J. Riesle, *The effect of PEGT/PBT scaffold architecture on oxygen gradients in tissue engineered cartilaginous constructs.* Biomaterials, 2004. **25**(26): p. 5773-80.

151. Brown, D., W. Maclellan, H. Laks, J. Dunn, B. Wu, and R. Beygui, *Analysis of oxygen transport in a diffusion-limited model of engineered heart tissue.* Biotechnol Bioeng, 2006.

152. Muschler, G.F., C. Nakamoto, and L.G. Griffith, *Engineering principles of clinical cell-based tissue engineering.* J Bone Joint Surg Am, 2004. **86-A**(7): p. 1541-58.

153. Kirschman, R.A., *Finding alternatives to blood transfusion.* Holist Nurs Pract, 2004. **18**(6): p. 277-81; quiz 282-3.

154. Riess, J.G., *Understanding the fundamentals of perfluorocarbons and perfluorocarbon emulsions relevant to in vivo oxygen delivery.* Artif Cells Blood Substit Immobil Biotechnol, 2005. **33**(1): p. 47-63.

155. Woitzik, J., N. Weinzierl, and L. Schilling, *Early administration of a second-generation perfluorochemical decreases ischemic brain damage in a model of permanent middle cerebral artery occlusion in the rat.* Neurol Res, 2005. **27**(5): p. 509-15.

156. Contreras, J.L., C. Eckstein, C.A. Smyth, G. Bilbao, M. Vilatoba, S.E. Ringland, C. Young, J.A. Thompson, J.A. Fernandez, J.H. Griffin, and D.E. Eckhoff, *Activated protein C preserves functional islet mass after intraportal transplantation: a novel link between endothelial cell activation, thrombosis, inflammation, and islet cell death.* Diabetes, 2004. **53**(11): p. 2804-14.

157. Giuliani, M., W. Moritz, E. Bodmer, D. Dindo, P. Kugelmeier, R. Lehmann, M. Gassmann, P. Groscurth, and M. Weber, *Central necrosis in isolated hypoxic human pancreatic islets: evidence for postisolation ischemia.* Cell Transplant, 2005. **14**(1): p. 67-76.

158. O'Brien, R.N., A.J. Langlais, and W.D. Seufert, *Diffusion coefficients of respiratory gases in a perfluorocarbon liquid.* Science, 1982. **217**(4555): p. 153-5.